PROTEOMICS STUDIES OF ENVIRONMENTAL EFFECTS AND SYSTEMIC GENE INTERACTIONS IN DISORDERS OF FATTY ACID BETA-OXIDATION

by

Wang, Wei

MPH, Harvard University, 2005

MMed, Shandong Medical University, China, 1999

BMed, Qingdao University, China,1992

Submitted to the Graduate Faculty of

Graduate School of Public Health in partial fulfillment

of the requirements for the degree of

Doctor of Philosophy

University of Pittsburgh

2011

UNIVERSITY OF PITTSBURGH

GRADUATE SCHOOL OF PUBLIC HEALTH

This dissertation was presented

by

Wang, Wei

It was defended on

July 25, 2011

and approved by

Dissertation Director: Jerry Vockley, M.D. Ph.D., Professor,
Pediatrics, School of Medicine, University of Pittsburgh

Michael Barmada, Ph.D., Associate Professor, Human Genetics,
Graduate School of Public Health, University of Pittsburgh

Billy Day, Ph.D., Professor, Pharmaceutical Sciences,
School of Pharmacy, University of Pittsburgh

Robert Ferrell, Ph.D., Professor, Human Genetics,
Graduate School of Public Health, University of Pittsburgh

David Finegold, Ph.D., Professor, Pediatrics,
School of Medicine, University of Pittsburgh

Jerry Vockley, MD, PhD

PROTEOMICS STUDIES OF ENVIRONMENTAL EFFECTS AND SYSTEMIC GENE INTERACTIONS IN DISORDERS OF FATTY ACID BETA-OXIDATION

Wei Wang, PhD

University of Pittsburgh, 2011

Fatty acid β-oxidation disorders (FAODs), the most frequent group of inborn errors of metabolism, are clinically heterogeneous and clear genotype-phenotype correlations have not been described. Very long chain acyl-CoA dehydrogenase (VLCAD) deficiency and short chain acyl-CoA dehydrogenase (SCAD) deficiency result from mutations on the *ACADVL* and *ACADS* genes, respectively. Multiple mutations have been described in both disorders. Acute symptoms are often induced by physiological stress such as fasting, but the pathophysiologic mechanism underlying disease symptoms and phenotypic heterogeneity remains unknown. The aim of this dissertation was to explore the biological changes induced by genetic mutations and the gene-gene interactions and environmental effects on these defects.

Proteomic changes in SCAD and VLCAD deficient mice, as well as the changes induced by fasting in VLCAD deficiency, were measured quantitatively using a combination of proteomics techniques. Broad mitochondrial dysfunction and derangements in multiple energy metabolism related proteins were altered in SCAD deficiency, indicating a complex mechanism for development of symptoms. Overall, a pattern associated with hepatotoxicity implicated in mitochondrial dysfunction and alteration of fatty acid metabolism was identified. Affected pathways converge on disorders with neurologic symptoms, suggesting that even asymptomatic individuals with

SCAD deficiency may be at risk to develop more severe symptoms. Several candidate biomarkers were suggested through Ingenuity Pathway Analysis. Numerous proteomic changes were characterized in VLCAD deficient mice in both fed and fasting states, and relevant biological pathway were identified. Fasting in both deficient and wild type animals induced alterations in several proteins. The pattern of alterations induced by fasting was different in VLCAD deficient mice from that in wild type animals. Mitochondrial chaperonins HSP60 and HSP10 altered differently in VLCAD deficient mice depending on the feeding state. Fasting altered an apparent compensatory increase in oxidative phosphorylation seen in the fed state. Thus, environmental factors and gene-environment interaction play important roles in the pathogenesis of VLCAD deficiency. The diversity of protein changes in variable pathways due to deficiencies in SCAD and VLCAD may help explain the phenotypic heterogeneity in patients.

These proteomic studies present new paradigm for exploring the mechanisms of disease, gene-environment interactions, and their contribution to gene-gene interactions in FAODs, one group of the mandatory target diseases in newborn screening program. The results advanced the knowledge about FAODs and had the public health significance by offering the benefits for the improvement in the diagnosis and treatment of theses disorders of great public health interest. Future characterization of functionally interactive genes and association studies in humans will provide further insight into disease mechanism. Further studies on candidate biomarkers are necessary to identify novel markers for prognosis prediction, adjunct diagnosis and therapy guidance in patients.

TABLE OF CONTENTS

LIST OF TABLES

LIST OF FIGURES

ACKNOWLEDGEMENTS

Special thanks goes to Dr. Jerry Vockley and Dr. Billy W. Day, for their guidance and support over the past several years. They have provided me tremendous help in my research project, for which I will always be grateful. Specifically, I would like to thank Dr. Vockley for giving me the great opportunity to work on these exciting projects and learn such a wide range of proteomic methods. I am thankful to Dr. Day for his valuable support and guidance. I appreciate their tolerance to me when I was having difficulties in the process of these projects. Without their constant support and guidance, the fulfillment of these projects would not have been possible.

I would like to acknowledge Dr. Michael Barmada for his suggestions on the biostatistics analysis and Dr. Robert Ferrell and Dr. David Finegold for all of their valuable feedback and care throughout my dissertation work and life in Pittsburgh, for which I will always remember. I also want to thank the proteomics core lab staff and Dr. Manimalha Balasubramani for their support. Additionally, I acknowledge all the members of the Vockley lab for their support over the years and my collaborators in Dr. Niels Gregersen's lab. I also thank Dr. Steven Ringquist and Ying Lu for their assistance in the initiation of the proteomic experiments.

Finally, I would like to thank the Research Advisory Committee of the Children's Hospital of Pittsburgh for funding support. Special thanks also to Drs. George Tseng, Eric Goetzman, Al-Walid Mohsen, Stephanie Mihalik, and Yudong Wang who were willing to provide me handful assistance. All of the support staff and faculties in the Department of Human Genetics and the Graduate School of Public Health have helped me in some way in completing

this dissertation. Special apologies and thanks to my son and mother for their sacrifice and support over the years. Last but not least, I am grateful to all my friends in Pittsburgh and other cities for their invisible support and influence in the process of this dissertation.

ABBREVIATIONS

ACADs - acyl-CoA dehydrogenases
ACADD- acyl-CoA dehydrogenases deficiency
ACAD9-acyl-CoA dehydrogenase 9
ACN-acetonitrile
BCA - bicinchoninic acid
BSA- bovine serum albumin
CHAPS- 3-[(3-Cholamidopropyl)dimethylammonio]-1-propanesulfonate
CID - collision-induced disassociation
2D-two dimension
2DGE-two dimensional gel electrophoresis
DIGE -difference gel electrophoresis (DIGE)
DTT- dithiothreitol
EMA- ethylmalonic acid
ETC-electron transport chain
ETF-electron transferring flavoprotein
ESI--electrospray ionization
FAO- fatty acid β-oxidation
FAOD-Fatty acid β-oxidation disorders
GO - gene ontology
H_2O_2 - hydrogen peroxide
HSP - heat shock protein
IEF-isoelectric focusing
IEM- Inborn Errors of Metabolism (IEM)
IPA-Ingenuity Pathway Analysis
IPG- Immobiline DryStrip
iTRAQ - isobaric tags for relative and absolute quantitation
KCL-potassium chloride
LCAD-long chain acyl-CoA dehydrogenase
LC-MS/MS-liquid chromatography
-mass spectrometry/mass spectrometry
MALDI-TOF/TOF- matrix assisted laser desorption ionization
-time of flight/time of flight
MCAD-medium-chain acyl- CoA dehydrogenase
MCT-medium chain triglyceride
MMTS-methyl methanethiosulfonate
MOPS - 3-(N-morpholino)propanesulfonic acid

MS - mass spectrometry
nano-LC-ESI- nanoscale-liquid chromatography electrospray ionization
nano-LC- nanoscale-liquid chromatography
NBS-newborn screening
OXPHOS-oxidative phosphorylation
PMSF - phenylmethanesulfonyl fluoride
PPARα-peroxisome proliferator-activated receptor- α
PQD-Pulsed Q dissociation
SCAD-short chain acyl-CoA dehydrogenase
SCADD- short chain acyl-CoA dehydrogenase deficiency
SCX - strong cation exchange
St Dev -standard deviation
TCA- tricarboxylic acid
TEAB- triethylammonium bicarbonate buffer
TCEP - tris(2-carboxyethyl)phosphine
TFA-trifluoroacetic acid
VLCAD-very long chain acyl-CoA dehydrogenase
VLCADD- very long chain acyl-CoA dehydrogenase deficiency

1.0 INTRODUCTION

1.1 INBORN ERRORS OF METABOLISM

Inborn Errors of Metabolism (IEM) are a group of genetic disorders caused by impairment of a specific biochemical reaction in a metabolic pathway. They have traditionally been viewed as Mendelian traits resulting from mutations in single gene and have served as important models for understanding the mechanism of pathogenesis of monogenic disorders (Lanpher et al, 2006). But while most IEMs are inherited as monogenic traits, they are typically caused by heterogeneous mutations and exhibit extremely variable clinical spectra with poor correlation of genotype with phenotype. The diagnosis of IEM often relies on the detection of abnormal metabolites that accumulate as a result of the deficient enzyme. While a diagnostic evaluation for IEMs is traditionally triggered by clinical symptoms in an individual, newborn screening that aims to detect disease before the development of symptoms has become increasingly important in recent years, and has expanded to include nearly 50 disorders. Pre-symptomatic identification of disease adds a further need to understand the etiology, pathogenesis and natural history of these disorders. Environmental factors such as diet, stress, and intercurrent illnesses also often impose important effects on clinical symptoms and outcomes. However, the exact mechanism and role that such environmental effectors play in most disorders are unknown. Discerning the relative impact of genes and environment on

Mendelian disorders presents many of the same challenges faced in the study of complex genetic diseases, and serve as good models to examine the relative role of genetic factors, environmental factors, and their interactions in determining phenotypes. Thus, exploration of gene interactions and environmental effectors would not only help in understanding the pathogeneses of these disorders and the diversities of phenotypes in this group of clinically recognizable deficiencies, but also would help in elucidating the pathogenesis and genotype-phenotype correlations in other more complex genetic diseases.

1.2 FATTY ACID B-OXIDATION AND ITS DISORDERS

FAO is a complex process involving transport of activated acyl-CoA moieties into mitochondria, followed by sequential removal of 2 carbon units in the form of acetyl-CoA (Figure 1)(Courtesy J.Vockley). These products, in turn, are used as fuel by the tricarboxylic acid (TCA) cycle or for the production of ketone bodies. Energy derived from various steps of the cycle is efficiently utilized to generate ATP through oxidative phosphorylation. β-oxidation represents an important source of energy for the body during times of fasting and metabolic stress. At least 25 enzymes and specific transport proteins are involved in mitochondrial fatty acid metabolism(Eaton et al, 1996; Saudubray et al, 1999). Of these, defects in at least 22 proteins have been shown to cause disease in humans(Andersen et al, 2002). The most common of these are deficiencies of acyl-CoA dehydrogenases (ACADs). The ACADs are a group of evolutionarily related enzymes that consists of at least 9 family members, each with characteristic substrate specificity. The ACADs involved in energy metabolism are very long chain acyl-CoA dehydrogenase (VLCAD), long chain acyl-CoA dehydrogenase (LCAD), acyl-

CoA dehydrogenase 9 (ACAD9), medium-chain acyl- CoA dehydrogenase (MCAD), and short chain acyl-CoA dehydrogenase (SACD). All of them catalyze the α−β-dehydrogenation of acyl-CoA esters with a conserved enzyme mechanism(Aoyama et al, 1995; Binzak et al, 1998), transferring electrons to electron transferring flavoprotein (ETF). They have been purified to homogeneity and share 30-35% identical amino acid residues (Tanaka & Indo, 1992). VLCAD catalyzes the initial reaction in the fatty acid oxidation cycle in the mitochondrial matrix, and is the rate-limiting step in that compartment. It is most active against activated fatty acids with a chain length of 14 to 20 carbons. SCAD catalyzes short chain acyl-CoAs with a length of 4-6 carbons.

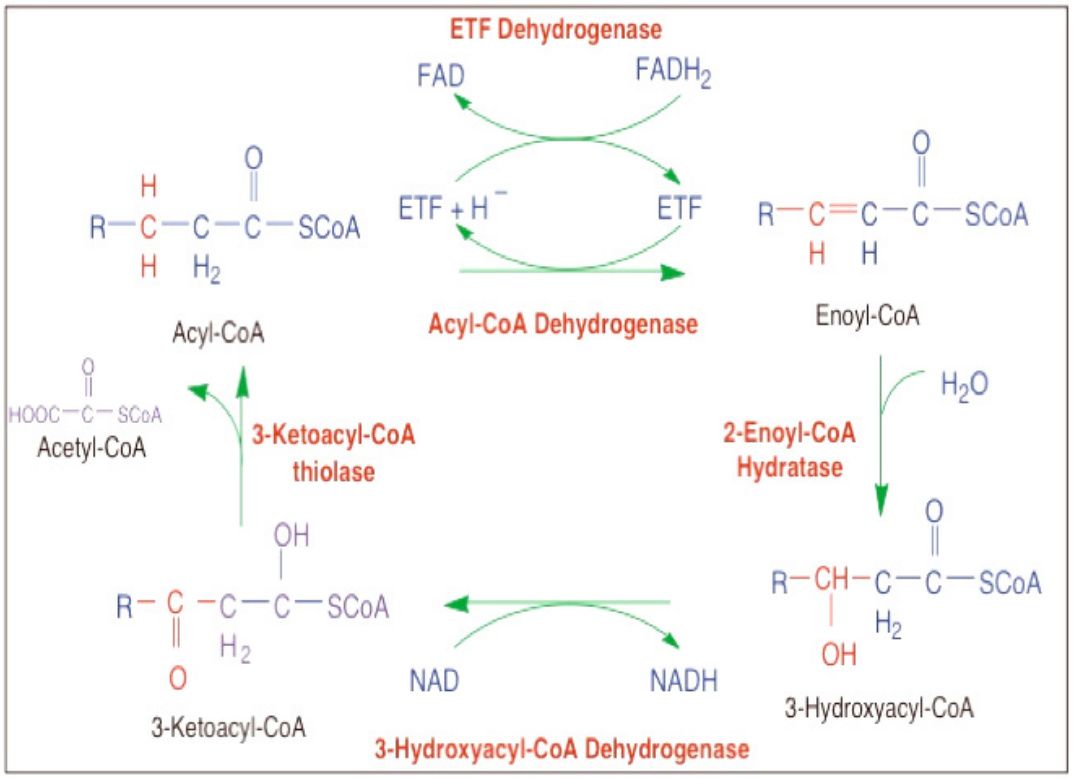

Figure 1. Mitochondrial ß-oxidation spiral

Disorders of mitochondrial fatty acid β-oxidation (FAOD), one of the most frequent groups of IEMs in humans, offer an excellent example of the multifactorial nature of clinical disease in IEMs. IEMs affecting this pathway are typically inherited in a recessive fashion. Affected individuals with FAODs may present at any age with recurrent rhabdomyolysis, hypoglycemia, hypotonia, and peripheral neuropathy, but they may also remain asymptomatic for a lifetime (Bennett et al, 2000; Vockley & Whiteman, 2002). Symptoms are most often induced by fasting or physiologic stress. As an additional complexity, patients with multiple partial defects in FAO have been described (Vockley et al, 2000) and multiple genetic variations have been identified in asymptomatic individuals (Pedersen et al, 2008; Tein et al, 2008; van Maldegem et al, 2006). The identification of FAO disorders has been tremendously improved through the introduction of acylcarnitine analysis by tandem mass spectrometry. Mutation analysis of specific genes may confirm the diagnosis, but explanation of differences in the phenotype of patients with the same enzyme deficiency remains a challenge. Importantly, different mutations have variable effects on protein function. Missense mutations that result in misfolded but stable proteins may have different effects on the integrity and function of the putative FAO metabolome than null mutations with absence of protein (Gregersen & Olsen, 2010). Systematic clinical and laboratory studies are needed to elucidate the pathophysiology of the different FAO disorders.

VLCAD and SCAD deficiencies are caused by mutations in the *ACADVL* and *ACADS* genes, respectively, that impair gene expression or enzyme stability or function. Some genotype-phenotype correlations have been described in VLCAD deficiency (Andresen et al, 1999). Mutations causing severe disease including hypoglycemia and cardiomyopathy with a high

mortality rate have been reported, however, genotype alone remains limited in its ability to predict phenotype (Coughlin & Ficicioglu, 2010; Wilcken, 2010). SCAD deficiency provides an even greater example of complexities in FAODs with extreme heterogeneous clinical presentations and a large number of genetic variations in *ACADS*. Whereas this condition was regarded a potentially life-threatening disorder prior to expanded newborn screening (NBS), patients identified by NBS for the most part remain asymptomatic despite confirmation of severe enzyme deficiency (Lindner et al, 2010). No clear genotype-phenotype relationships have ever been seen in either group of patients (Waisbren et al, 2008; Wilcken et al, 2003). Affected individuals with VLCAD deficiency may also present with acute symptoms in the newborn period, with milder symptoms in early childhood and rhabdomyolysis in adults. The observed acute symptoms are often induced by physiological stress or by conditions such as fasting or endurance exercise. However, the pathophysiologic and molecular mechanism underlying stress-induced illness in patients with VLCAD deficiency is not yet well understood.

As a group, FAO disorders are among the most prevalent autosomal recessive conditions in humans (Spiekerkoetter et al, 2009a). However, the individual gene defects only offer a partial view of the spectrum of disease related to this family of genes. Patients with some of these disorders can remain asymptomatic for life, and many require exposure to environmental stressors to express disease. Thus, a more complicated mechanism may exist in the pathogenesis of this group of diseases. Gene expression and functional cellular studies detailing secondary dysfunction at multiple levels would offer such a potential in help understand the complexities in the disease mechanism. In addition, multiple partial defects in energy pathways have been described in patients presenting with symptoms of energy dysfunction (Vockley et al, 2000). The presence of concurrent partial defects in more than one gene in individual or related metabolic

pathways has been termed “synergistic heterogeneity”, a genetic phenomenon that shares much in common with multifactorial and polygenic disease. A systemic examination of the interaction of genes and environment would be of great value in understanding the pathogenesis of FAODs and explaining the variations in phenotype. However, such studies are difficult or impossible in humans.

1.3 MOUSE MODELS

Mouse models for many of the fatty acid oxidation disorders have been described and have been helpful in studying the pathophysiology of these diseases (Schuler & Wood, 2002; Spiekerkoetter & Wood, 2010). The VLCAD gene for mouse was mapped to mouse chromosome 11 and has been found to be similar to that of the human VLCAD locus (*ACADVL*) (Cox et al, 1998b). Two mouse models of VLCAD deficiency have been produced independently using different strategies and presented with biochemical and pathological features resembling those of human VLCAD deficiency (Cox et al. 2001; Exil et al. 1998, 2003). The Cox model of VLCAD deficiency was generated by targeting the *ACADVL* gene using a replacement approach that resulted in a null allele with deletion of exons 7 to 19 (Cox et al. 2001). Clinical findings in these animals included mild hepatic steatosis, mild fatty change in the heart in response to fasting, and cold intolerance (Cox et al. 2001; Exil et al. 1998, 2003). The gene for mouse SCAD (*Acads*) originally known as butyryl-CoA dehydrogenase (*Bcd*-1) was mapped to chromosome 5 and later renamed as *ACADS*. A mouse with SCAD deficiency was serendipitously discovered in a mutant strain of BALB/cByJ mice (Armstrong et al. 1993; Wood et al. 1989). The complete enzyme deficiency in these mice resulted from a 278-base pair deletion involving exons 9 and 10

of *Acads* gene(Hinsdale et al, 1993). Mice with SCAD deficiency manifested the biochemical and pathological features of human SCAD deficiency after fasting but remained asymptomatic. Mouse studies with animal heterozygous for mutations at multiple loci of fatty acid oxidation related genes have confirmed the physiologic relevance of the accumulation of mutations at multiple loci in related pathways(Schuler et al, 2005).

Stress-induced changes have been investigated in several FAO deficient mouse models. Fasting and cold exposure resulted in severe hypoglycemia and hypothermia with lethality in one third of VLCAD deficient mice (Spiekerkoetter et al, 2004). Long chain acylcarnitines in the blood of these animals were elevated and free carnitine was decreased as compared to unstressed wild type animals after fasting. However, a lesser increase in C14-C18 acylcarnitines and a decrease of free carnitine were also observed in fasted heterozygous compared to wild-type mice. Fatal cold intolerance and fasting induced microvesicular fatty changes in hepatocytes have been described in SCAD deficient mice (Armstrong et al, 1993). Differential induction of several genes regulated by peroxisome proliferator-activated receptor-α (PPARα) in liver and brown adipose tissue during fasting and cold exposure in LCAD and VLCAD null mice has also been reported (Goetzman et al, 2005). The similarities between these mouse models and human disease make them an ideal platform to rigorously study the effects of the primary gene mutations, and the interaction of environmental stressors with these mutations, on cellular functions.

1.4 PROTEOMICS TECHNOLOGY

The global survey of functionally related genes offers the potential to gain insight into the complex molecular events related to the introduction of a mutant gene into a cell. Gene expression profiling using cDNA and oligonucleotide arrays to examine mRNA, as well as other genotyping approaches, have proven to be powerful tools to address gene interactions in complex diseases. However, they suffer from several inherent limitations. mRNA abundance does not typically correlate well with protein abundance. Moreover, protein structure, function, and interactions can be altered and regulated by subcellular localization or post-translational modifications such as phosphorylation, glycosylation, ubiqination, or acylation that are not predicted by mRNA abundance. In contrast, a screening approach with mass spectrometry based on differential detection of proteins in isolated organelles from samples of interest offers the potential to measure all such changes directly.

Proteomics takes a broad, comprehensive and systematic approach to understand biology, which is generally unbiased and not dependent upon existing knowledge. For the last three decades, proteomics techniques have emerged to deal with complicated issues that cannot be approached by genomic analysis. Global analysis of protein abundance based on differential detection of proteins in isolated organellar compartments using high-throughput mass spectrometry offers great potential to study the complex disease. Integrated analyses of gene expression and proteomic profiling of mouse mitochondria have identified a network of at least 90 co-regulated genes involved in oxidative phosphorylation, β-oxidation, and the TCA cycle and highly expressed in brown fat, skeletal muscle and heart. It has been estimated that there are approximately 1500 mitochondrial proteins or so different polypeptides in the mitochondria (Kislinger et al, 2006; Mootha et al, 2003). One combined proteomic and transcriptomic

profiling study using tandem mass spectrometry (MS/MS) created an inventory of 667 mitochondrial proteins in heart and 776 proteins in liver (Kislinger et al, 2006).

Comparative proteomics aims to quantitatively compare proteins levels from two or more samples. The most commonly used method for comparative proteomic studies is two-dimensional gel electrophoresis (2DGE). This technology has been used to investigate differential protein abundance in large-scale proteomic experiments prior to mass spectrometric identification(Gygi et al, 2000; Tanaka & Indo, 1992). Difference gel electrophoresis (DIGE) allows comparison of multiple two-dimensional (2D)-gels and allows different samples to be analyzed concurrently on the same gel (Unlu et al, 1997). Compared with conventional 2DGE, in which protein samples are separated on individual gels, stained and quantified, followed by image comparison with computer aided image analysis programs, DIGE shortens the procedure, eliminates to a great extent gel-gel variations, and has a large dynamic range allowing both the differential analysis of abundant proteins, as well as proteins present at low concentration (Ong et al, 2003). Development in quantitative proteomics has led to the application of fluorescent cyanine dyes (Cy2, Cy3 and Cy5) to label proteins before they are separated on a single 2D gel. In DIGE, the proteins in each sample are covalently tagged with different color fluorescent cyanine dyes that are designed to have no effect on the relative migration of proteins during electrophoresis(Tonge et al, 2001; Viswanathan et al, 2006)

With the rapid expansion of protein sequence databases, mass spectrometry based identification of proteins is becoming more realistic and more reliable. The development of liquid chromatography-mass spectrometry (LC-MS) based profiling techniques has emerged as a robust tool in this area. Isobaric tags for relative and absolute quantification (iTRAQ) have been recently applied in proteomic studies (Ross et al, 2004; Wiese et al, 2007). It employs

incorporation of 4 to 8 different mass labels into peptides in different samples that can then be compared in one experiment. During peptide sequencing by tandem mass spectrometry, differentially labeled peptides are selected in the mass spectrometer as a single mass precursor ion since a balance group equalizes the size difference of the tags. The quantification values are determined by the mass labels, which give rise to distinct low mass peptide fragment ions. Labeling multiple peptides per protein increases confidence in identification and quantitation. This technique also offers a greater tolerance to any steric hindrance effect associated with labeling and provides access to peptides whose labeling sites may otherwise not be accessible to CyDyes used in DIGE analysis (Wiese et al, 2007; Wu et al, 2006).

No global analysis of proteomic changes has been performed on either animals or humans with VLCAD deficiency or SCAD deficiency. The objective of my projects employing multiple proteomic approaches was to examine global changes in mouse models of these disorders in order to identify secondary changes related to the primary gene defects and to characterize the effects of those changes on the physiologic response to environmental stress.

1.5 HYPOTHESES AND SPECIFIC AIMS

The hypotheses addressed in this dissertation were as follows. 1) The qualitative pattern and/or relative abundance of mitochondrial proteins changes in mice deficient in *ACADVL* and *ACADS* will help explain the heterogeneous symptoms in these two deficiencies. 2) Specific cellular functions and pathways as determined by the pattern of proteins altered in the mouse models will provide insight into the pathogenesis of these disorders. 3) Measuring proteomic

changes from the deficient mouse models would identify novel markers for diagnosis and to follow treatment in humans with these diseases. My project had three specific aims.

Specific Aim 1 was to examine changes in mitochondrial protein expression in SCAD deficient mice, characterize the cellular functions and canonical pathways associated with altered proteins, and explore candidate biomarkers for diagnosis and treatment.

Specific aim 2 was to examine changes in mitochondrial protein expression in VLCAD deficient mice under fed and fasting conditions, analyze the cellular functions and canonical pathways associated with altered proteins under each condition, and explore candidate biomarkers and related pathological damage.

Specific aim 3 was to identify mitochondrial proteins overlapping and differentiating VLCAD and SCAD deficiency in mice, and elucidate the roles of annotated cellular functions and associated pathways in the pathogenesis of two FAO disorders.

2.0 PROTEOMIC STUDY ON SHORT CHAIN ACYLCOA DEHYDROGENASE DEFICIENT MOUSE

2.1 ABSTRACT

Short-chain acyl-CoA dehydrogenase deficiency (SCADD) is an autosomal recessive inborn error of metabolism that leads to the impaired mitochondrial fatty acid ß-oxidation of short chain fatty acids. It is clinically heterogeneous and multiple mutations have been identified in patients .No clear genotype-phenotype relationships have been seen. Nor is there a good correlation between the genotypes and the current biochemical marker for the diagnosis. The mechanism and definition of this deficiency remain unclear. The aim of this study was to better understand the mechanism of molecular changes at a global level, gain insight into the pathophysiology of this deficiency and to identify biomarkers that predict the development of symptoms. The quantitative changes of mitochondrial proteome in SCAD deficient mice compared to wild type mice were examined using two-dimensional gel difference electrophoresis (2DIGE) followed by protein identification with MALDI-TOF/TOF and iTRAQ labeling followed by nano-LC/MALDI-TOF/TOF. A broad spectrum of mitochondrial dysfunction and multiple energy metabolism related proteins were identified indicating that a more complex mechanism for development of symptoms may exist. Affected pathways converge on disorders with neurologic symptoms, suggesting that even asymptomatic individuals with SCAD

deficiency may be at risk to develop more severe disease. The results from this study largely identified a pattern associated with hepatotoxicity implicated in mitochondrial dysfunction, fatty acid metabolism, decrease of depolarization of mitochondria and mitochondrial membrane and swelling of mitochondria demonstrating that SCAD deficiency relates more directly to mitochondrial dysfunction and alteration of fatty acid metabolism. I proposed several candidate biomarkers that can serve as potential markers for adjunct diagnosis and monitoring of therapy.

2.2 INTRODUCTION

Short-chain acyl-CoA dehydrogenase deficiency (SCADD) is an autosomal recessive inborn error of metabolism that leads to the impaired mitochondrial fatty acid ß-oxidation of fatty acids with a chain length of 4 to 6 carbon units. Short chain acyl-CoA dehydrogenase (SCAD) is a member of the acyl-CoA dehydrogenase (ACAD) family that catalyzes the initial reaction of the fatty acid oxidation spiral with sequential cleavage of two carbon units, and serves as an important energy source for the body during times of fasting and metabolic stress. Electrons from reduced SCAD are passed to electron transfer flavoprotein and then directed into the electron transport chain via electron transfer flavoprotein-ubiquinone oxidoreductase (ETF-QO), an inner mitochondrial membrane protein (Ghisla et al, 1984); (Thorpe & Kim, 1995).

SCAD is a homotetrameric enzyme that is encoded in the nuclear genome and functions in mitochondria. It shares structural and functional similarity with other ACADs (Ikeda et al, 1987; Matsubara et al, 1989a) but differs from them in substrate specificity. The human *ACADS* gene is located at chromosomal position 12q22-qter and spans approximately 13 kb, consisting

of 10 exons (Corydon et al, 1997). The mouse *ACADS* gene maps to chromosome 5 at the Bed-1 locus (Prochazka and Leiter 1986), and is a compact, single-copy gene approximately 5kb in size containing 10 exons (Kelly & Wood, 1996). An SCAD deficient Balb/cByJ mouse has been described and is due to a 278-bp deletion in the 3' end of the *ACADS* gene leading to reduced steady-state levels of SCAD mRNA (Hinsdale et al. 1993).

Deficiency of SCAD results in the accumulation of butyryl-CoA, which in turn leads to accumulation of butyrylcarnitine, butyrylglycine, ethylmalonic acid (EMA), and methylsuccinic acid in blood, urine, and cells (Amendt et al, 1987; Coates et al, 1988; Corydon et al, 1996). It was originally identified in symptomatic children and adults with heterogeneous symptoms including metabolic acidosis, ketotic hypoglycemia, epilepsy, myopathy, hypotonia, developmental delay and behavioral changes (Amendt et al, 1987; Corydon et al, 2001; Kurian et al, 2004; van Maldegem et al, 2006). However, other patients were reported have minimal or no symptoms (Ribes et al, 1998). With the widespread implementation of expanded newborn screening programs through tandem mass spectrometry measurement of acylcarntines in blood spots, many SCAD deficient infants have been identified. However, most or all of these infants have remained asymptomatic (van Maldegem et al, 2010). This has led to the recognition of many individuals carrying *ACADS* mutations but lack of related symptoms.

Approximate 70 genetic variations have been identified in the *ACADS* gene in symptomatic and asymptomatic individuals (Pedersen et al, 2008; Tein et al, 2008; van Maldegem et al, 2006). No clear genotype-phenotype relationships have been seen in either clinical patients or those identified through newborn screening (Waisbren et al, 2008; Wilcken et al, 2003). Nor is there a good correlation between the genotypes and the biochemical characteristics of EMA and butyrylglycine excretion (Bhala et al, 1995; van Maldegem et al,

2006). In addition, two common coding polymorphisms in the *ACADS* gene have been identified that lead to variant proteins and increased EMA excretion in some individuals, but seem not to be disease causing. Finally, decreased SCAD activity in skin fibroblasts or muscle is not a good predictor of clinical symptom (Ribes et al, 1998). Thus the clinical relevance of the biochemical defect and the need to treat affected individuals remain unclear. In the SCAD deficient mouse, most of the biochemical findings parallel those seen in the human disease, including organic aciduria with excretion of ethylmalonic, methylsuccinic acids and N-butyrylglycine, and development of a fatty liver upon fasting or dietary fat challenge (Wood et al. 1989; Schiffer et al. 1989). In contrast to the complicated genetic situation in humans with heterogeneous SCADD, the mouse provides an excellent model to study pathogenesis of this disease *in vivo*.

The clinical heterogeneity seen in SCADD raises fundamental questions about the pathophysiologic changes induced by deficiency of this enzyme, as they appear to differ from the other fatty acid oxidation disorders. However, the reason for these differences, and the heterogeneity seen within the disorder, remain unknown. It is clear that the biomarkers currently characterized in SCADD patients, including increased urinary EMA and butyrylglycine, increased plasma butyrylcarnitine, and decreased SCAD activity, are not sufficient to predict clinical symptoms and disease severity. Thus, additional biomarkers to categorize the effects of SCADD would be of great value. Recent experiments have called attention to the possible role of abnormal protein folding and interactions in cell lines from patients with SCADD and proposed the hypothesis that misfolded SCAD protein may play a role in the mitochondrial toxicity (Schmidt et al, 2010).

In the last three decades, proteomics has found broad application in many areas of biology, biochemistry and biomedicine. Several proteomic approaches have been developed for

quantitatively assessing proteomes to study the systemic differences between the healthy and diseased state. Two quantitative proteomic approaches, two-dimensional gel difference electrophoresis (2DIGE) and isobaric tags for relative and absolute quantification (iTRAQ) are available to measure the molecular changes induced by mutations in disease models. DIGE allows comparison of multiple 2D-gels and different samples to be analyzed concurrently on the same gel eliminating a great extent gel-gel variations (Unlu et al, 1997), and has advantages in allowing both the differential analysis of abundant proteins and proteins at relative low concentration as compared to 2DGE. iTRAQ analysis has recently come into more general use in quantitative proteomics (Ross et al, 2004; Wiese et al, 2007). It utilizes the incorporation of 4 to 8 different mass labels into peptides in different samples of interest for comparison in one experiment. The quantification values are determined by the distinct mass labels with low mass peptide fragment ions. This technique offers an increased confidence in identification and quantitation by labeling multiple peptides per protein and provides access to peptides whose labeling sites may otherwise not be accessible to CyDyes used in DIGE analysis (Wiese et al, 2007; Wu et al, 2006). In this study, quantitative changes in the mitochondrial proteome of SCAD deficient mice compared to wild type were examined to better understand the biological changes induced by SCAD deficiency and identify the potential biomarkers predictive of clinical outcome. The use of two quantitative proteomic approaches has allowed us to generate complementary information on the quantification and identification of changes in the mitochondrial proteome and explore the novel potential protein markers of disease pathogenesis and severity. Characterization of such changes will offer new insight into the mechanisms of disease and provide novel markers for diagnosis.

2.3 MATERIALS AND METHODS

2.3.1 Mice

SCAD deficient mutant mouse (BALB/cByJ) and wild type mice (BALB/cBy) were originally purchased from the Jackson Laboratory (Bar Harbor, Maine) at age of 4-5 weeks, and further propagated in the animal facilities at the Children's Hospital of Pittsburgh of UPMC. All mice were maintained pathogen-free, complying with standard housing procedures. 3 or 5 male offspring mice for each genotype were obtained before tissue harvest. All animals were sacrificed at age 6-8 weeks following standard protocols approved by the Animal Care and Use Committee of the University of Pittsburgh. Tissues were removed immediately after rapid euthanasia with CO2.

2.3.2 Isolation of mitochondria

Freshly removed liver was finely minced in ice cold isolation buffer A containing 225 mM mannitol, 75 mM sucrose, 10 mM HEPES free acid, 10 mM EDTA, pH7.4, then gently homogenized with a glass Dounce homogenizer in isolation buffer B containing 225 mM mannitol, 75 mM sucrose, 10 mM HEPES free acid, 0.1% BSA fatty acid free, 10 mM EDTA, pH 7.4, with the addition of 10 µl/ml HaltTM protease inhibitor cocktail (Pierce, Rockfold, IL). The homogenate was centrifuged at 1,300 x g for 10 minutes at 4 °C, and the supernatant was recovered and centrifuged at 10,000 x g for 10 minutes. The pellet was carefully preserved and resuspended in 12% Percoll solution, then layered on top of a 30-70% Percoll gradient and

centrifuged at 62,000 x g for 35 minutes at 4 °C. The mitochondrial band located between the 30% and 70% layers was removed and washed with cold isolation buffer A, then collected by centrifugation at 10,000 x g for 10 minutes 4 °C. A small aliquot of the sample was taken for organelle marker analysis and purity testing by western blotting. Twenty micrograms of the remaining sample were run on a 10% SDS acrylamide gel and transferred to PVDF membrane for western blotting. The membrane was probed with anti-cytochrome C (a mitochondrial marker) and anti-calreticulin (an ER marker) antibodies (Santa Cruz Biologicals). Two approaches to examine the mitochondrial proteome in the final samples were employed. The overall workflow is shown in Figure 2.

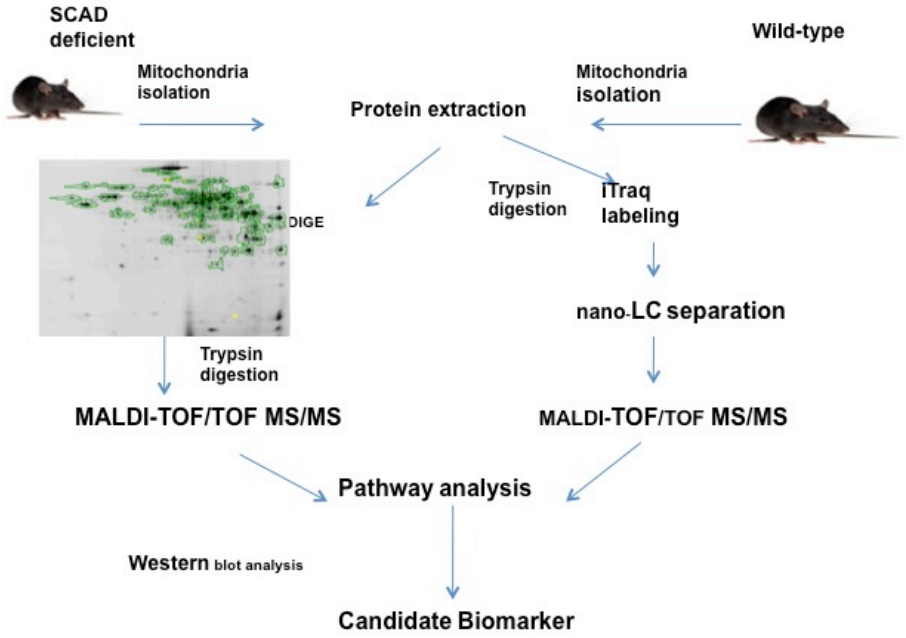

Figure 2. Overall workflow of experiment

2.3.3 Difference gel electrophoresis

Mitochondrial protein was extracted using M-PER Mammalian Protein Extraction Reagent (Pierce, Rockfold, IL). Ten microliters per milliliter of sample of HaltTM protease inhibitor cocktail (Pierce, Rockfold, IL) and 1µl/ml phosphatase inhibitor cocktail 2 (Sigma, Saint Louis, MO) were added to the extraction buffer. The mixture was shaken gently for 10 minutes at 4 °C, and cellular debris was removed by centrifugation at 14,000 x g for 15-30 minutes at 4 °C. Protein samples were then treated with the 2D Clean-up Kit (GE Healthcare, Piscataway, NJ) according the manufacturer's instructions. Briefly, approximately 100 µg of protein were precipitated, and resuspended in 7 M urea, 2 M thiourea, 4% 3-[(3-cholamidopropyl) dimethylammonio]-1-propanesulfonate (CHAPS) and 2% Amidosulfobetaine-14 (ASB-14). Protein concentration was measured with the 2-D Quant Kit (GE Healthcare, Piscataway, NJ) according the manufacturer's instructions.

Cy-dye labeling. A stock solution of PrCy3-N-hydroxysuccinimide ester and MeCy5-N-hydroxysuccinimide ester (Cy3 and Cy5, respectively), were prepared as described (Unlu et al, 1997) and stored in anhydrous N,N-dimethylformamide (DMF) at -80 °C. Cyanine dye 2 (Cy2) was purchased from GE Healthcare. Equal amounts of protein samples from SCAD deficient and wild type mice were individually labeled in a reciprocal manner with equal volumes of Cy3 or Cy5 to produce balanced covalent labeling of 1–5% of the available lysine side chains without significantly altering the protein isoelectric points. An equal amount of pooled samples from both genotypic mice was labeled with Cy2 as an internal standard for the normalization of each gel. The labeling reaction was incubated on ice in the dark for 30 min and

then terminated by addition of 1 μl of quench (40% aqueous methylamine, pH 8.0) (Beckner et al, 2005) and further incubation on ice in the dark for 10 minutes.

Difference gel electrophoresis (DIGE). Equal volumes of samples In buffer containing 7 M urea, 2 M thiourea, 2% amidosulfobetaine-14, 10 mg/ml DTT and 1% Pharmalytes 3–11 (GE Healthcare, Piscataway, NJ) were added to each of the labeled protein samples and paired protein samples from deficient and wild type mice were mixed together for subsequent isoelectric focusing on long wide pH range Immobiline DryStrips, 24 cm, pH 3-11 nonlinear (3-11 NL). After active rehydration for 10 hours at 30 v, IEF was performed with an Ettan IPGphor Π system (GE Healthcare, Piscataway, NJ) at 300 v for 30 minutes, 500 v for 30 minutes, 1000v for 1 hour and up to 80000 vh, and then maintained at 30 v as needed. After equilibration with 50 mM Tris-HCl pH 8.8, 6M urea, 30% glycerol, 2% SDS plus 100 mg DTT added per gel for 10-15 minutes, and additional alkylation by 250 mg iodoacetamide per gel, the strips were placed on freshly made 12.5% SDS-polyacrylamide gels. The resolved proteins were separated with a vertical Ettan DALTsix electrophoresis system (Amersham Bioscicences) in a running buffer of 1X TGS (Tris-Glycine-SDS, Bio-Rad, Hercules, CA).

Gels were visualized and evaluated with the Typhoon 9400 Variable Imager (GE Healthcare, Piscataway, NJ). Appropriate emission filters and lasers were selected to give optimum results with minimal cross talk. The Cy3 images were scanned using a 532 nm laser and a 580 nm band pass BP30 emission filter; Cy5 images were scanned using a 633 nm laser and a 670 nm-BP30 emission filter; and Cy2 images were scanned using a 488 nm laser and an emission filter of 520 nm BP40. All gels were scanned at 100 microns pixel size for the best resolution. The photomultiplier tube voltage was chosen to achieve the best image quality. The photomultiplier tube was set to ensure a maximum pixel intensity between 40–60 000 pixels. A

focal plane of +3mm b/c of glass plates was chosen. ImageQuant v5.2 (GE Healthcare, Piscataway, NJ) was used to crop the images to exclude the nonessential information prior to image analysis.

Gel analysis was performed using DeCyder DIA v5.2 (GE Healthcare, Piscataway, NJ). Quantitative comparison of proteins between samples was performed using the differential in-gel analysis module for each gel, comparing the normalized volume ratio of each spot from a Cy3- or Cy5-labeled sample to the corresponding Cy2 signal from the pooled sample internal standard. The estimated number of spots for each co-detection procedure was set to 2000. Dust or other artifacts were detected and removed by applying an exclusion filter with peak slope values of greater than one or as clusters of sharp spikes. Visual inspection confirmed the differences indicated by the DeCyder software prior to removal. The biological variation analysis module, which allows integral matching and calculation of average abundance for each protein spot, was used to match the multiple images from three different gels and provide statistical data on differential protein expression levels between deficient and wild type groups collectively. Student's t-test was selected to compare differences in protein levels. Though a threshold of 1.25 was set to call differences, only proteins with ≥1.3 fold changes and visible spots were picked and subjected to mass spectrometric analysis. Coomassie blue stain was used to detect abundant proteins.

Identification of differentially expressed proteins from DIGE analysis. Protein spots that differed on DIGE between deficient and wild type animals were manually retrieved, digested with trypsin, and submitted for mass spectrometry analysis. The peptides derived from each protein spot were analyzed with matrix assisted laser desorption ionization time of flight mass spectrometry (MALDI-TOF-MS) in a 4700 Proteomics Analyzer with TOF/TOF (Applied

Biosystems, Foster City, CA). Each peptide sample was spotted four times onto a MALDI plate. The reflector positive ion mode acquisition and processing methods were chosen to collect peptide spectra in the mass range of 800-4000 Da with minimum s/n filter set to 10 and mass exclusion tolerance set to 50 ppm. The highest ten intensity peptides were selected for analysis using MS/MS acquisition mode of the 1kV positive ion, and the processing method with a mass exclusion tolerance of 100 ppm and minimum s/n filter of 10 in the mass range 60 Da to 20 Da.

Data were processed with a GPS Explorer Workstation (Applied Biosystems, Foster City, CA,). The MASCOT algorithm (Matrix Science, Boston, MA) was used to search the Mass Spectrometry Protein Sequence DataBase (MSDB). MASCOT parameters were set to include only Mus species with the following parameters: tolerance of one missed trypsin cleavage per protein, allowance of cysteine modification by acrylamide, oxidation of methionine, carbamidomethyl oxidation peptide charge of +1, and peptide tolerance of 100 ppm with MS/MS fragment tolerance of 0.2Da. Protein identifications were accepted when scores over 65 indicated nonrandom identification at a significance level of P=0.05 and the protein IDs were consistent in at least 3 of 4 quadruplicates spots on MALDI plates from two individual gels.

2.3.4 iTRAQ experiments

Mitochondrial pellets isolated as above were suspended in sample buffer containing 0.5 M triethylammonium bicarbonate buffer (TEAB, pH 8.5), 0.1% SDS at 4°C. The samples were sonicated 3 times for 10 seconds at 4°C, and debris was removed by centrifugation at 14,000 x g for 15 minutes at 4°C. The protein concentration was measured using the BCA protein assay

reagent according to the manufacturer's protocol (Pierce, Rockford, IL). Absorbance was measured at 590 nm on a microplate reader (Bio-Rad, Hercules, CA)

iTRAQ labeling. Equal amounts of 100 µg of protein from both genotypes were precipitated with acetone and resuspended in 0.5 M TEAB and 0.5% Rapigest (Waters, Milford, MA). Protein samples were denaturated, reduced, alkylated, and digested with trypsin according to the manufacturer's protocol (Applied Biosystems, Foster City, CA). Four iTRAQ reagents (Applied Biosystems, Foster City, CA) with mass labels of 114, 115, 116 and 117 Da were used to separately label samples from deficient or wild type mice. Each sample was labeled twice for each experiment, and a total of 3 experiments were performed with the tagged samples in a reciprocal manner (Table 1). Equal amounts of pooled samples from 2 of the same genotype samples were used as an individual sample in the second and third experiments in order to reduce the sample variations. Three hundred microliters of 0.5% formic acid in H2O were added to the tubes, and the samples were stored at 4 °C overnight to quench the unreacted iTRAQ reagent and hydrolyze the Rapigest. The samples were dried by vacuum and reconstituted in 20 µl of 10 mM potassium phosphate pH 3.0, 25% acetonitrile (ACN). The reporter ions were checked in a 4700 MALDI-MS/MS (Applied Biosystems, Foster City, CA) to ensure sample labeling. All of the iTRAQ labeled peptide samples were then pooled for fractionation.

Table 1. Experimental design for iTRAQ proteome profiling

Experiment No.	Labeled Samples	Labeled Samples	Labeled Samples	Labeled Samples
1	114-SCAD+/+ 1	115-SCAD-/- 1	116- SCAD +/+ 1	117- SCAD-/- 1
2	114 -SCAD -/- 2&3*	115-SCAD+/+ 2&3	116- SCAD -/- 2&3	117- SCAD+/+ 2&3
3	114-SCAD+/+4&5**	115-SCAD-/- 4&5**	116- SCAD +/+ 4&5**	117- SCAD-/- 4&5**

*2&3: pooled sample from animals 2 and 3 **4&5: pooled sample from animals 4 and 5

Strong cation exchange fractionation. PolySULFOETHYL A macro-Spin columns (12 µm, 300 Å, 50-450 µL (The Nest Group, Inc, Southborough, MA) were employed to fractionate peptide samples. The columns were pretreated with methanol and with water, and then equilibrated with 10 mM potassium phosphate, pH 3.0, 25% ACN. The samples were then diluted in 10 mM potassium phosphate, pH 3.0, 25% ACN, and loaded onto the column. Six fractions were collected by stepwise elution with 20 mM potassium chloride (KCL), 40 mM KCL, 80 mM KCL, 100 mM KCL, 200 mM KCL and 400 mM KCL in 10 mM potassium phosphate, pH 3.0, 25% ACN. The eluted fractions were lyopylized, resuspended in 0.5% trifluoroacetic acid, 5%ACN, and desalted using a PepClean C-18 column (Pierce, Rockford, IL) according to the manufacturer's instructions.

Nano-LC separation. Peptide samples were further separated using an RP LC-Packing Ultimate system (Dionex, Sunnyvale, CA) with a trap column (300 µm i.d. x 5 mm, PepMap 100 C18 material 5 µm, 100 Å) (Dionex). The system was washed with a 5-85% ACN gradient

containing 1% trifluoroacetic acid (TFA) for 9 minutes then 85% ACN, 0.1% TFA for 30 minutes at a flow of 300 nl/min before loading onto an analytical column (75 μm i.d. x 100 mm, ProtePep II C18 material 3 μm, 100 Å; New Objective, Woburn, MA). The peptide samples were fractionated using a multi step protocol as follows: Buffer A was 5% ACN, 0.1% TFA, and buffer B was 85% ACN, 5% isopropyl alcohol and 0.1% TFA. A gradient of 0-56% B in 115 minutes, 56%-100% B in 5 minutes, 100% B for 5 minutes was run all at a flow rate of 300 nl/min. Before and after the runs, BSA peptides were loaded as control. The BSA peptide samples were fractionated using a multiple gradient of 0-56% B in 30 minutes, 56%-100% B in 5 minutes, 100% B for 5 minutes all at a flow rate of 300 nl/min. The fractionated peptides were collected using the Probot™Micro Fraction Collector system. 30 second flow spots were spotted on an ABI 4800 LC-MALDI metal target plate (ABI, Foster City, CA) in a 16 x 48 array. A total of 576 spots were collected for each strong cation exchange (SCX) fraction of samples and 192 spots were collected for each fraction of control BSA peptides. BSA fractions were spotted on the plate before and after the sample fractions. During the LC run, 10 mg/ml α-cyano-4-hydroxy cynnamic acid (CHCA) with 10 mM ammonium citrate dibasic and 10 fM angiotensin II in 85% ACN, 0.1% TFA were mixed with the flow and co-spotted on the plate using a μTee mixer at a flow rate of 1.5 μl/min.

Mass Spectrometry of iTRAQ labeled peptides. A 4800 Analyzer equipped with TOF/TOF ion optics (Applied Biosystems) was used to analyze the MALDI target plates and MS-MS/MS data were acquired using the 4000 Series Explorer software, version 3.5.1. The instrument was calibrated before each run. The operating mode of MS was set to MS reflector positive. MS spectra were acquired from 900 to 4000 Da with a focus mass of 2000 Da to determine the mass of the precursor peaks of interest. MS was performed using angiotensin II

spiked into the matrix as an internal standard with a 5-ppm maximum outlier error. The top 10 peptide peaks with a S/N filter of 20 were selected for MS/MS analysis. Peptide CID (air) was performed at 2 kV in positive mode with an accumulation of 2000 shots for each spectrum. The MS/MS default calibration was updated before each target was run by using a peptide in the calibration mix spots.

Protein quantification and identification of iTRAQ labeled samples. MS/MS data were collected and processed using ProteinPilotTM Software 2.0 (Applied Biosystems). All 6 fractions of each experiment were combined into one dataset for the analysis. The LC-based Paragon algorithm was used to search against the mouse International Protein Index (IPI) database v 3.68. The species Mus musculus was specified. The ID search was focused on biological modifications. Search parameters also included iTRAQ labeling of the N-terminus and lysine residues, cysteine modification by methylmethanethiosulfonate (MMTS), and digestion by trypsin. Isoform specific identification and quantification was done by excluding all shared peptides and including only unique peptides. The bias and background correction was processed to optimize quantification data. Proteins with ProtScore ≥ 1.3 (unused) at a significance level of 0.05 (95% confidence) were selected for further analysis.

Proteins were identified on the basis of having at least 2 peptides with an ion score above 99% confidence. Only peptides identified with ≥95% confidence were confirmed and included in the quantitative analysis. Only peptides for which peaks corresponding to the iTRAQ labels were detected were included. The protein sequence coverage (95%) for a specific protein was estimated as the percentage of matching amino acids from the identified peptides having confidence greater than or equal to 95% divided by the total number of amino acids in the sequence. Estimates of fold change ratios of differential expression between labeled protein

samples and the error factors provided by ProteinPilot were utilized. Proteins with at least 2 peptides (sequence coverage 95%) and error factor lower than 1 were then exported into Excel for further data analysis.

Data analysis. All quantification values in one experiment used for the calculation of proteins ratios were summed and averaged to obtain the averaged reference baseline value in one data set. The quantification value of each protein was then normalized to this reference value by setting it to 1. Student's t-test was used to test the difference at $p \leq 0.05$ between the quantification values of mutant and wild type for each protein. The averaged fold change of a protein expression in mutant compared to that in wild type was recalculated. The cut-off fold change of significant proteins was set to 1.3 or 0.7. Proteins with significant changes ($p \leq 0.05$) and over 1.3 fold change or less than 0.7 fold change in at least 2 experiments were classified as significantly changed proteins.

2.3.5 Pathway and network analysis

The complete set of differentially expressed proteins from two proteomic analysis approaches with their gene symbol names as identifiers and corresponding expression values were examined with Ingenuity Pathways Analysis software (Ingenuity Systems, Redwood City, CA; www.ingenuity.com). Each identifier was mapped to its corresponding object (gene/protein) in the Ingenuity Knowledge database. These focus genes were overlaid onto a global molecular network developed from knowledge-based information previously reported in the literature. The canonical pathway analysis utilizes well characterized metabolic and cell signaling pathways that were available prior to data input. The filters and general settings for the core analysis were set to

consider all molecules including endogenous chemicals, as well as both direct and indirect relationships. The taxae of human and mouse were selected. All data sources, including cell lines and liver tissue, were considered, and a stringent filter for molecules and relationships was chosen. Networks of the focus genes were then algorithmically generated based on their connectivity and ordered by score. The software computes a score for each possible network according to the fit of that network to the input proteins/genes. This score is calculated as the negative base-10 logarithm of the p-value that indicates the probability that the network-eligible molecules are found together as a result of random chance. Scores 2 or higher have at least a 99% confidence of not being generated randomly. Networks were also associated to the biological functions (and/or diseases) that were most related to the genes in the network. Genes or gene products are represented as nodes, and the biological relationship between two nodes is represented as an edge. All edges are supported by at least one reference from the literature or from canonical information in the software. The intensity of the node color indicates increased (red) or decreased (green) abundance. Nodes are displayed using various shapes that represent the functional class of the gene product. I utilized the toxicity analysis function incorporated in IPA software to assess the secondary physiologic impact of the primary *ACADS* gene deficiency.

2.3.6 Western blotting

To validate significant findings, western blot analysis was performed on several selected proteins that were likely to be of biological interest. Equal amounts of 50 µg or 100 µg of mitochondrial protein from wild type mice and mutant mice were separated on 10% Bis-Tris SDS polyacrylamide gels (Bio-Rad, Hercules, CA) in MOPS buffer (Bio-Rad, Hercules, CA). The separated proteins were transferred to 0.2 um nitrocellulose membrane (Bio-Rad, Hercules,

CA) using a TE Series Transphore Electrophoresis Unit (Hoefer Scientific Instruments, San Francisco, CA). The membrane was immunoblotted with the desired antibodies. Primary antibodies used were SCAD and LCAD (Vockley Lab), Complex III subunit core 2 (Mitoscience, Eugene, OR), SCP2 and HSP60 (Santa Cruz Biotech, Santac Cruz, CA). SDH (Complex II) antibody (Santa Cruz Biotech, Santa Cruz, CA) was used as loading control. The secondary antibodies conjugated to horseradish peroxidase included rabbit anti-goat IgG and anti-mouse IgG (Santa Cruz Biotech), selected based on the primary antibody. Bound secondary antibody was detected with Western Blotting Luminol Reagent (Santa Cruz Biotech) and scanned using Fujifilm LAS-3000 (Fujifilm Medical Systems, Stanford, CT).

2.4 RESULTS

To characterize mitochondrial proteome changes related to SCAD deficiency, DIGE analysis of purified mitochondria followed by protein identification with MALDI-TOF/TOF was first utilized. iTRAQ labeling followed by peptide separation and identification with LC-MALDI-TOF/TOF was then performed. An overview of the experimental approach is shown in Figure 2. A total of 49 proteins with differential expression in SCAD deficient mice were identified. A variety of energy metabolism related proteins were identified to be altered.

2.4.1 Differentially expressed proteins in SCAD deficient mice identified through DIGE analysis

An identical internal standard comprised of pooled aliquots from all samples from each experiment was incorporated to enable the comparison of protein abundance between samples on different 2D gels. This standard allowed accurate comparison of protein spots across all gels. Protein samples were also labeled in a reciprocal manner to eliminate the variation in labeling with the cyanine dyes. Three individual images corresponding to Cy2-, Cy3-, and Cy5-labeled samples from each gel were analyzed using DeCyder software. Biological Variation Analysis was used for integral matching and calculation of the average abundance of each protein spot across all gels. After applying an exclusion filter and manually excluding the control spots by inspection, a total of 161 spots were matched among all gels through biological variation analysis of the 1354 detected spots. A standardized average spot volume ratio exceeding 1.25 in three analyzed gels (Student's t-test, $p \leq 0.05$) was considered to be a significant change. Analysis identified a significant increase in 12 (7.5%) spots and a decrease in 16 spots (9.9%) in mitochondria from SCAD deficient mice. These spots are depicted on a DIGE gel image shown in Figure 3. Proteins spots with at least 1.3 fold change were excised manually and subjected to in-gel digestion, and their mass spectra were analyzed by MALDI-TOF-TOF.

A Mascot database search of the MS spectra resulted in the identification of 10 proteins obtained from quadruplicate MALDI spots in 2 individual gels (Table 2). A consistent identification from at least 3 MALDI spots with a score ≥100 was considered reliable ID for the specified protein. Protein spots with the same protein IDs were reported with an averaged ratio. Proteins identified and their average ratios are listed in Table 2 with information on experimental or theoretical molecular weight and PI values, accession number, Mascot scores, and involved

pathway or functions. A representative 2D DIGE image showing the significantly changed proteins in SCAD deficient mice was shown in Figure 3. Sterol carrier protein 2 and sterol carrier protein X were identified in 2 different positions. They represent the same protein with synonymous names in the UniPro database (non-specific lipid-transfer protein). Catalase/mutant catalase was assigned to 3 spots (5, 6, and 14). Beta-alanine oxoglutarate amino-transferase and its synonymous 4-aminobutyrate aminotransferase were identified as spot 9. The database search revealed that all of the identified proteins were predicted to be located in mitochondria. Catalase, typically viewed as a peroxisomal protein, has been shown to be more abundant in rat liver mitochondria than in peroxisomes (Jiang et al, 2005);(Murayama et al, 2001).

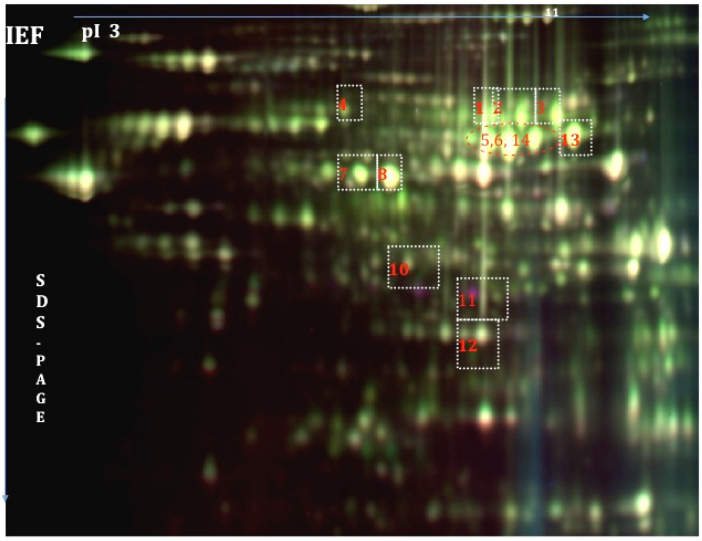

Figure 3. Representative 2D DIGE image showing the significantly changed proteins in SCAD deficient mice.

Mitochondrial proteins were separated in the first dimension by IEF with pH range from 3-11 then 12.5% SDS-polyacrylamide in the second dimension. Proteins from deficient and wild type mice were labeled with Cy3 or Cy5 in a reciprocal manner. In each gel, an internal standard from pooled samples was labeled with Cy2 to allow matching of spots in different gels and to normalize the amount of loaded protein. Protein spots that were differentially expressed (over 1.3 fold change, $p \leq 0.05$) and successfully identified with MALDI-TOF/TOF are marked with numbers.

Table 2. Differentially expressed mitochondrial proteins identified by DIGE in SCAD deficient mice

Protein name	Accession No.	Protein MW	Protein PI	Spot	Mascot score	SCAD-/- : SCAD+/+		Function
						Average ratio	p-value	
Sterol carrier protein2/ Sterol carrier protein X	AAH18384 JU0157	59087.8	7.16	2	217	+1.92	0.018	Lipid transport
H+-transporting two-sector ATPase, alpha-chain	JC1473	59715.6	9.22	13	427	+1.72	0.031	OXPHOS
Aldehyde dehydrogenase 4 family, member A1	Q8BXM3	61713.6	8.7	3	260	+1.62	0.012	Amino acid metabolism
Catalase	A36695	59727.6	7.72	5,6,7	277	+1.59	0.038	Fatty acid oxidation
Epoxide hydrolase	A47504	62489.6	5.85	4	248	+1.50	0.017	Amino acid metabolism
Sterol carrier Protein X/ Sterol carrier protein 2	JU0157	59119.7	7.15	1	112	+1.46	0.008	Lipid transport
Aldehyde dehdrogenase2 precursor, mitochondrial	I48966	56501.8	7.53	8	443	+1.32	0.026	Amino acid metabolism
Ornithine carbamoyltransferase precursor	OWMS	39739.6	8.81	12	435	-1.30	0.0005	Urea cycle
4-aminobutyrate aminotransferase	AAH58079	56415.6	8.35	9	191	-1.47	0.041	GABA shunt
Beta-alanine oxoglutarate aminotransferase	Q8BZA3	50204.8	8.79	9	265	-1.47	0.041	GABA shunt
Acetyl-Coenzyme A dehydrogenase, short chain	Q91w85	44861.1	8.68	11	188	-3.53	0.0005	Fatty acid beta-oxidation

Table 3. Differentially expressed mitochondrial proteins identified by iTRAQ experiment.

Unused score	%Cov (95)	Accession	Gene symbol	Protein Name	Peptide (95%)	Averaged Ratio **SCAD-/-: SCAD+/+**	No. Exp.	Function
15.86	15.61	IPI00111218.1	Aldh2	Aldehyde dehydrogenase, mitochondrial	8	3.11	3	Amino acid metabolism
10.61	12.33	IPI00134809.2	Dlst	Isoform 1 of Dihydrolipoyllysine-residue succinyltransferase component of 2-oxoglutarate dehydrogenase complex	6	2.42	2	Amino acid metabolism
4.02	6.38	IPI00129178.1	Oat	Ornithine aminotransferase, mitochondrial	2	2.1	3	Amino acid metabolism
2	2.12	IPI00124372.3	Aldh9a1	Aldehyde dehydrogenase 9A1	1	1.88	2	Amino acid metabolism
7.4	7.30	IPI00890092.1	Aldh7a1	Alpha-aminoadipic semialdehyde dehydrogenase	4	1.67	2	Amino acid metabolism
4.01	5.32	IPI00759940.2	Fh1	Fumarate hydratase 1 precursor	2	1.49	3	Amino acid metabolism
3.75	5.85	IPI00379694.4	Hmgcl	3-hydroxy-3-methylglutaryl CoA lyase precursor	2	2.22	2	Ketogenesis& AA
32.72	52.64	IPI00653158.1	Acaa2	Acetyl-Coenzyme A acyltransferase 2, isoform CRA K	23	2.6	3	Fatty acid oxidation
8.52	9.49	IPI00894588.1	Acadl	Long-chain acyl-CoA dehydrogenase precursor	5	2	2	Fatty acid oxidation
6.28	14.11	IPI00116753.4	Etfa	Electron transfer flavoprotein subunit alpha	5	1.98	2	OXPHOS
12.97	6.11	IPI00943457.1	Pcx	Pyruvate carboxylase isoform 1	6	1.56	3	TCA cycle
18.71	29.59	IPI00323592.2	Mdh2	Malate dehydrogenase, mitochondrial	9	1.36	3	TCA cycle
3.16	14.99	IPI00331692.1	Dci	Dodecenoyl-Coenzyme A delta isomerase precursor	4	1.5	2	Lipid /fatty acid metabolism
14.63	14.83	IPI00308885.6	Hspd1	Isoform 1 of 60 kDa heat shock protein	7	1.65	3	Mito protein folding/import
4.05	1.50	IPI00755120.2	Rrbp1	Ribosome binding protein 1 isoform a	2	1.74	2	Gene translation
4.3	4.20	IPI00454008.1	Shmt2	Serine hydroxymethyltransferase	2	1.71	2	One-carbon unit metabolism
2	8.50	IPI00885646.1	Coq9	Coq9 Protein	2	2.29	2	biosythesis of CoQ
2	11.76	IPI00556699.1	Gcsh	Isoform CRA_b	1	2.54	2	Unknown
6	24.54	IPI00133034.3	Hint2	Histidine triad nucleotide-binding protein 2, mitochondrial	3	2.27	2	Undefined
3	14.00	IPI00133215.3	Ndufb7	NADH dehydrogenase [ubiquinone] 1 beta subcomplex subunit 7	2	0.47	3	OXPHOS/ETC-Complex I
6.15	8.83	IPI00119138.1	Uqcrc2	Cytochrome b-c1 complex subunit 2, mitochondrial	3	0.47	2	OXPHOS/ETC-Complex III
3.92	7.66	IPI00133240.1	Uqcrfs1	Cytochrome b-c1 complex subunit Rieske,	2	0.61	2	OXPHOS/ETC

Table 3 Continued

				mitochondrial				Complex III
2.39	4.46	IPI00120232.1	Ndufs7	NADH dehydrogenase [ubiquinone] iron-sulfur protein 7, mitochondrial	1	0.59	2	OXPHO/ETC-Complex I
12.74	52.00	IPI00130322.5	Ndufa7	NADH dehydrogenase [ubiquinone] 1 alpha subcomplex subunit 7	6	0.57	2	OXPHOS/ETC-Complex I
3.52	15.32	IPI00555000.2	Uqcrb	Cytochrome b-c1 complex subunit 7	2	0.3	2	OXPHOS/ETC-Complex III
3.48	17.44	IPI00225390.5	Cox6b1	Cytochrome c oxidase subunit 6B1	3	0.45	2	OXPHOS/ETC-Complex IV
2	7.00	IPI00881401.1	Cpt2	Carnitine O-palmitoyltransferase precursor	2	0.37	2	Lipid metabolism, FAO
9.33	10.22	IPI00114209.1	Glud1	Glutamate dehydrogenase 1, mitochondrial	6	0.49	2	Ubiquitous--Carbon and Nitrogen metabolism
5.6	3.62	IPI00776047.1	Aifm1	Apoptosis-inducing factor, mitochondrion associated 1	3	0.65	3	apoptosis
3.53	7.60	IPI00322760.7	Prodh	Proline dehydrogenase	2	0.56	2	Amino Acid metabolism
2.52	4.10	IPI00319973.3	Pgrmc1	Membrane-associated progesterone receptor component 1	2	0.56	2	Receptor for Progeserone
92.81	29.20	IPI00111908.8	Cps1	Carbamoyl-phosphate synthase [ammonia], mitochondrial	59	0.49	3	Urea cycle
10.48	18.38	IPI00133440.1	Phb	Prohibitin	6	0.56	2	Transcription activator
8.67	4.88	IPI00330747.2	Nphp3; Acad11	Acyl-CoA dehydrogenase family member 11	4	0.55	3	Unknown
3.52	9.59	IPI00125325.1	Decr2	Peroxisomal 2,4-dienoyl-CoA reductase	2	0.63	2	
6.55	3.16	IPI00554845.2	Immt	Isoform 5 of Mitochondrial inner membrane protein	3	0.67	2	Undefined
8.27	25.62	IPI00623553.1		Hypothetical protein	4	0.66	3	Undefined
2.01	2.66	IPI00625588.1		Hypothetical protein	2	0.6	2	Undefined

Differentially expressed mitochondrial proteins identified by iTRAQ analysis. 38 unique proteins showed significant increase in SCAD deficient mice in at least two replicate experiments with ≥95% confidence, corresponding to a protein score cutoff 1.3. The table details the altered proteins with unused scores (uniqueness of peptides used, protein confidence), gene names; accession numbers; average ratios and p-values of expression between knock-out and wild type mice, percent coverage of matching amino acids from identified peptides (95%) (%Cov95), number of experiments that showed significant changes, and biological functions described for these proteins. Averaged ratio values were calculated from 2 or 3 experiments if significant alterations ($p \leq 0.05$) were seen in the same direction. Additionally, proteins in a single experiment were considered to show a significant up-regulation or down-regulation if their expression ratios were 1.3 or 0.7, respectively.

2.4.2 Differentially expressed proteins in SCAD deficient mice identified by iTRAQ experiments

Mitochondrial membrane proteins are typically amphipathic with large hydrophobic domains, often leading to inconsistent iTRAQ labeling. To counter this problem, we added SDS to 0.1% before labeling followed by use of Rapigest after labeling to increase the solubility of mitochondrial membrane proteins. Two different reagents were also used to label the same peptide sample to better control for variation in labeling efficiency. Moreover, to minimize the effect of biological variance among individual mice, mitochondria from two individual mice were pooled together to give one mixed protein sample. Peptide samples were first fractionated via strong cation exchange chromatography and then separated by nano-LC. BSA was spiked into each step of the procedure to control for experimental processing.

A total of 741 proteins with unused score ≥1.3 (95% CI) were identified by iTRAQ in three different experiments, giving an average of 247 proteins with high confidence of unambiguity. Only peptides with over 95% confidence were included in the quantification calculation for that protein using the algorithm in the ProteinPilot software. Proteins identified by at least 2 peptides were used for further analysis. Among the proteins that were differentially expressed in SCAD deficient mice, 38 proteins were classified as being increased by 1.3-fold or decreased by 0.7-fold in at least 2 experiments. Key identifiers are provided in Table 2. Some proteins identified are not recognized as being mitochondrial in location, whereas others are reported to localize to multiple organelles (Table 2).

Examination of the biological functions associated with up-regulated proteins revealed that 5/19 (26%) of them are involved in amino acid metabolism, 2/19 (10%) are related to fatty

acid oxidation, and 2/19 (10%) proteins are in the TCA cycle. The down-regulated proteins included 7 proteins belonging to complexes of I, III and IV of the mitochondrial electron transport chain. Only 1 down-regulated protein was associated with fatty acid oxidation. About 18% (7/38) were not associated with clear or defined functions.

2.4.3 Overview of differentially expressed proteins in SCAD deficient mice

All Differentially expressed proteins identified by combined DIGE analysis and iTRAQ experiments were further grouped and characterized according to their basic biological function annotation in UniPro/Swiss-Prot. (Figure 4A, 4B). A 1.3-fold-change cutoff was applied to classify proteins as up- or down-regulated. 48 proteins displayed in Table 2 and Table 3 were grouped into different clusters based on their functional relations. Expression of 25 proteins was significantly increased and 21 proteins (not counting SCAD) showed a significantly decreased level. Among the up-regulated proteins, 4/25 (16%) were associated with fatty acid metabolism and 9/25 (36%) were associated with amino acid metabolism, whereas, among down-regulated proteins, only 1/21 (5%) proteins was associated with fatty acid metabolism and 1/21 (5%) proteins was associated with amino acid metabolism. Therefore, both fatty acid metabolism and amino acid metabolism were generally up-regulated in response to defect in fatty acid beta-oxidation. Several different aldehyde dehydrogenases had increased expression in both DIGE analysis and iTRAQ experiments (Table 2 and 3).

Most of identified down-regulated proteins (29%) were involved in oxidative phosphorylation including components of complexes I, III, and IV in the electron transport chain. While, complex V was observed to be up-regulated by DIGE analysis, this complex was identified as being down-regulated in iTRAQ experiments. However, it did not meet the

minimum cutoff of 0.7x. Two enzymes/proteins in the TCA cycle were up-regulated but none of enzymes in TCA cycle were down-regulated.

Several proteins were identified as being altered similarly in DIGE and one, but not all of the iTRAQ experiments. For example, ornithine transcarbamylase (OTC) was found to be reduced by DIGE analysis and one of the iTRAQ experiments but it didn't meet the defined criterion in the second study. Thus, the two approaches appear to be complementary rather than providing identical information. Data derived from iTRAQ labeling was more consistent following strong cation exchange fractionation and LC separation.

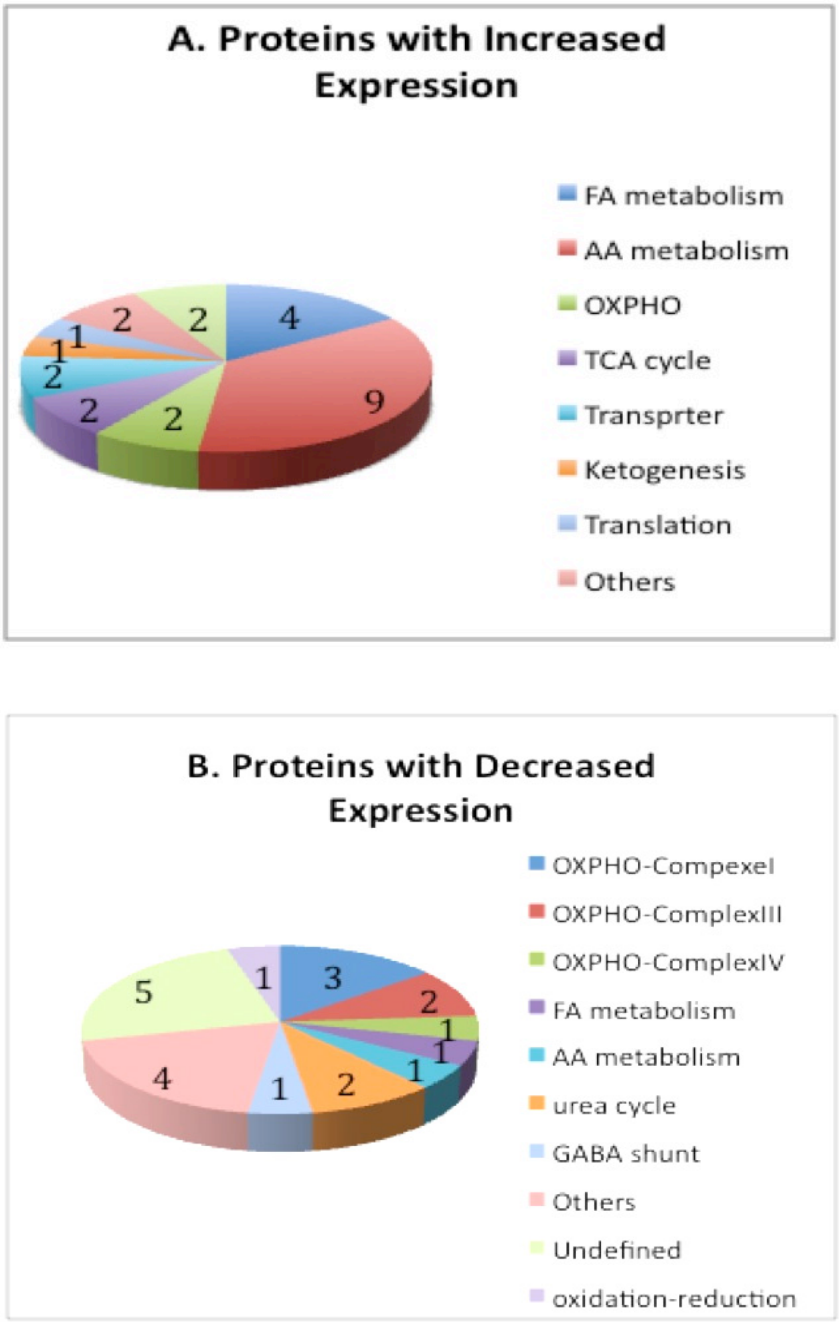

Figure 4. Functional distributions of differentially expressed proteins

(A) Proteins increased in level; (B) Proteins decreased in level. The numbers of proteins that are grouped related biological functions were marked. Biological functions are as follows: fatty acid oxidation metabolism (FAO), amino acid metabolism (AA), lipid trasferation or lipid metabolism (LM), protein folding or import (PFI), oxidative phosphorylation (OXPHOS), gene translation (GT), not any of the above (others) and undefined.

2.4.4 Western blot analysis

It is important to validate DIGE and mass spectrometry data by independent techniques when possible. To provide further support of the previous findings, three proteins of high biological interest were selected to validate by western blotting. Not surprisingly, SCAD was almost absent in western blot analysis and was 3-4 fold reduced on DIGE gels and one of iTRAQ experiments (Figure 5C). As was seen in the proteomic experiments, expression of complex III, cyctochrome b-c1 subunit 2 (uqcrc2) differed between deficient mice and wild type mice (Figure 5A), though the difference was less dramatic than was seen with iTRAQ (Table 3). Similarly, the expression of sterol carrier protein 2 was increased in SCAD deficient mice, though the change was less than appeared by DIGE analysis (Figure 5B). HSP60 (heat shock protein 60) appeared unchanged by western blot analysis (Figure 5E) but at least one isoform was identified as being significantly altered in the proteomic experiments. The level of the housekeeping protein succinate dehydrogenase (complex II) was constant in both western blot and proteomic analysis (Figure 5C).

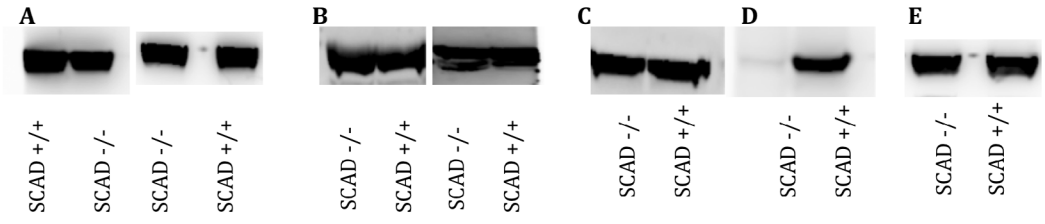

Figure 5. Western blot analysis

A, cytochrome b-c1 complex subunit 2 using anti-UQCR2 antibody; B, sterol carrier protein 2 using anti-SCP2 antibody; C, succinate dehydrogenase (complex II) using anti-SDH antibody; D, SCAD using anti-SCAD antibody, and E, heat shock protein 60 using anti-HSP60 antibody. Mitochondria proteins were isolated from SCAD deficient (-/-) and wild type (+/+) mouse livers. Samples were run on 10% polyacrylaminde, tris-bis gels.

2.4.5 Ingenuity pathway and Gene Ontology Analysis

IPA was next used to classify changed proteins into different functional groups (Appendix A for definitions in IPA) and identify cellular activities and related pathways that were altered due to SCAD deficiency. Of the identified 48 proteins with differential changes, 20 could be inputted for network analysis and 37 could be used for canonical pathway analysis. The remainder of the differentially expressed proteins could not be included in the analysis due to the lack of the information in current literature, or inadequate identification. The proteins that were classified into the top 5 molecular and cellular functional groups are shown in (Table 4).

Table 4. Top 5 significant molecular and cellular functions associated with altered proteins in SCAD deficient mice

Name	p-value	# Molecules
Molecular and Cellular Functions		
Free radical scavenging	2.2 E-5 —2.2E-5	4
Cell death	7.22 E-5 —3.27 E-2	8
Amino acid metabolism	3.22 E-4—2.73 E-3	2
Small molecule biochemistry	3.22 E-4—4.84 E-2	1
Carbohydrate metabolism	2.73 E-3—2.16 E-2	4
Physiological System Development and Function		
Cardiovascular system development and function	2.81 E-3 —2.43E-2	2
Organismal development	2.81 E-3 —2.43 E-2	2
Tissue morphology	2.81 E-3—2.40 E-2	2
Reproductive system development and function	5.46 E-3—8.17 E-3	2
Embryonic development	8.17 E-3—8.17 E-3	1

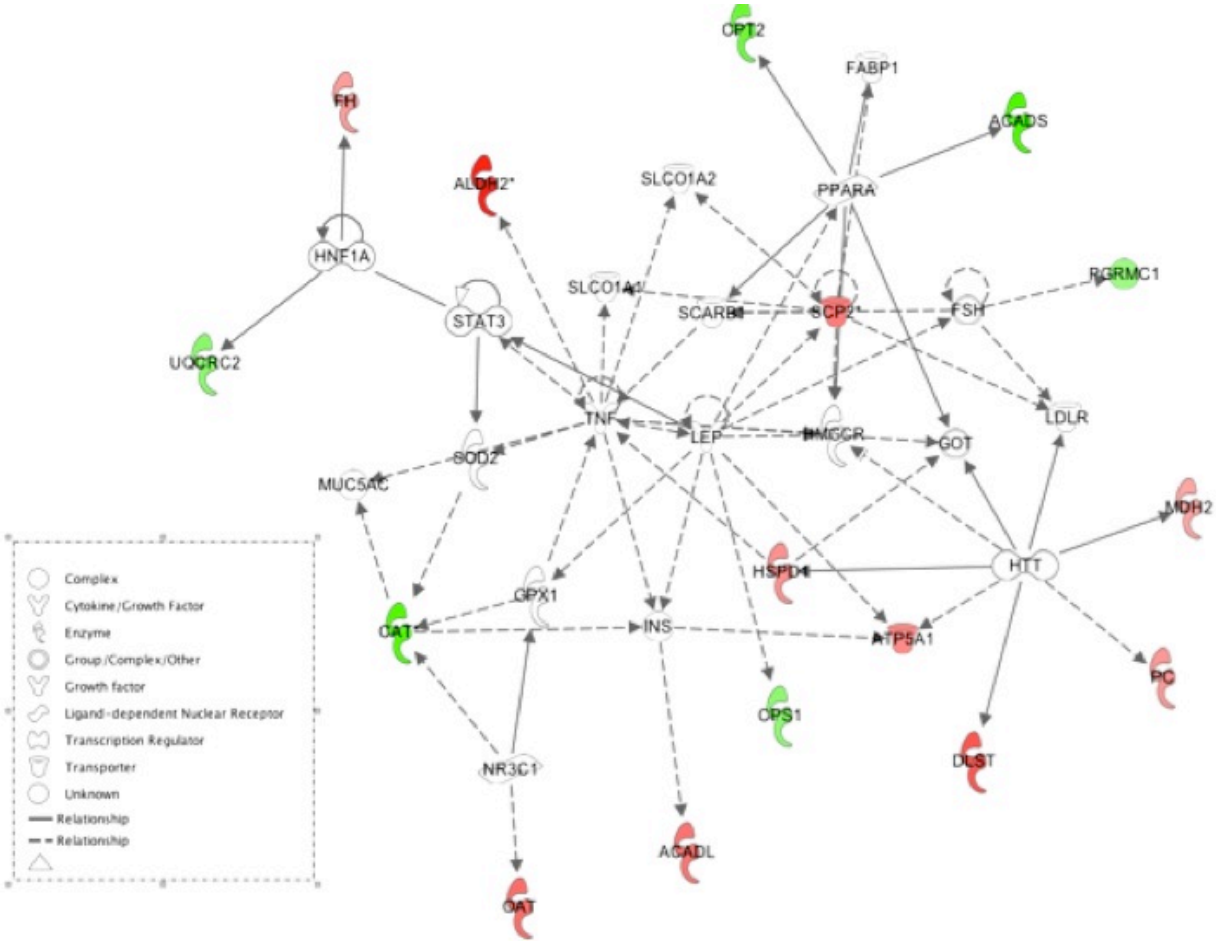

Figure 6. Top-rated network of lipid metabolism, molecular transport in SCADD mice

The network of "lipid metabolism, molecular transport" associated with altered proteins in SCAD deficient mice was generated and scored as the top-rated network by IPA. Red nodes indicate that the protein is up regulated in SCAD deficient mice. Proteins colored green indicate that the protein is down-regulated. The color intensity corresponds to the degree of abundance. Proteins in white are those identified through the Ingenuity Pathways Knowledge Base. The shapes denote the molecular class of the protein. A solid line indicates a direct molecular interaction, and a dashed line indicates an indirect molecular interaction. A full explanation of lines and relationships is provided in Appendix B.

Five protein networks (score >2) containing a total of 20 proteins were generated. Figure 6 shows the most significant network with a score of 32. This network, named "lipid metabolism, molecular transport and small molecules biochemistry", was composed of 16 proteins identified experimentally and 19 proteins known from the Ingenuity Pathways Analysis database to interact with them. 5 down-regulated and 8 down-regulated proteins in this group with the greatest changes were enzymes. Two transporters were shown to be up-regulated. This network is linked by several transcription regulators described in the literature including *HNF1A, STAT3* and *HTT*, as well as the transporters *SLCO1A1, SCARB1* and *LDLR*. The transmembrane transporter H+ transporting ATPase (Complex V) in the oxidative phosphorylation pathway, which also has the functions of "protein, nucleotide and ATP binding", also function in this group, suggesting an up-regulation of ATPase activity in mitochondrial function. SCP2, a non-specific lipid transfer protein with multiple functions of protein and lipid binding, and as a sterol carrier, was up regulated in SCAD deficient mice in the DIGE analysis. Similarly, *HPSD1* with the activity in the ubiquitination pathway and functions in unfolded protein and chaperone binding was also implicated as being up regulated.

Table 5. Top 5 Significant diseases and disorders associated with changed proteins

Diseases and Disorders	p-value	# Molecules
Neurologic Disease	3.05 E-6—4.28 E-2	6
Metabolic Disease	1.87 E-4 — 2.43 E-2	18
Endocrine System Disorders	2.73 E-3 — 2.43 E-2	2
Genetic Disorders	2.73 E-3 — 4.02 E-3	26
Hematologic Disease	2.73 E-3 — 2.73 E-3	1

A number of proteins could be further grouped according to the diseases with which they have been associated (Table 5***).*** The largest number of altered proteins (18/37) have previously been associated with metabolic diseases, including 8 down-regulated proteins (encoded by *ABAT, AIFM1, CPS1, CPT2, GLUD1, IMMT, OTC* and *PRODH*) and 9 up-regulated proteins. Six proteins encoded by *NDUFS7, GLUD1, MDH2, OTC, ABAT* and *HSPD1* have previously been associated with neurologic disease. Specifically, abnormalities in *NDUFS7* are seen Leigh syndrome in human, and *GlUD1, MDH2* and *OTC* are reported altered in Reye syndrome (Deshmukh et al, 1985; Holt et al, 1983; Mitchell et al, 1985) Reye syndrome is a fatal disease of unknown cause with symptoms that overlap many disorders of energy metabolism. It is characterized by acute encephalopathy and hepatic failure presenting with confusion, behavioral changes, seizures and loss of consciousness. Patients show multi-organs involvement, especially the brain and liver. Glutamate dehydrogenase, malate dehydrogenase, medium chain acyl-CoA

dehydrogenase, and ornithine carbamoyltransferase deficiencies (among many others) have been documented in patients with Reye-like symptoms (Deshmukh & Remington, 1984; Deshmukh et al, 1985; Holt et al, 1983; Lai et al, 1994; Mitchell et al, 1980).

Two enzymes known to be altered in other metabolic disorders were decreased in SCAD deficient mice: carbamylphosphate synthetase 1, an enzyme in the urea cycle that catalyzes the reaction of ATP and bicarbonate to produce carbonylphosphate and ADP, and 4-aminobutyrate transaminase, an enzyme that catalyzes the conversion of 4-aminobutanoic acid (GABA) and 2-oxoglutarate into succinic semialldehyde and glutarate in mitochondria. Additionally, 4-aminobutyrate aminotransferase (*ABAT)* abnormalities are reported in spinal muscular atrophy and other neurological diseases. This enzyme metabolizes gamma-aminobutyric acid (GABA), an important, mostly inhibitory neurotransmitter in the central nervous system) into succinic semialdehyde. Patients with *ABAT* deficiency show psychomotor retardation, hypotonia, hyperreflexia, lethargy, refractory seizures, and electroencephalogram (EEG) abnormalities(Gibson et al, 1985; Medina-Kauwe et al, 1999).

Table 6. Top-rated canonical pathways and functions associated with changed proteins

Pathway	p-value	Ratio
Valine, leucine, and isoleucine degradation	6.23 E-12	8/65 (0.123)
Mitochondrial dysfunction	1.7 E-11	9/117 (0.077)
Arginine and proline metabolism	2.04 E-11	8/75 (0.107)
Fatty Acid Metabolism	1.29 E-9	8/125 (0.063)
ß-alanine metabolism	3.49 E-9	6/49 (0.122)

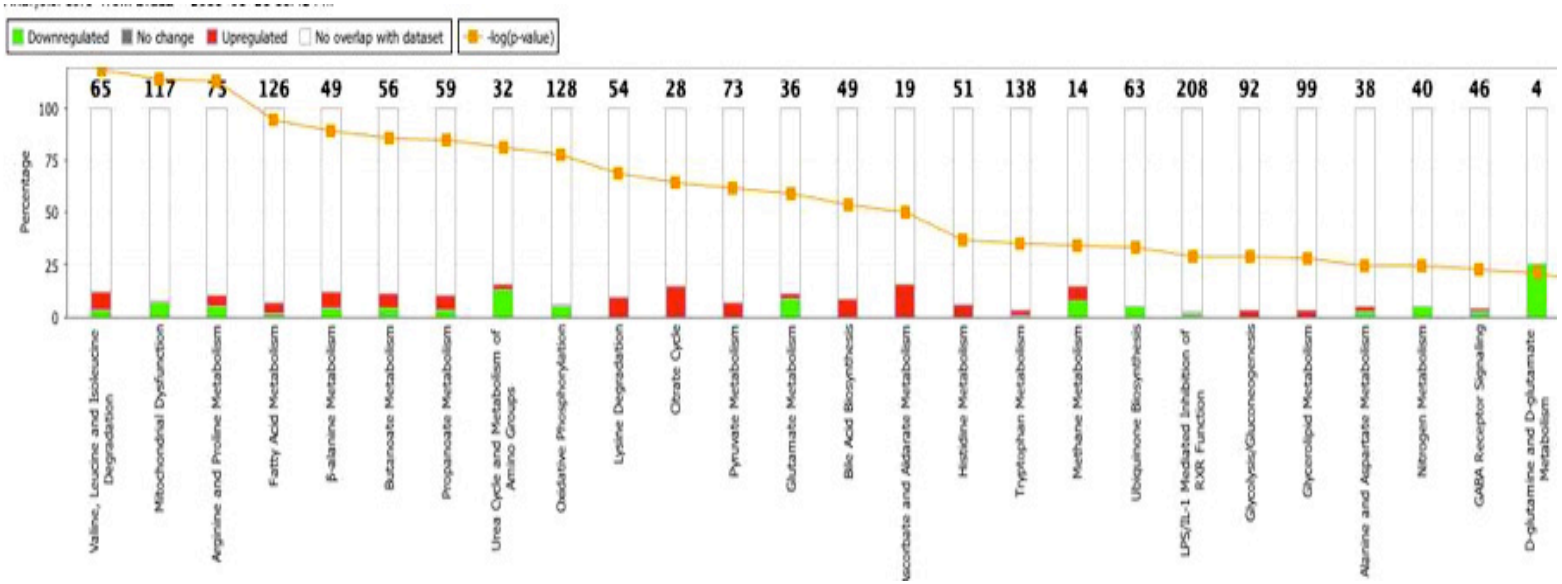

Figure 7. The most significantly affected pathways in SCAD deficient mice

The Canonical Pathways that are associated with changed proteins are displayed along the x-axis. The y-axis displays the percentage which is calculated as follows: number of genes in a given pathway that meet cutoff criteria, divided by total number of genes that make up that pathway. The orange dotted line displays the Significance of –log (p-value) ($P \leq 0.05$, Fisher's exact test). Red denotes the gene/protein that is up-regulated, green denotes the gene/protein that is down-regulated.

Ingenuity Pathways Analysis highlighted several canonical pathways as being affected in SCAD deficient mice. The most affected canonical pathway was that of “branched chain amino acid metabolism and mitochondrial dysfunction (Figure 7, Table 6)**.** A total of 8 changed proteins were mapped to branched chain amino acid metabolism“ with coverage of 12.3% molecules (8 of possible 65 molecules, $p \leq 0.05$) in this pathway. Besides SCAD, only one protein encoded by *ABAT* was reduced, while the other 6 proteins were increased (1.62-2.60 fold). Nine proteins were involved in “mitochondrial dysfunction“, comprising 7.7% of all molecules in this pathway ($p \leq 0.05$; Table 6). The other two top-related canonical pathways were involved in amino acid metabolism and fatty acid metabolism, the latter of which included all altered proteins in the OXPHOS pathway.

To further explore the connections of significant networks, the network was reconstructed by merging the three top-rated networks overlaid with the canonical pathways involved (Figure 8). This analysis suggests that reduced proteins were mostly involved in the urea cycle and oxidative phosphorylation. Three of the up-regulated proteins were involved in pyruvate metabolism. The highest proportion of changed proteins was in the mitochondrial dysfunction and branched chain amino acid metabolism pathways.

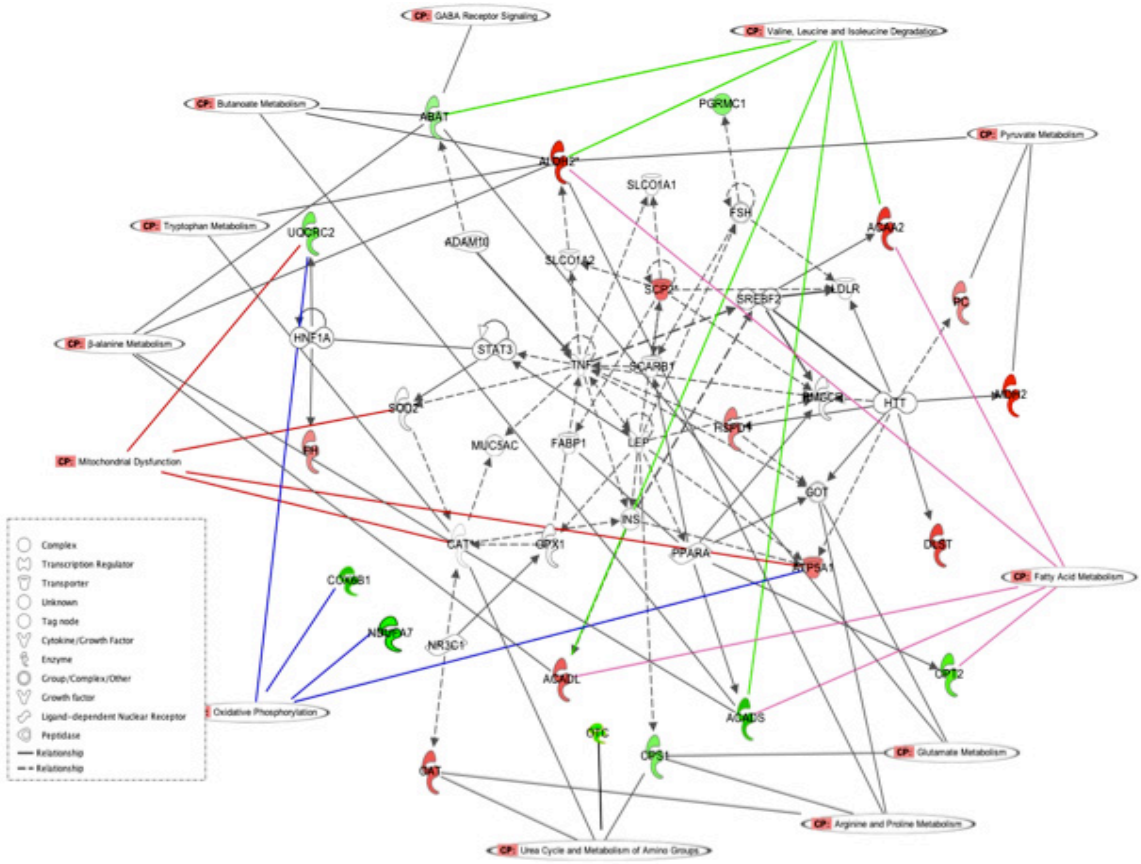

Figure 8. Merged networks overlay with pathways identified from SCADD mice

Proteins colored in green indicate decreased expression in SCAD deficient mice. Proteins colored in red indicate increased expression. The color intensity corresponds to the degree of abundance. Proteins in white are those identified through the Ingenuity Pathways Knowledge Base. The shapes denote the molecular class of the protein. A solid line indicates a direct molecular interaction, and a dashed line indicates an indirect molecular interaction. The CP (canonical pathway) in ovals denotes the significant pathways identified. A full explanation of lines and relationships is provided in Appendix B (Software legend).

Among the 9 proteins involved in mitochondrial dysfunction, 7 proteins were down-regulated in SCAD deficient mice (Table 3, Figure 4, Figure 7), 6 of which were involved in OXPHOS. Most of the proteins associated with the fatty acid oxidation pathway were increased in SCAD deficient mice except for carnitine palmitoyltransferase II (*CPT2*), which was less

abundant. Transcription regulators such as *HNF1A, STAT3, SREBF2* and *HTT*, and transporters such as *ATP5A, FABP1* and *SCARB1* link these pathways as illustrated in Figure 8. The nuclear receptor PPARA also participates in the regulation of both networks. Although these regulators were not identified as significantly altered in all experiments, smaller changes in their levels may play important roles in determining the pattern of protein abnormalities seen in SCAD deficiency. For example, *ACADS* is connected to *CPS1* through *PPARA* and *LEP*. Such unidentified changes may also be important in the development of pathophysiologic changes and symptoms.

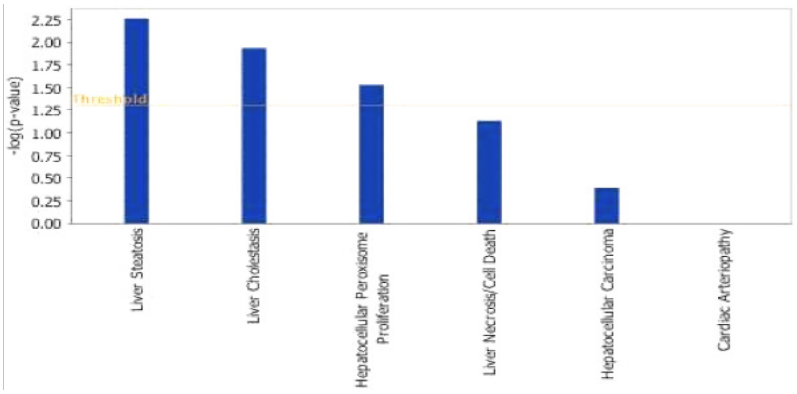

Figure 9. Hepatotoxicity of changed proteins

The prediction of clinically relevant pathologies associated with altered proteins in SCAD deficiency. Y-axis displays the significance of association ($p \leq 0.05$).

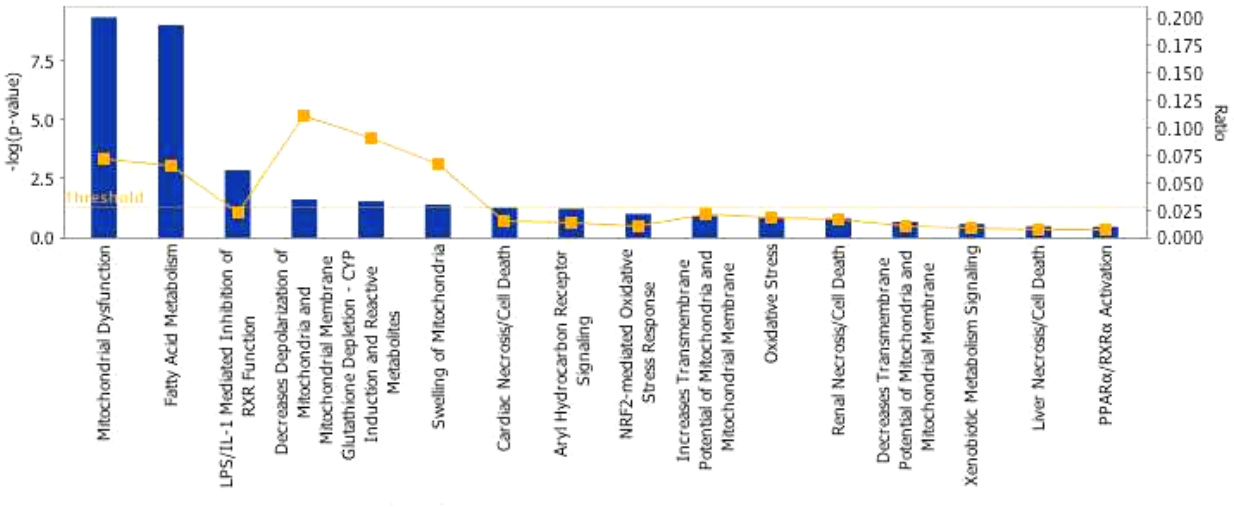

Figure 10. The "toxicity" of altered proteins in SCAD deficient mice

This bar chart shows the significance of altered proteins associated with the Ingenuity Tox Lists of molecules that are known to be involved in a particular type of toxicity. The left Y-axis displays the significance and corresponds to the height of the bars; the right Y-axis displays the ratio and corresponds to the dotted line.

To help characterize the clinically relevant secondary changes associated with SCAD gene deficiency and provide additional insight into the pathologic alterations induced by SCAD gene deficiency, the toxicity analysis function in the IPA software was utilized. In this analysis, SCAD deficiency was essentially defined as a "toxin", secondary changes identified in the proteome was assessed and assigned to functional pathways as with more traditional small molecule studies. The results largely identified a pattern associated with hepatotoxicity and significant toxicity on implicated in mitochondrial dysfunction, fatty acid metabolism, decrease of depolarization of mitochondria and mitochondrial membrane and swelling of mitochondria involving 5 down-regulated proteins (Figure 9, 10). The analytical tool does not provide parameters to assess specific impacts on skeletal muscle, thus, the toxicity changes on skeletal muscles were not identifiable.

Table 7. Candidate biomarkers identified in differentially expressed proteins

Gene Symbol	Entrez Gene Name	Family	GenPept/IPI/UniProt/Swiss-Prot Accession	Fold Change
ACAA2	acetyl-CoA acyltransferase 2	enzyme	IPI00653158.1	2.600
ACADL	acyl-CoA dehydrogenase, long chain	enzyme	IPI00894588.1	2.000
ACADS	acyl-CoA dehydrogenase, C-2 to C-3 short chain	enzyme	Q91W85	-3.580
ALDH2	aldehyde dehydrogenase 2 family (mitochondrial)	enzyme	IPI00111218.1	3.110
CPT2	carnitine palmitoyltransferase 2	enzyme	IPI00881401.1	-2.703
EPHX1	epoxide hydrolase 1, microsomal (xenobiotic)	peptidase	Q9D379	1.500
GLUD1	glutamate dehydrogenase 1	enzyme	IPI00114209.1	-2.041
PC	pyruvate carboxylase	enzyme	IPI00943457.1	1.560

One goal of proteomic analysis is to identify biomarkers that identify disease or predict the development of symptoms. Biomarker analysis by IPA identifies and prioritizes the most relevant and promising molecular biomarker candidates from the differentially expressed proteins. The Biomarker filter to explore molecular biomarker candidates was selected to focus on contextual information related to human and mouse genes associated with diseases shown to be significantly altered in SCAD deficient mice. 7 candidate markers that have been associated with related diseases (Table 7) were identified. Five of them were up regulated. *ACAA2* encoding protein is involved in fatty acid elongation and valine, leucine and isoleucine degradation. It is associated with non-insulin dependent diabetes mellitus and microvesicular hepatic steatosis.

Proteins encoded by *ACADL* and *CPT2* were identified as potential biomarkers but with changes in opposite directions. *GLUD1* is associated with Reye's syndrome and hyperinsulinism-hyperammonemia disorders. To magnify the filter findings, the analysis was filtered for all body fluids where a biomarker has been used in the diagnosis, efficacy, prognosis, progression, response or safety as well as identification of a specific disease. However, when applying more restricted filter parameters on human or mouse and including only tissue specificity of liver did, the analysis did not identify any additional biomarker candidates.

2.5 DISCUSSION

A wide array of symptoms has been in reported in patients affected with SCAD deficiency, but the vast majority of infants identified through newborn screening remain well. The clinical and physiologic ramifications of SCAD deficiency are unknown. The purpose of this study was to gain insight into the pathophysiology of this condition and to identify biomarkers that predict the development of symptoms by surveying changes in the mitochondrial proteome of SCAD deficient mice. Proteomic changes in liver mitochondria from SCAD deficient mice were first profiled. These experiments revealed a broad mitochondrial dysfunction beyond fatty acid oxidation induced by SCAD deficiency. Multiple energy related metabolism pathways were altered, indicating that a more complex mechanism for development of symptoms may exist. This finding differentiates SCAD from other fatty acid beta-oxidation disorders such as very long chain and medium chain acyl-CoA dehydrogenase deficiency in spite of the fact that they are caused by the genes within the same ACAD family.

While only limited data are available on the secondary effects of fatty acid oxidation defects on the proteome, the primary symptoms in most of these disorders can be viewed as a direct manifestation of the energy deficit caused by interruption of fatty acid oxidation. Specifically, patients experience stress or fasting induced hypoglycemia with or without rhabdomyolysis and may have long term skeletal or cardiomyopathy. The severity of SCADD varies from asymptomatic in most individuals, to rare life threatening metabolic crises in some of them, but rarely includes the more common symptoms seen in the longer chain defects. The diverse changes in energy metabolism in SCAD deficiency may, in part, explain these heterogeneous symptoms. The diversity of other pathways altered in SCAD deficient mice suggests that differential compensatory or secondary deleterious effects may play the dominant role in determining the pathophysiology of this deficiency. Up regulated amino acid catabolism and TCA cycle enzymes imply that short chain fatty acids are less available to produce energy, and that the mice compensate by generating energy from other sources. While these compensatory changes may overcome the primary deleterious effects of impaired energy production in SCAD deficiency, it provides opportunities for variable expression of other genes to impact phenotypes leading to the less severe symptoms in most patients with this deficiency.

A decrease of almost all complexes in electron transport chain implies that less efficient fatty acid oxidation is magnified by a secondary defect in oxidative phosphorylation, thus further impairing ATP production. Deficiency of the respiratory chain complexes is a common cause of Leigh syndrome, a rare neurometabolic condition presenting with seizures, hypotonia, fatigue, nystagmus, poor motor function and ataxia (DiMauro and Schon 2003;(de Lonlay et al, 2001; Lebon et al, 2007; Tiranti et al, 1999; Triepels et al, 1999). In addition to one subunit of NADH dehydrogenase (iron-sulfur protein 7) previously implicated in the pathogenesis of Leigh

syndrome, reduction of 5 subunits of other respiratory chain complexes and UGRCB encoding complex III binding protein (cytochrome b-c1 complex subunit 7), which is also part of the ubiquinol-cytochrome c oxidoreductase complex, was also demonstrated. Mutations in this gene are associated with mitochondrial complex III deficiency. This correlation between fatty acid oxidation and oxidative phosphorylation is consistent with the recognition that many patients with respiratory chain complex deficiencies accumulate metabolites suggestive of fatty acid beta-oxidation dysfunction, and the recent description of a multi-functional enzyme complex encompassing all the activities of fatty acid oxidation and the respiratory chain (Schuck et al, 2009);(Wang et al, 2010) In addition, mutations in *ACAD9*, another member of the *ACAD* gene family can lead to either a fatty acid oxidation defect of deficiency of respiratory chain complex I deficiency (He et al, 2007) Sauer et al, 2008; (Bortolami et al, 2008; Gianazza et al, 2006; Haack et al, 2010; Sauer et al, 2008; Wang et al, 2010). Thus, to understand SCAD deficiency, it becomes necessary to consider other energy pathways as well.

Various proteins related to other metabolic pathways were also altered in SCADD mice. These include carbamylphosphate synthase I (*CPS1*), carnitine palmitoyltransferase II (*CPT2*), pyroline-5-carboxylate reductase (*ALDH4A1)*, fumarase (*FH*), ornithine carbamoyltransferase (*OTC)*, and pyruvate carboxylase (*PC*), as well as the enzymes implicated in glutaric aciduria (*ETFA*), hyperinsulinism-hyperammonemia syndrome (*GLUD1)*, hyperprolinemia 1(*PRODH*), and hypolipidemia of mice (*SCP2*). While the physiologic cause of these changes and their effect on cellular metabolism are unknown, they underscore the complexity of secondary alterations that must be taken into account to fully understand the physiologic effects of a single gene defect such as SCADD.

It has also been noted that most symptomatic patients have presented with predominantly neurologic manifestations, which are rarely seen in the other ACAD defects. Disease association analysis identified additional genes involved in neurological disease as being altered in SCAD deficient mice. For example, 4-aminobutyrate aminotransferase encoded by *ABAT*, also named GABA transferase, is an enzyme that catalyzes the conversion of 4-aminobutanoic acid (GABA), an inhibitory neurotransmitter, and 2-oxoglutarate into succinic semialdehyde and glutamate. The phenotype of GABA-transferase deficiency includes psychomotor retardation, hypotonia, hyperreflexia, lethargy and refractory seizures (Medina-Kauwe et al, 1999). It is also interesting to note that SCADD deficient mice have very abnormal EEGs, though overt seizures are not seen. Further assessment of GABA metabolism in SCAD deficient patients may provide further insight into the role of this pathway in the development of clinical symptoms. The most frequent clinical findings reported in SCAD deficiency in humans are hypotonia and developmental delay. Many disorders with prominent neurologic symptoms, including Parkinson disease, cystic fibrosis, alpha 1-antitrypsinogin deficiency, and spinal cerebellar atrophies, share a common cellular pathology related to abnormal protein folding, aggregation, and eventual cellular damage. Point mutations in the *ACADS* gene are predominate in SCADD in humans. Many of these point mutations have been demonstrated to lead to abnormal protein folding and degradation but the physiologic relevance of these findings remains unclear. Alteration of proteins in the neurologic disease category in SCADD mice and the heat shock protein HSP60 (*HSPD1*) provide further impetus to better characterize these changes and their role in the development of symptoms in humans.

Network analysis revealed that components of the most highly altered network in SCADD mice are linked by several transcription regulators and transporters. In addition, several

transporters, including transmembrane transporter *ATP5A1* and heat shock protein HSP60 *(HSPD1),* functioning in protein and ATP binding and protein folding in mitochondria were identified as altered. These findings highlight yet an additional level of secondary cellular response resulting from SCAD deficiency. While alterations in other transporters or transcription regulators were not seen, it is important to realize that most are of very low abundance in the cell and present in other cellular locations than mitochondria. They therefore are not likely to be identified in the current experiments. However, their potential importance is highlighted by identification of factors such as *PPARA, HNF1A, STAT3* and *HTT* and transporters *SLCO1A1, SCARB1* and *LDLR* that serve as hubs in networks encompassing many of the proteins/enzymes altered in SCAD deficiency. Further studies will be necessary to elucidate their role in mitochondrial dysfunctions.

One goal of the current study was to identify biomarkers to distinguish asymptomatic SCAD deficiency from individuals at risk to develop symptoms that thus can serve as potential markers for adjunct diagnosis and monitoring of therapy. To examine this question, biomarker analysis was performed with filtering for all body fluids and all tissues but excluding cell lines, and including known diseases in humans and mice. These analyses identify *ACADL* and *CPT2* as candidate biomarkers. Both are of interest due to their role in fatty acid oxidation and that they are significantly changed in SCAD deficiency mice, though in opposite directions. In addition, *GLUD1*, linked with Reye's syndrome and hyperinsulinism-hyperammonemia is also of interest. Future studies are necessary to determine if these markers are better than the current biochemical markers (urinary EMA and butyrylglycine and plasma butyrylcarnitine) that provide a sensitive means of diagnosing SCAD deficiency, but not determining its severity.

Animal models of inborn errors of metabolism provide an ideal system to explore the potential biological relevance of specific markers, eliminating the diverse effects introduced by a heterogeneous genetic background. This study is the first large scale quantitative proteomics profiling of SCAD deficient animals. Historically, a combination of histopathology and clinical chemistry has been used to estimate the toxicity of a specific treatment, and differentiating toxic effects of treatment from disease-associated changes was problematic. Nucleotide array profiling is helpful to identify global expression changes that correlate with clinical pathology and to generate a hypothesis as to the causes of cellular toxicity. I have applied the traditional pharmacologic approach of molecular toxicity analysis to evaluate the clinically relevant toxic effects as defined by changes in the proteome in SCAD deficient mice that reflect pathologic processes in the animals. In these analyses, I treated the presence of SCAD deficiency essentially as a pharmacologic agent, and queried the analytical software for evidence of "treatment" toxicity. The result revealed that these changes were majorly correlated with hepatotoxicity which involved changed gene/proteins resulting in abnormalities in mitochondrial dysfunction, fatty acid metabolism, decrease of depolarization of mitochondria and mitochondrial membrane and swelling of mitochondria. The toxicity analysis revealed a change in one protein linked to oxidative stress (but without a known role) making this an unlikely mechanism of cellular toxicity. A previous report of proteomic screening of SCAD deficient human fibroblasts found that the level of superoxide dismutase 2 was reduced, a finding of unknown significance (Pedersen et al, 2010; Zolkipli et al, 2011). In contrast, eight proteins with altered levels were involved in toxicity related to mitochondrial dysfunction and eight were linked to the toxicity of fatty acid metabolism. Thus, it appears that the major toxicity arising from SCAD deficiency relates more directly to mitochondrial dysfunction and alteration of fatty acid metabolism. Such a

toxicity analysis approach should be of general use in studying the pathophysiologic effects of single gene mutations in genetic models of disease.

The novelty of this study lies in the application of proteomic approaches to identify alterations in molecular pathways induced by SCAD deficiency, and provides additional insight into the fundamental pathophysiology of this condition. Variability of symptoms in humans with SCAD deficiency suggests that this autosomal recessive genetic disorder behaves more as a polygenic disorder than as a traditional monogenetic trait. Additional study of the primary deficiency on other genetic backgrounds will help provide insight into the other critical genes that affect the biochemical and clinical phenotype in this disorder. Multiple experimental details provide robustness to the final conclusions. Replicate experiments and complementary proteomic approaches serve to provide confidence in the changes seen, as does verification by western blotting. Use of multiple separation and sample preparation techniques also increases the ability to identify disease specific markers within a complex proteome containing thousands of proteins. Of the two methods used, iTRAQ labeling proved to be more sensitive and more robust at generating data for statistical comparisons. However, protein changes could be independently confirmed by western blotting and DIGE. Liver is a mitotic tissue with a high rate of cell division and thus, typically, rapid protein turnover and a high level of innate variation in protein abundance. The range of biological variation that can be tolerated by the cell depends on the individual protein. Such inherent biological variations cannot be eliminated completely, however, their effects on experimental outcome can be minimized by analyzing multiple samples in each genotypic group and pooling of samples. The proteomic analysis in this study evaluated both proteins encoded in the nuclear genome and imported into mitochondria as well as those encoded on the mitochondrial chromosome. Thus, the changes identified in mutant mice reflect a

compilation of all dynamic changes including gene expression as well as protein modification and the processes of mitochondrial targeting, import, and protein folding. It is important to note that a protein must be relatively abundant to be detected by the techniques used in this study, although additional changes can be underrated by network analysis.

In conclusion, changes in the mitochondrial proteome in animals with SCAD deficiency were first identified and quantitated. The secondarily changed proteins implicate a complicated process of cellular toxicity with multiply altered metabolic pathways and disease associated networks. Additionally, these pathways converge on disorders with neurologic symptoms, suggesting that even asymptomatic individuals with SCAD deficiency may be at risk to develop more severe disease. Several candidate biomarkers that can serve as potential markers for adjunct diagnosis and monitoring of therapy were then proposed. Further studies will allow delineation of changes in the proteome that can serve as biomarker(s) for the development of symptoms, and provide opportunities to develop therapies based on the recognition of new cellular protein interactions.

3.0 PROTEOMIC STUDY ON VERY LONG CHAIN ACYLCOA DEHYDROGENASE DEFICIENT MOUSE

3.1 ABSTRACT

Very long chain acyl-CoA dehydrogenase (VLCAD) deficiency identified through newborn screening is a clinically heterogeneous fatty acid ß-oxidation disorder without clear genotype-phenotype correlations. Acute symptoms are often induced by physiological stress such as illness and fasting. The pathophysiologic mechanisms underlying disease symptoms and phenotypic heterogeneity remain unclear. The interaction between the genetic and environment factors is typically measured in epidemiologic studies on individuals with a specific genetic susceptible to the exposure. However, ascertaining reproducible cellular changes in an individual at risk due to environmental effects remains a challenge. The objective of this study was to better understand the mechanism of molecular changes at a global level and to explore the environmental effects on the gene products and the relevant biological pathways that interact. The mitochondrial proteome of VLCAD deficient mice was quantitatively compared to wild type mice in fed and fasted states. Isobaric tags for relative and absolute quantification (iTRAQ) labeling followed by nano-LC/LTQ-Orbitrap mass spectrometry were employed to identify the changes in both deficient and wild type groups and the differences in response to fasting. The affected pathways and clinical relevance associated with altered proteins were evaluated using

Ingenuity Pathway Analysis. Numerous proteomic changes associated with gene deficiency and fasting as well as gene-gene interactions within relevant pathways were identified. Most of changes induced by fasting were different in deficient mice as compared to wild type mice and few changes induced by fasting were shared in the mutant and wild type mice. The pattern of changes in chaperone proteins including HSP60 and HSP10 upon fasting was different in them. Fasting altered the compensatory increase in oxidative phosphorylation in fed deficient mice. Secondary changes in fasted deficient mice were involved in cardiac dysfunction. Fasting induced different proteomic changes in deficient mice indicating differences in the interactions of genes and gene-environment, and important roles of these interactions in the pathogenesis of VLCAD deficiency. Particularly, fasting in mutants reversed the protective response in oxidative phosphorylation pathway induced by genetic deficiency alone. Global survey of fasting effects on a genetic mouse model presents an approach to explore gene-environment interaction and their contribution to gene-gene interactions. Future characterization of functional interactive genes and association studies in humans will provide further insight into disease mechanism and guidance in therapy.

3.2 INTRODUCTION

Mitochondrial fatty acid ß-oxidation plays a major role in energy production in the body, especially during fasting conditions. At least 25 enzymes and transport proteins are involved in mitochondrial FAO, which is predominantly responsible for the oxidation of fatty acids of carbon chain length 20 or less. Fatty acids are transferred across the mitochondrial membrane as carnitine esters by carnitinepalmitoyl transferase 1 and 2 in conjunction with the carnitine-

acylcarnitine translocase. The four reactions of the ß-oxidation cycle, catalyzed by four enzymatic activities [acyl-CoA dehydrogenase (ACAD), enoyl-CoA hydratase, L-3-hydroxyacyl-CoA dehydrogenase, and 3-ketoacyl-CoA thiolase], sequentially remove two carbons until the acyl-CoA is converted to acetyl-CoA molecules. Electrons are transferred to respiratory chain through complex I of the electron transfer chain or directly to coenzyme Q (ubiquinone) by electron transfer flavoprotein (ETF). Very long-chain acyl-CoA dehydrogenase (VLCAD) is the initial enzyme involved in mitochondrial fatty acid -oxidation, fueling hepatic ketogenesis during periods of high energy demand after hepatic glycogen stores have been depleted. VLCAD is a member of the ACAD enzyme family, which currently has eleven known members. The ACADs catalyze the rate-limiting step in the mitochondrial β-oxidation of activated fatty acids and branched-chain amino acids. Each possesses a characteristic pattern of substrate utilization but these partially overlap for some enzymes. VLCAD appears to be the major ACD responsible for the catalysis of acyl-CoAs 16 to 20 carbons in length in human liver, heart, and muscle.

VLCAD deficiency (VLCADD) is an autosomal inborn error resulting from mutations in the *ACADVL* gene that impair enzyme expression or function. Patients with VLCAD deficiency present with a broad spectrum of clinical symptoms ranging from lethal hypoketotic hypoglycemia, hepatomegaly, and cardiomyopathy in infancy to episodic rhabdomyolysis in adolescents and adults. The underlying mechanisms leading to heterogeneous manifestations in these patients at different periods of ages still remain unknown. Acylcarnitine analysis of dried blood spots by electrospray ionization tandem mass spectrometry (MS/MS) allows pre-symptomatic identification of VLCAD deficiency in newborns. However, some children may escape detection and present with later onset symptoms (Boneh et al, 2006; Ficicioglu et al,

2010). In addition, as some asymptomatic newborns may develop rhabdomyolysis after excessive physical exercise at an older age, it is still unknown whether those individuals may remain asymptomatic throughout their life-time (Spiekerkoetter et al, 2009a). The observed acute symptoms are often induced by physiological stress or by conditions such as fasting or endurance exercise that fatty acid oxidation, through mechanisms that are not well understood. The pathophysiologic and molecular mechanism underlying stress-induced symptoms and the clinical heterogeneity in this disease is unknown.

Numerous mutations have been reported in VLCADD patients. They include null, missense, frameshift, and splice consensus sequence mutations as well as in-frame deletions (Andresen et al, 1996a; Andresen et al, 1996b; Mathur et al, 1999). A genotype-phenotype correlation was described on the basis of clinical phenotype in 55 unrelated VLCAD deficient patients with known mutations. Children with the severe phenotype tended to have null mutations while patients with the two milder forms of the disease were more likely to have missense mutations(Andresen et al, 1999). Nevertheless, a few missense mutations were clearly associated with the severe phenotype(Coughlin & Ficicioglu, 2010).Genotype alone remains limited in its predictive ability to determine the phenotype. The clear correlations between genotype and phenotypes have not been well established.

Clinical diagnosis of VLCAD deficiency relies on tandem mass spectrometry to identify elevations of the hallmark metabolites in blood (C14: 1, C12: 1, 14:2, 16:2, and C18:1 carnitines) followed by molecular analysis of the *ACADVL* gene. Urine dicarboxylic aciduria may be present during acute illness but is typically normal otherwise. Additional diagnostic tools include assay of enzyme activity and functional measurements of whole cell fatty acid ß-oxidation in fibroblasts or lymphocytes. As with most enzyme disorders, the level of residual enzyme activity

correlates with the severity of the clinical phenotype, but the relationship is inexact (Andresen et al, 1999; Gregersen et al, 2001). The genetic and pathophysiological basis for this variation is not known.

The severe episodes of metabolic crisis or sudden death in patients with fatty acid ß-oxidation disorders were usually induced by the physiologic stressor, fasting, in adolescence or early childhood. The fasting was the most important inducer in the episodes of metabolic crisis and sudden death in VLCAD deficient individuals. During fasting, glucose supplies become limited. Under this condition, the liver converts fatty acids into ketone bodies, which serve as an additional energy source for all tissues but are of particular importance in brain, heart, and skeletal muscle. Therapy of VLCAD deficiency focuses on avoiding the stressors that induce catabolism and provide alternative fuel sources that can bypass the metabolic block. These efforts include avoidance of fasting, and addition of medium chain fats as a dietary supplement (Brown-Harrison et al, 1996; Cox et al, 1998a). It is noteworthy, however, that there are no formal studies evaluating the effectiveness of any of these therapies (Spiekerkoetter et al, 2009a; Spiekerkoetter et al, 2009b), and in spite of them, 10–20% or more of treated patients still have episodic rhabdomyolysis (Wilcken, 2010). The heterogeneous biochemical abnormalities and the variable outcomes in treated patients suggest that secondary abnormalities in pathways other than fatty acid oxidation, as well as other genetic and environmental factors, play roles in the pathophysiology of this disorder. However, the full scope of biological changes induced by VLCAD deficiency with or without fasting has been impossible to characterize directly in patients.

Mouse models of human inborn errors of metabolism offer an excellent opportunity to explore more complicated questions than is often possible in patients with these disorders. Two

independently VLCAD-deficient mouse models have been developed and characterized (Cox et al, 2001b; Exil et al, 2003). Both animals exhibit metabolic and biochemical abnormalities resembling the human deficiency and have been used to study the stress-induced metabolic changes that occur in VLCAD deficiency (Spiekerkoetter and Wood). The *ACADVL* gene maps to mouse chromosome 11 and has a similar gene structure to that of the human locus (Cox et al, 1998b). However, some key differences are seen in biochemical abnormalities in mouse models. In human VLCADD, C14:0 and C14:1 acylcarnitines accumulate predominantly, whereas in VLCAD-deficient mice, the C16 and C18:1 species are the "signature" acylcarnitines (Spiekerkoetter et al, 2004). VLCAD deficient mice with the genetic background of C57BL/6+129svJ have lower concentrations of free carnitine and elevated C14-C18 acylcarnitines in blood, similar to the metabolite patterns seen in humans with VLCADD (Exil et al, 2003). Fasting and cold exposure result in severe hypoglycemia, hypothermia, skeletal myopathy and death in one third of VLCAD-deficient mice resembling human VLCADD (Spiekerkoetter et al, 2004). Additional studies have documented the development of hepatosteatosis in response to fasting with death after prolonged fasting (Cox et al, 2001b). Long-term supplementation of VLCAD deficient mice medium chain triglyceride (MCT) oil also induces severe hepatosteatosis (Tucci et al, 2010). However, the broader impact of fasting on the mouse transcriptome and proteome has not been examined.

To help understand the underlying mechanism leading to heterogeneous phenotypes and response to environmental factors that may involve in the disease manifestation, systematic study of the accumulated biological effects of the primary metabolic deficiency is needed. Currently available proteomics approaches allow measuring biological changes at a global scale induced by mutations and fasting in disease models. A discovery approach with mass spectrometry based on

differential detection of proteins by labeling amino acid residue in tryptic peptides offers the potential to measure all protein changes directly in subcellular compartments. Isobaric tags for relative and absolute quantification (iTRAQ) analysis have recently come into general use in quantitative proteomics (Ross et al, 2004; Wiese et al, 2007). iTRAQ reagents are a set of multiplexed, amine-specific, stable isotope reagents that can label N-terminus residue of lysine of all peptides in up to eight different biological samples enabling simultaneous identification and quantitation of different samples that can be compared in one experiment. The labeled peptides are identical in mass and hence identical in single MS mode, but each produces strong, diagnostic, low mass MS/MS signature ions allowing for quantitation of different samples simultaneously. In addition, information such as post-translational modifications is not lost using this chemistry. The proteome coverage is expanded and the confidence in identification and quantitation is improved by labeling multiple peptides per protein. Utilization of 8-plex reagents allows quantitative measurement of the proteomic changes induced by VLCAD deficiency or fasting in a simplified experiment by mixing multiple proteome samples from animals with and with deficiency or with or without fasting. While, the complexity of the MS and MS/MS data is not increased.

Ingenuity Pathway Analysis is a software that helps understand biology at multiple levels by integrating data from various experimental platforms and provide insight into the molecular interactions, cellular phenotypes, and disease processes of the biological system under investigation (Ingenuity Systems, www.ingenuity.com). It leverages the Ingenuity Knowledge Base, a repository of biological interactions and functional annotations created from individually modeled relationships between proteins, RNAs, genes, metabolites, complexes, cells, tissues, drugs, and diseases. It has been adopted by the research community to understand the complex

biological and chemical systems. The pathways and functions associated with the secondarily changed proteins resulted from VLCAD defects or fasting could be analyzed using this tool to help extend the current understanding and gain further insight into the biological mechanism.

It is widely accepted that the full clinical spectrum of most diseases is determined by the interplay of genetic and environmental factors. In patients with inborn errors of metabolism, the primary mutation dictates a specific and severe susceptibility to an otherwise normal biomolecular or physiologic state, but a wide range of clinical phenotypes can still be seen. The effect of environmental factors is usually measured in epidemiological studies of individuals with some genetically susceptibility to an exposure, but such studies are usually not tenable in patients with metabolic disorders. In this study, a mouse model of a fatty acid oxidation defect (VLCAD deficiency) was used to characterize changes in the mitochondrial proteome in mice that are genetically identical except for one mutation and exposure to a specific stressor (fasting) to identify the interaction of genes and environment in determining clinical symptoms. No such a systemic study has been done in human beings or animals at a global scale.

3.3 MATERIALS AND METHODS

3.3.1 Mice

VLCAD knock out (C57BL/6+129svJ) and corresponding wild type mice with the same genetic background were purchased from Jackson Laboratory (Bar Harbor, Maine) at age 4-5 weeks. The animals were housed in the animal facilities in Children's Hospital of Pittsburgh of UPMC and bred for all experiments and tissue harvest. At least 6 male mice of each genotype

were used for each tissue harvest experiment. For fasting studies, 6 pairs of male mice were fasted 16 hours before sacrifice. All animals were sacrificed at 6-8 weeks of age by CO2 asphyxiation followed by standard protocols as approved by the University of Pittsburgh IACUC. Liver was removed immediately after death.

3.3.2 Isolation of mitochondria from mice liver

Freshly removed liver was finely minced in ice cold isolation buffer A containing 225 mM mannitol, 75 mM sucrose, 10 mM HEPES free acid, 10 mM EDTA, pH7.4, then gently homogenized with a glass Dounce homogenizer in isolation buffer B containing 225 mM mannitol, 75 mM sucrose, 10 mM HEPES free acid, 0.1% BSA fatty acid free, 10 mM EDTA, pH 7.4, with the addition of 10 µl/ml HaltTM protease inhibitor cocktail (Pierce, Rockfold, IL). The homogenate was centrifuged at 1,300 x g for 10 minutes at 4 °C, and the supernatant was recovered and centrifuged at 10,000 x g for 10 minutes. The pellet was carefully preserved and resuspended in 12% Percoll solution, then layered on top of a 30-70% Percoll gradient and centrifuged at 62,000 x g for 35 minutes at 4 °C. The mitochondrial band located between the 30% and 70% layers was removed and washed with cold isolation buffer A. The purified mitochondria were then collected by centrifugation at 10,000 x g for 10 minutes 4 °C. A small aliquot of the sample was taken for organelle marker analysis and purity testing by western blotting. 20 µg of the remaining sample were run on a 10% SDS acrylamide gel and transferred to PVDF membrane for western blotting. The membrane was probed with anti-cytochrome C (a mitochondrial marker) and anti-calreticulin (an ER marker) antibodies (Santa Cruz Biologicals).

3.3.3 iTRAQ experiments

Preparation of mitochondrial protein. Mitochondrial pellets isolated from wild type and deficient mice were suspended in sample buffer containing 0.5 M triethylammonium bicarbonate buffer (TEAB, pH 8.5), 0.1% SDS. The samples were sonicated 3 times for 10 seconds at 4°C, and debris from each sample was removed by centrifugation at 14,000 x g for 15 minutes at 4°C. The protein concentration was measured using the BCA protein assay reagent according to the manufacturer's protocol (Pierce, Rockford, IL). Absorbance was measured at 590 nm on a microplate reader (Bio-Rad, Hercules, CA). One hundred micrograms of protein from each sample were placed in an eppendorf tube, mixed with pre-chilled acetone, and the tubes were incubated at -20°C until precipitate formed (30 minutes -4 hours). The acetone was then decanted and the samples dried in air at room temperature.

iTRAQ labeling. An 8-plex isobaric reagent kit (Applied Biosystems, Foster City, CA) was used to label samples for each set of experiment. Each sample was labeled twice to represent biological replicates for each sample from deficient or wild type mice in the fasted or fed status. The labeling procedure for each biological replicates was performed based on the manufacturer's protocol (Applied Biosystems, Foster City, CA). The labeling strategy was designed as shown in Table 8. A total of 6 experiments were performed with the tagged samples in a reciprocal manner to conduct 3 pairs of comparisons between deficient mice and wild type mice under both normal feeding and fasting conditions. Briefly, 100 μg of precipitated mitochondrial proteins from each of 8 different samples (Table 8) were resuspended in 20 μL of 0.5 M triethylammonium bicarbonate (TEAB), and 1 μl of 2% SDS was added with mixing to allow denaturation. 2 μL of the reducing reagent 50 mM tris- (2-carboxyethyl) phosphine (TCEP) were then added to each sample and incubated at 60°C for 1 hour. After cooling, the samples were alkylated with 1 μL of

the cysteine blocking reagent 200 mM methyl methanethiosulfonate (MMTS) at room temperature in the dark for 20 min. Four micrograms of N-tosyl-L-phenylalanine chloromethyl ketone (TPCK) treated trypsin were then added to each sample, and the samples were incubated at 37° C overnight. Prior to labeling, the 8 iTRAQ reagents (Applied Biosystems, Foster City, CA) 113,114, 115, 116,117,118,117, 119 and 121 were brought to 37° C. 50 μL of isopropanol were added to each iTRAQ vial. The iTRAQ reagents were then added to the appropriate digested sample as shown in table 1. The pH of each sample was then adjusted to pH 8-8.5 by adding an appropriate volume of the TEAB buffer. Tubes were incubated at room temperature for 2 hours, and all 8 samples were combined into one tube for peptide purification.

Table 8. Experimental design for proteome profiling using iTRAQ labeling

Experiment No.	Labeled Samples	Labeled Samples	Labeled Samples	Labeled Samples	Labeled Samples	Labeled Samples	Labeled Samples	Labeled Samples
1	113-VLCAD-/- 1 (fed)	114-VLCAD+/+1 (fed)	115-VLCAD-/2 (fed)	116-VLCAD+/+2 (fed)	117-VLCAD-/-1 (fed)	118-VLCAD+/+1 (fed)	119-VLCAD-/2 (fed)	121-VLCAD+/+2 (fed)
2	113-VLCAD+/+ 3&4* (fed)	114-VLCAD-/- 3&4*(fed)	115-VLCAD+/+ 5&6**(fed)	116-VLCAD-/- 5&6**(fed)	117-VLCAD+/+ 3&4*(fed)	118-VLCAD-/- 3&4*(fed)	119-VLCAD+/+ 5&6**(fed)	121-VLCAD+/+ 5&6**(fed)
3	113-VLCAD-/- 1 (fasting)	114-VLCAD+/+1 (fasting)	115-VLCAD-/2 (fasting)	116-VLCAD+/+2 (fasting)	117-VLCAD-/-1 (fasting)	118-VLCAD+/+1 (fasting)	119-VLCAD-/2 (fasting)	121-VLCAD+/+2 (fasting)
4	113-VLCAD-/- 1&2 (fed)	114-VLCAD-/-1&2 (fasting)	115-VLCAD-/- 3&4 (fed)	116-VLCAD-/- 3&4 (fasting)	117-VLCAD-/- 1&2&3*** (fed)	118-VLCAD-/- 3&4&5&6 (fasting)	119-VLCAD-/ 3&4&5 (fed)	121-VLCAD-/- 3&4&5&6 (fasting)
5	113-VLCAD+/+ 3&4* (fed)	114-VLCAD+/+ 3&4*(fasting)	115-VLCAD+/+ 5&6**(fed)	116-VLCAD+/+ 5&6**(fasting)	117-VLCAD+/+ 3&4*(fed)	118-VLCAD+/+ 3&4*(fasting)	119-VLCAD+/+ 5&6**(fed)	121-VLCAD+/+ 5&6**(fasting)

*3&4 : pooled samples from mice 3 and mice 4; **5&6: pooled samples from mice 5 and mice 6; ***1&2&3: pooled samples from mice 1,2 and mice 3; 3&4&5&6: pooled samples from mice 3,4,5 and mice 6.

SCX purification. Peptide samples were purified using strong cation exchange (SCX) cartridges, Strata 55 μum,70 Å (Phenomenex, Torrance, CA). Samples were diluted in Buffer A (10 mM phosphoric, pH 3.0, 25% acetonitrile) to ensure that the pH was below 3.0. The Strata cartridges were conditioned using ACN and Buffer A at a flow rate of 2-4 ml / minutes. Each mixed sample for one experiment was then loaded onto the solid phase extraction (SPE) column at a rate of 2-4 ml/minute. The column was rinsed with 1-2 ml of Buffer A and dried by aspirating air through the syringe. The peptides were eluted from the column using Buffer B (5% ammonium hydroxide, 30% methanol). The purified peptides were vacuum dried.

Peptide fractionation. Peptides were fractionated using isoelectric focusing (IEF) with 18 cm pH 3.5-4.5 Immobiline DryStrip (IPG) strips (GE Healthcare, Uppsala, Sweden). The dried peptides were resuspended in 340 μl of 8M urea, 2mg/ml DTT, 0.1% Triton X-100, and 1% ampholytes. The IPG strip was rehydrated in the sample solution for 10-20 hours. The IEF for experiment 1 and 2 was performed on a Multiphor II Electrophoresis Unit (Pharmacia Biotech AB, Uppsala, Sweden) at 20 °C with a current of 2 mA in gradient mode. The IEF for peptide samples for experiment 3, 4, and 5 was run with an Ettan IPGphor Π system (former Amersham Biosciences, Piscataway, NJ) following the program with 300v for 10 minutes, 3500v for 17.5 hours, 800v for 3 hours and then maintained at 30v as needed (Table 2). After the completion, the IPG strip was cut into 10 fragments and placed into tubes containing 100 μl 5% acetonitrile (ACN), 0.5% trifluoroacetic acid (TFA). Peptides were extracted 2 or 3 times by incubation in 5% ACN, 0.5% TFA at room temperature for 60 minutes. The supernatant solutions were then pooled together for the clean-up step.

Peptide clean-up. Eluted fractions were desalted using PepClean C-18 spin columns (Pierce, Rockford, IL) according to the manufacturer's protocol. Briefly, 200 μl of activation

solution (50% methanol) was loaded onto the column to wet the resin. The column was equilibrated with 0.5% TFA in 5% ACN. The fractionated peptides were loaded onto the column and washed with 0.5% TFA in 5% ACN. Peptides were then eluted from the column using 70% ACN and dried by speed vacuum. Cleaned peptides were resuspended in 0.1% TFA, 2% ACN for nano-LC separation.

Nano-LC Mass spectrometry. The purified peptide mixtures were separated by reverse phase nano-Liquid chromatography on an Easy nLC system (Proxeon, Odense, Denmark). The peptides were loaded onto a trap column (0.3 mm id x 5mm Kromasil C18, 5 μm particles) followed by the separation with an analytical column (75 μm id x 100 mm, packed with Kromasil C18, 3.5 μm)(Eka Chemicals, Bohus, Sweden) at a flow rate of 300 nl/minute using a gradient of 5%-35% ACN in 0.4% acetic acid for 100 minutes. Between each analytical run, 100 fmol bovine serum albumin was run for 31 min to serve as a quality control and equilibration of the system. The effluent was directly applied by electrospray with a stainless steel emitter (Proxeon, Odense, Denmark) into a LTQ-Orbitrap mass spectrometry (Thermo Fisher Scientific, Waltham, USA) system. The electrospray voltage applied was 2 kV.

The mass spectrometry was operated with Xcalibur v 2.0.7 (Thermo Fisher Scientific, Waltham, USA) in a data-dependent mode to alternate between one MS full scan and 6 MS/MS scans with linear ion trap (LTQ) detection of the most intense ions. The MS detection parameter was set to constitute a full scan of m/z 400–2000 with Orbitrap resolution R = 60,000 at m/z 400. The top four MS spectra data were acquired for the most intensive precursor ions in the MS survey scans. The m/z values selected for MS/MS were dynamically excluded for 25 s. Rejection of charge state +1 was selected. The internal calibration was performed using a lock mass ion ($Si(CH_3)_2O)_6H$, m/z 445.120025) from ambient air (Olsen et al, 2005). Pulsed Q dissociation (PQD)

fragmentation was performed with the following settings: activation time of 0.1 s, activation Q of 0.7, and normalized collision energy of 33.

Bioinformatics and Database Searching. The MS/MS spectra (RAW files) were processed using extract_msn.exe from February 15, 2010 (Thermo Fischer Scientific). The MS/MS data from 10 different fractions of peptides from each experimental study were combined to search against the IPI-mouse database (version 3.65 with 56775 sequences, released 10/16/2009) using Mascot version 2.2.04 (Matrix Science, London, UK, www.matrixscience.com) with the multidimensional protein (MudPIT) scoring algorithm(Kersey et al, 2004). Up to two missed cleavages, with trypsin as the digestion enzyme, were allowed. The full scan tolerance of 5 ppm and MS/MS tolerance of 0.75 Da were accepted. Searches were performed allowing variable oxidation of methionine residues (16 Da) and iTRAQ labels on tyrosine, and fixed modification of iTRAQ labels on lysine and N terminus, and methylthio modification of cysteines. The threshold of protein identification was set to have significance at $p \leq 0.001$ corresponding to a false discovery frequency of 0.002 for searching against a decoy database. iTRAQ values were reported for proteins with four or more measured iTRAQ values when each peptide had an expectation value of 0.02 or below. When the identification of a protein in an analysis resulted in several possible protein isoforms, all of them were considered for quantification. In the quantitative calculations, only protein isoforms with iTRAQ values in all analyses were included. The mass spectrometry for the analysis of purified peptides from fasted animals and fasted wild type animals and database search was performed by Dr. Johan Palmfeldt, PhD, and Research Unit for Molecular Medicine, Aarhus University Hospital, Denmark.

For each protein, the relative ratio was calculated as the ratio of peptide signals belonging to that protein compared to the corresponding peptides signals with label 113 according to the Mascot algorithm. The data set was exported for further biostatistics analysis. Proteins with a minimum of at least 2 labeled peptides and a mascot score of over 65 were selected for further data analysis. In experiments of normal fed mice (experiment 1 and 2), values of all of proteins corresponding to wild type in each independent experiment were summed up and averaged to obtain a reference value to take into account the lower variation in wild type samples. Correspondingly, due to the low coverage of captured proteins in experiments on fasted mice, all of proteins with 8 labeled values were summed and averaged to obtain a reference value for each data set. Each iTRAQ value was recalculated in its own data set by setting the reference label value to be 1 and then log2 transformed to have a normalized value (Appendix C). The equal variance was tested for each protein. Student's *t*-test was used to test the difference at $p \leq 0.10$ between the log transformed values of mutant and wild type for each protein. The mean of the biological and technical replicates were calculated to obtain the averaged fold change of a protein expression in mutant compared to that in wild type or fasted compared to that in normal fed. Proteins that were significant ($p \leq 0.10$) and over 1.25 folds change or less than 0.75 folds change in 2 experiments (experiment 1 and 2) were classified as significant changed proteins. However, in order to maximize the detection of significant changed proteins in the rest of experiments, the *p*-value for the significance was set to be at $p \leq 0.10$ (Student's *t*-test) and the cut-off of protein changes was also set to have 1.25 or 0.75 but in only one experiment.

3.3.4 Pathway and network analysis

All proteins altered in deficient mice in either the fed or fasting state compared to wild type under the same conditions were separately analyzed for independent biological network building and pathway analysis by the Ingenuity Pathways Analysis (IPA; Ingenuity Systems, Redwood City, CA; www.ingenuity.com). The differentially expressed proteins from direct comparison of fasted mice and normal fed mice were analyzed independently. Each identifier of changed protein was mapped to its corresponding object (gene/protein) in the Ingenuity Knowledge database. The filters and general settings for the core analysis were set to consider all molecules including endogenous chemicals, as well as both direct and indirect relationships. The taxonomy of mouse was selected. All data sources except cell lines were considered and a stringent filter for molecules and relationships was applied. Networks of the focus genes were algorithmically generated based on their connectivity and ordered by an IPA score according to a global molecular network developed from Ingenuity Knowledge-Base. IPA computes a score for each possible network according to the fit of that network to the input proteins/genes. This score is calculated as the negative base-10 logarithm of the *p*-value that indicates the probability of the network-eligible molecules that are part of a network being found together as a result of random chance (Fisher's exact test). Scores 2 or higher have at least a 99% confidence of not being generated by random chance alone. The association to biological functions (and/or diseases) that were most significant to the genes in the network was also grouped. Genes or gene products are represented as nodes, and the biological relationship between two nodes is represented as an edge. All edges are supported by at least one reference from the literature or from canonical information in the software. The intensity of the node color indicates the increased (red) or de-creased (green) abundance. Nodes are displayed using various shapes that represent the

functional class of the gene product. In this analysis, we selected the top 2 networks with the highest as the most significant networks.

The Global Functional Analysis (GFA) and Global Canonical Pathways (GCP) analysis utilizes well characterized metabolic and cell signaling pathways incorporated in IPA that are available prior to data input. The canonical pathways and associated diseases related to the differentially expressed proteins were generated according to the algorithms in the software and listed in order of the significance of relation to the database. In this study, we compared the top-rated canonical pathways changed in the fed state and fasting state. The *p*-value associated with a function or a pathway is calculated by considering the number of focus genes that participate in that process and the total number of genes known to be associated with that process in the selected reference set by IPA using the right-tailed Fisher Exact Test.

3.4 RESULTS

To characterize changes in protein expression induced by VLCAD deficiency as well as fasting, mitochondrial proteome profiles in livers from male VLCAD deficient mice and corresponding wild type mice were quantitatively examined. Three pairs of comparisons were conducted in five independent experiments to identify the changes in protein expression between deficient mice and wild type mice under both normal feeding and fasting conditions. An overview of experimental approach is shown in Table 1. The aim of the first two experiments was to identify proteins altered in VLCAD deficient mice in the fed state in comparison with the wild type mice. The third experiment examined protein alterations in VLCAD deficient mice as

compared to wild type animals in the fasted state. The fourth and fifth experiments were designed to identify the proteins altered in response to fasting regardless of genotypes. 8-plex ITRAQ reagents were utilized to label trypsin-digested peptides. Proteins were identified and quantitated with nano-LC/LTQ-Orbitrap mass spectrometry. Numerous protein were identified and in each dataset. IPA was employed to identify the affected pathways and reconstruct the networks as inferred from proteins with altered expression.

3.4.1 Differentially expressed proteins in VLCAD deficient mice in the fed state

A total of 721 proteins and 490 proteins were identified with at least 2 peptides for each protein at $p \leq 0.001$ corresponding to a false discovery frequency of 0.002 in two independent experiments. Two different reagents were used to label the same peptides sample to minimize the variations of labeling efficiency. Moreover, to reduce the biological variance among individual mice, mitochondrial protein samples from two individual mice were pooled together to give one mixed protein sample. Peptide samples were first fractionated using isoelectric focusing with IPG strips at a range of pH 3.5-5.0 for the best resolution of peptides, and then were separated chromatographically by nano-LC, which separated the peptides efficiently.

Among the proteins that were differentially expressed, 43 proteins were classified as significantly changed in VLCAD deficient mice when compared to the wild type (Table 9). Only those proteins with consistently over 1.3-fold changes or less than 0.7-fold changes and their changes were significant ($p \leq 0.05$) in both of two experiments in VLCAD deficient mice were considered as significantly altered. The detailed description of the identification and quantification information including gene symbol, gene names, minimum peptides detected in two experiments, averaged ratios of protein values in deficient mice compared to those in wild

types and the biological annotations related to these proteins are provided in the table. Among the changed proteins, 31 proteins were decreased and 12 proteins were increased. The location of some identified proteins in this experiment are not indicated if they have been recognized as being in only mitochondria, whereas the mitochondrial location of others are reported if they have been localized to multiple organelles, and were identified and recognized in this experiment (Table 9).

Ingenuity Pathway Analysis was used to classify proteins altered in VLCAD deficient mice into different functional groups (Appendix A) and determine whether they were associated with related pathways and/or different cellular activities. Of the 43 altered proteins, 27 could be included in the network analysis and 36 could be used for canonical pathway analysis and functions analysis. Some of the remaining proteins that could not be included in the analysis may be due to the lack of the information from current literature, or being hypothetical proteins, duplicates with synonymous names or having the same encoding gene. Several significant functions that were associated with altered proteins were reported in *Figure 11*. The numbers of proteins that were classified into the top 5 molecular and cellular functional groups are shown in Table 11. The function that was most significantly associated with the altered proteins in VLCAD deficient mice in the fed state was lipid metabolism and small molecule chemistry (defined as those functions of small molecules not, included in the more specific categories of DNA, RNA, protein, lipids and carbohydrates). A larger number of molecules were classified into this functional group. 12 and 14 of them were altered respectively in the first and second experiment. IPA also identified an association with nucleic acid metabolism, however, only 4 molecules were detected involving in this function.

Table 9. Statistically significant altered proteins in VLCAD deficient mice in the fed state

Gene symbol	Gene Names	Minimum peptides	Minimum Protein score	Protein Mass	Ratio of protein expression (fed VLCAD-/-: fed VLCAD+/+)
ACADVL	Very long-chain specific acyl-CoA dehydrogenase	9	121	83625	-4.03
CP2A5	Cytochrome P450 2A5	32	567	67139	-3.5
CP239	Cytochrome P450	6	221	65895	-3.3
THIKB	3-ketoacyl-CoA thiolase B, peroxisomal	61	1058	49857	-3.10
SOX	Peroxisomal sarcosine oxidase	17	192	50913	-2.54
NUDT7	Peroxisomal coenzyme A diphosphatase	59	1399	31283	-2.29
GSTP2	Glutathione S-transferase P	2	70	27615	-2.13
MA2B1	Lysosomal alpha-mannosidase	4	96	127768	-2.08
CES3	Carboxylesterase 3	18	227	72626	-2.03
HIUH	5-hydroxyisourate hydrolase	10	85	15514	-1.98
PAHX	Phytanoyl-CoA dioxygenase, peroxisomal	33	309	45339	-1.96
NLTP	Non-specific lipid-transfer protein	210	5205	73857	-1.93
OCTC	Peroxisomal carnitine O-octanoyltransferase	11	184	81602	-1.83
GPDA	Glycerol-3-phosphate dehydrogenase [NAD+]	7	137	45659	-1.80
IDHC	Isocitrate dehydrogenase [NADP] cytoplasmic	9	157	58512	-1.78
GSTP1	Glutathione S-transferase P 1	10	245	27687	-1.76
PPA5	Tartrate-resistant acid phosphatase type 5	3	77	41485	-1.75
ECHP	Peroxisomal bifunctional enzyme	91	1236	92343	-1.74
HAOX1	Hydroxyacid oxidase 1	30	346	48202	-1.70
CATA	Catalase	470	1766	69996	-1.69
CP3AB	Cytochrome P450	14	193	72999	-1.65
ALDOB-	Fructose-bisphosphate aldolase B	13	185	46847	-1.64
CP2CT	Cytochrome P450 2C29	15	241	67197	-1.64
HYES	Epoxide hydrolase 2	38	684	73582	-1.63
THIKA	3-ketoacyl-CoA thiolase A, peroxisomal	71	1060	49465	-1.60
NUD19	Nucleoside diphosphate-linked moiety X motif 19, mitochondrial	8	69	44057	-1.60
PECR	Peroxisomal trans-2-enoyl-CoA reductase	8	111	38399	-1.59
GNS	N-acetylglucosamine-6-sulfatase	6	87	70860	-1.53
AMACR	Alpha-methylacyl-CoA racemase	11	177	48052	-1.53
ACOX1	Peroxisomal acyl-coenzyme A oxidase 1	107	1543	87382	-1.51
CP2DQ	Cytochrome P450 2D26	3	87	64166	-1.50
ASSY	Argininosuccinate synthase	7	94	57128	-1.49
GABT	4-aminobutyrate aminotransferase	44	798	66398	1.33
ATPB	ATP synthase subunit beta	312	5985	63566	1.33

Table 9 Continued

CH60	60 kDa heat shock protein	129	3678	77787	1.33
QCR6	Cytochrome b-c1 complex subunit 6	20	869	13092	1.36
COX41	Cytochrome c oxidase subunit 4 isoform 1	37	240	24431	1.36
QCR1	Cytochrome b-c1 complex subunit 1	48	485	57546	1.37
ETHE1	Protein ETHE1, mitochondrial	7	196	30569	1.39
KMO	Kynurenine 3-monooxygenase	29	461	63169	1.43
NDUV1	NADH dehydrogenase [ubiquinone] flavoprotein 1	4	209	59567	1.45
IMMT	Mitochondrial inner membrane protein	34	624	101206	1.48
M2GD	Dimethylglycine dehydrogenase	68	799	113197	1.48
DHTK1	Probable 2-oxoglutarate dehydrogenase E1 component DHKTD1	10	85	115495	1.83

43 unique proteins were significantly changed ($p \leq 0.05$) in two experimental replicates. They were identified with a minimum of 2 peptides. The table includes the significantly changed proteins with gene symbol, gene names, minimum peptides detected for each protein (Min. Peptides), minimum proteins score, and protein mass and averaged ratios of expression in deficient mice to that in Wild type. p-values were not shown ($p \leq 0.05$, Student's t test. Averaged ratio values were calculated from their corresponding two experiments if they were significant ($p \leq 0.05$) in the same up-regulation or down-regulation directions. Additionally, the protein was considered to show a significant up-regulation or down-regulation if their expression ratios were □1.3 or 0.7, respectively.

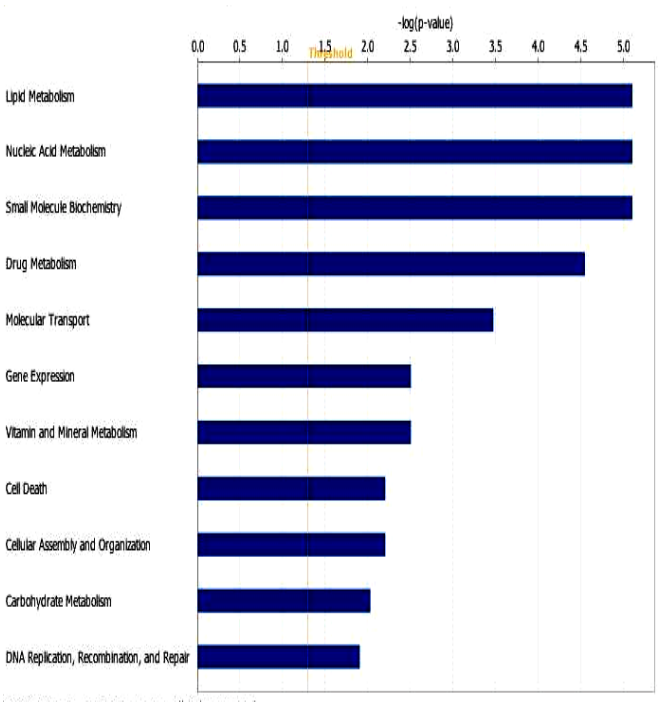

Figure 11. Molecular and cellular functions of altered proteins in fed VLCAD deficient mice

The molecular and cellular functions associated with altered proteins in fasted VLCAD deficient mice were analyzed by IPA. Definitions of functions are provided in Appendix A. The Y-axis denotes the associated functions. The X-axis represents the -log (*p*-value) of the association (Fisher's exact test). The altered proteins were those expressed differentially in fed VLCAD deficient mice as compared to fed wild type mice.

The top-rated network related to the 3 functions including lipid metabolism, molecular transport and small molecule chemistry was identified through Functional Analysis of IPA. A network (Figure 12) was generated by merging two networks with scores of 32 and 8 containing the same functions to provide an overview of the biological functions associated with them. It included a total of 19 proteins of the 27 eligible used for these network analyses. Of these proteins, 17 were enzymes. The same named network of lipid metabolism, molecular transport and small molecule chemistry were previously identified as being significantly altered in short chain acyl-CoA dehydrogenase deficient mice. However, more proteins classified into this network were down-regulated in VLCAD deficient animals than those in SCAD deficient animals.

Several transcription regulators inferred from the lPA knowledge base linked this network (Figure 12). They include the nuclear receptors of *PPARA*, *PPARG* and *PPARGC1A* and *HNF4A*. Expression of *SCP2*, a non-specific lipid transfer protein with multiple functions of protein binding, lipid binding and sterol carrier was decreased in VLCAD deficient mice. Interestingly, it has been previously identified as up-regulated in SCAD deficient mice. HSP60 *(HSPD1)*, a mitochondrial protein functioning in protein folding was identified as up regulated in VLCAD deficient mice as did in SCAD deficient mice in the fed state.

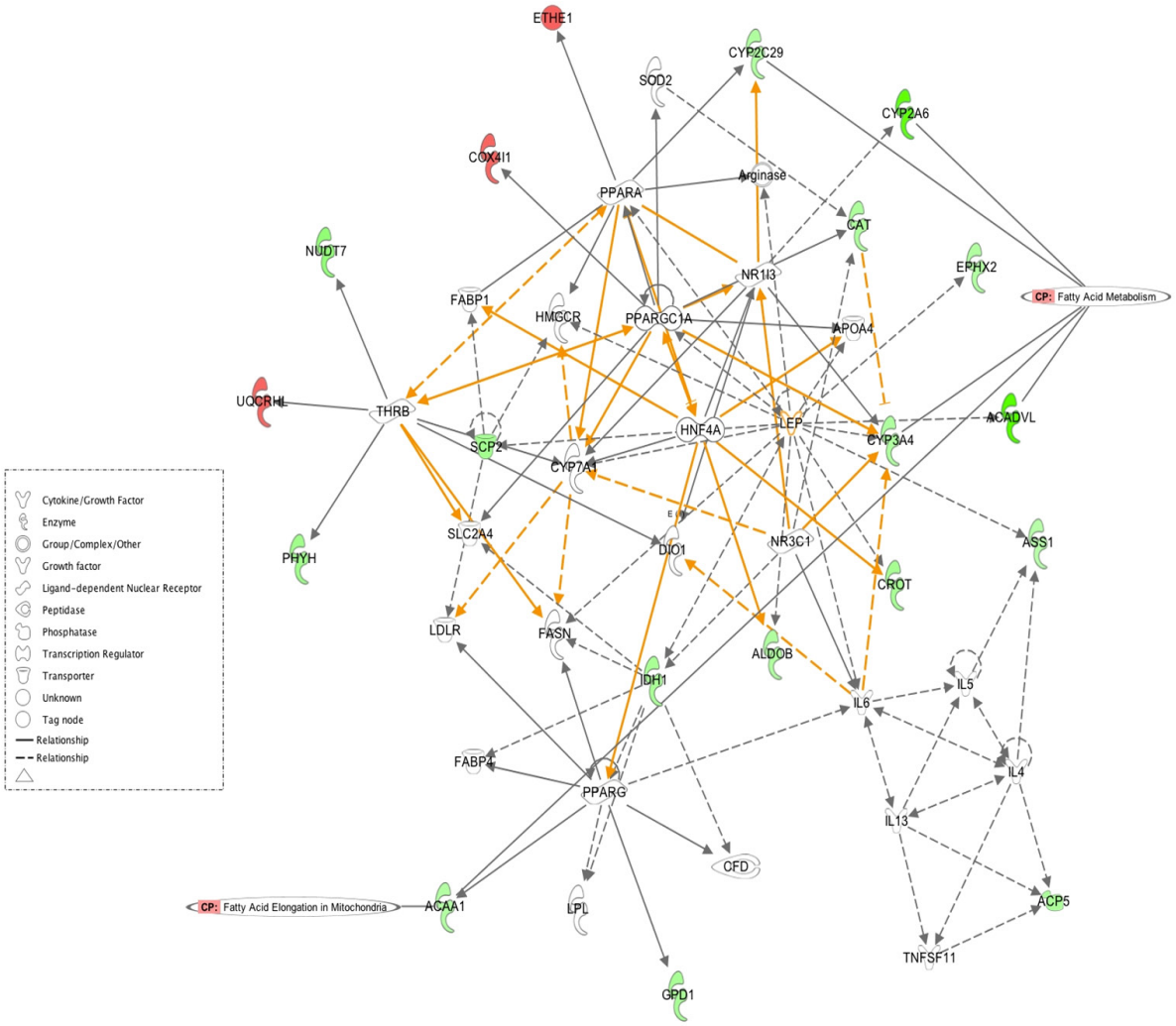

Figure 12. Top-rated network of altered proteins in fed VLCAD deficient mice

This network (lipid metabolism, molecular transport and small molecule chemistry) was generated by IPA. Red nodes indicate that the protein is up-regulated in fed VLCAD deficient mice compared to fed wild type mice. Green indicates that the protein is down-regulated. The color intensity corresponds to the degree of abundance. Proteins in white are those inferred from the Ingenuity Pathways Knowledge Base. The shapes denote the molecular class of the protein. A solid line indicates a direct molecular interaction, and a dashed line indicates an indirect molecular interaction. A full explanation of lines and relationships is provided in Appendix B.

An analysis of the canonical pathways that are associated with quantitatively changed proteins revealed that most of affected pathways were defined by down-regulated proteins (Figure 13.) The canonical pathways that were the most significant in association with altered proteins included the fatty acid metabolism, tryptophan metabolism, bile acid biosynthesis, and fatty acids elongation in the mitochondria. All of these canonical pathways were associated with down-regulated proteins in VLCAD deficient mice. In contrast, the oxidative phosphorylation pathway was significantly associated with up-regulation of components of all four electron transport chain complexes. As expected, fatty acid metabolism was identified as the top significantly changed canonical pathway in the analysis, involving 9 molecules among a total of 117 contained in this pathway. Fatty acid elongation in mitochondria was one of the most significantly associated pathways. Three down-regulated proteins were mapped to fatty acid elongation in mitochondrial with coverage of 19% of molecules in this pathway (3/16 molecules in the IPA knowledge database, $p \leq 0.05$; Figure 13). Additional altered proteins were associated with other diseases pathways such as skeletal and muscular diseases and hepatic system disease.

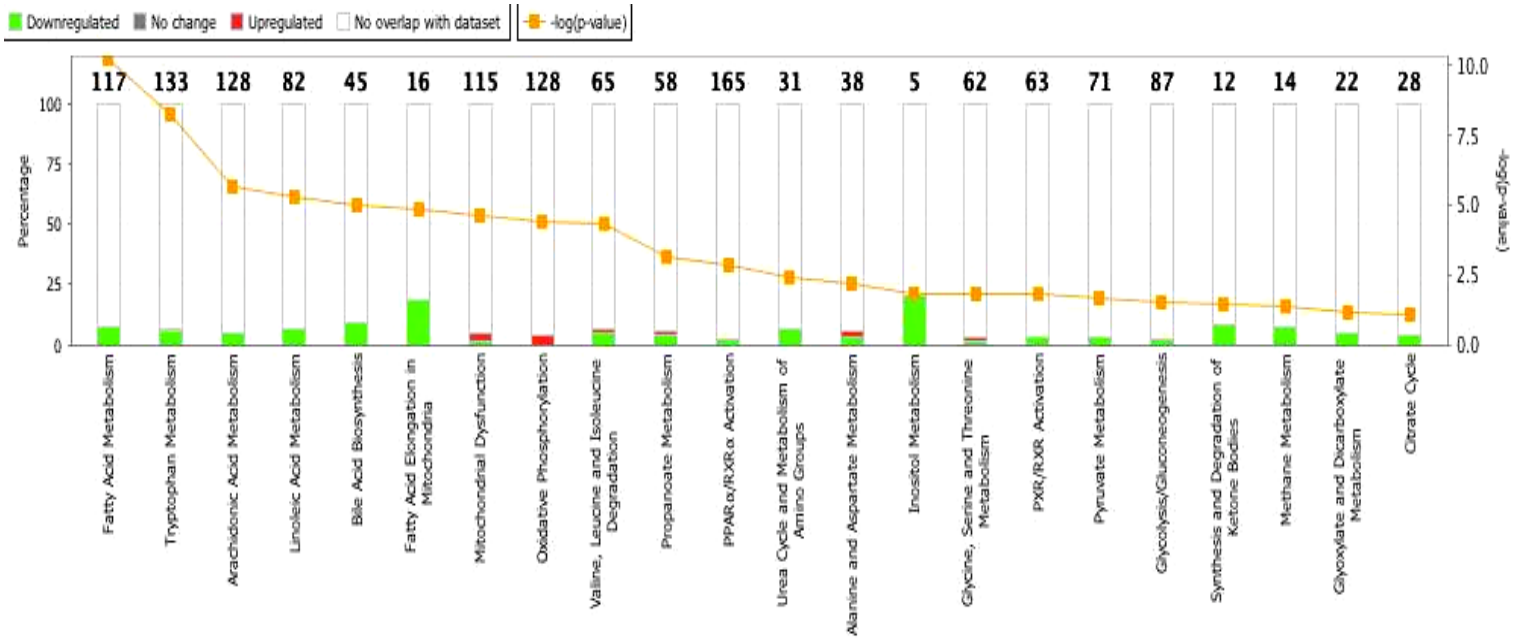

Figure 13. Affected canonical pathways in fed VLCAD deficient mice

The canonical pathways associated with altered proteins in fed VLCAD deficient mice compared to fed wild type mice were generated by IPA. Green indicates that the protein is down-regulated. Red indicates that the protein is up-regulated. Yellow dot represents the -log (*p*-value) of the association (Fisher's exact test). The X-axis denotes the associated functions. The Y-axis represents the percentage of altered proteins among all available molecules in Ingenuity Knowledge database associated with the functional group denoted by X-axis.

3.4.2 Differentially expressed proteins in VLCAD deficient mice in the fasted state

VLCAD deficient patients and mice exhibit an abnormal response to fasting, ultimately resulting in hypoglycemia and a wide range of metabolic derangements. To examine biological changes in the fasted state unique to VLCAD deficiency, the mitochondrial proteomic profiles in VLCAD deficient mice in the fasted state were compared to fasted wild type mice. All of mice were fasted for 16 hours before sacrifice. A total of 286 unambiguous proteins meeting the identification criterion having significance of $p \leq 0.001$ corresponding to a false discovery rate ≤ 0.002 were identified. Only those peptides identified with $\geq 95\%$ confidence were included in the quantification of the parent protein using the algorithm provided by Mascot software. Proteins with at least 2 peptides and mascot score of over 65 were used for further statistical data analysis. To increase the detection of significantly changed proteins, a selection criterion of significance $p \leq 0.10$ (student *t*-test) was set. Among the proteins that were differentially expressed in VLCAD deficient mice, 54 proteins were classified as significant (≤ 0.75-fold or ≥ 1.25-fold change; $p \leq 0.10$) in experiment 3 (Table 3). Detailed information about the identification and quantification information including accession number, gene symbol, number of minimum iTRAQ peptides related to these proteins identified, protein mass, and the minimum protein score obtained in Mascot were described. 31 proteins had decreased expression while 24 were increased (Table 10).

Table 10. Statistically significant altered proteins in VLCAD deficient mice in the fasted state

Gene symbol	Gene Names	Minimum Protein score	Protein Mass	Minimum peptides	Ratio of protein expression (fasted VLCAD -/-:fasted VLCAD+/+)
ACADVL	Very long-chain specific acyl-CoA dehydrogenase, mitochondrial	121	83625	2	-3.41
NUDT7	Peroxisomal coenzyme A diphosphatase	232	31283	10	-2.49
ALDH2	Aldehyde dehydrogenase, mitochondrial	683	66346	76	-2.35
DHRS4	Dehydrogenase/reductase SDR family member	69	35249	9	-2.22
OAT	Ornithine aminotransferase, mitochondrial	1113	56859	55	-2.2
PHS2	Pterin-4-alpha-carbinolamine dehydratase 2	74	17604	3	-2.17
GPX1	Glutathione peroxidase 1	171	25238	19	-2.13
ODO2	Dihydrolipoyllysine-residue succinyltransferase component of 2-oxoglutarate dehydrogenase complex, mitochondrial	607	57453	59	-2.03
IVD	Isovaleryl-CoA dehydrogenase, mitochondrial	193	54527	12	-1.99
CH10	10 kDa heat shock protein, mitochondrial	954	14606	118	-1.99
LACB2	Beta-lactamase-like protein 2	125	38439	7	-1.96
CYC	Cytochrome c, somatic	1336	17470	159	-1.92
NLTP	Non-specific lipid-transfer protein	1162	73587	150	-1.87
MMAB	Cob(I)yrinic acid a,c-diamide adenosyltransferase, mitochondrial	803	31658	13	-1.77
RT31	28S ribosomal protein S31, mitochondrial	440	55597	22	-1.67
THIM	3-ketoacyl-CoA thiolase, mitochondrial	3486	49804	215	-1.61
FUMH	Fumarate hydratase, mitochondrial	500	64559	17	-1.59
NDUV2	NADH dehydrogenase [ubiquinone] flavoprotein 2, mitochondrial	1165	32107	23	-1.56
ETHE1	Protein ETHE1, mitochondrial	467	30569	8	-1.56
AATM	Aspartate aminotransferase, mitochondrial	496	57133	64	-1.5
MCEE	Methylmalonyl-CoA epimerase, mitochondrial	133	23356	2	-1.53
SUOX	Sulfite oxidase, mitochondrial	605	67216	16	-1.51
FABPL	Fatty acid-binding protein, liver	509	19758	32	-1.49
SODM	Superoxide dismutase [Mn], mitochondrial	2476	29943	63	-1.47
SPYA	Serine--pyruvate aminotransferase, mitochondrial	106	52192	10	-1.45
3HIDH	3-hydroxyisobutyrate dehydrogenase, mitochondrial	87	42431	3	-1.43
KAD2	Adenylate kinase 2, mitochondrial	406	33070	23	-1.42
NFU1	NFU1 iron-sulfur cluster scaffold homolog, mitochondrial	107	32430	10	-1.42
SHC1	SHC-transforming protein 1	94	70283	2	-1.40
ETFA	Electron transfer flavoprotein subunit alpha, mitochondrial	3298	43477	65	-1.36
FKBP2	Peptidyl-prolyl cis-trans isomerase FKBP2	106	19427	11	1.32
PDIA1	Protein disulfide-isomerase	3175	72944	125	1.38

Table 10 Continued

GRP78	78 kDa glucose-regulated protein	3997	91330	247	1.44
RMD3	Regulator of microtubule dynamics protein 3	90	59878	3	1.50
QCR7	Cytochrome b-c1 complex subunit 7	241	17474	51	1.56
GLU2B	Glucosidase 2 subunit beta	258	69272	27	1.58
HMCS2	Hydroxymethylglutaryl-CoA synthase, mitochondrial	430	66631	15	1.61
PAHX	Phytanoyl-CoA dioxygenase, peroxisomal	540	45339	26	1.75
PECI	Peroxisomal 3,2-trans-enoyl-CoA isomerase	119	52992	3	1.84
NUCB1	Nucleobindin-1	599	62502	51	1.86
PRDX5	Peroxiredoxin-5, mitochondrial	69	27027	2	1.86
ACNT1	Acyl-coenzyme A amino acid N-acyltransferase	64	54272	3	1.86
MYH9	Myosin-9	462	289864	27	1.86
CP2DA	Cytochrome P450 2D10 /2D16	110	62948	5	1.87
PDIA3	Protein disulfide-isomerase A3	333	72829	49	1.91
RRBP1	Ribosome-binding protein 1	457	244936	38	1.95
ALR	FAD-linked sulfhydryl oxidase ALR	118	26272	2	2.08
ASPG	N(4)-(beta-N-acetylglucosaminyl)-L-asparaginase	107	43192	29	2.12
IMMT	Mitochondrial inner membrane protein	200	101206	19	2.16
TTHY	Transthyretin	549	18900	20	2.21
ACBD5	Acyl-CoA-binding domain-containing protein 5	264	66727	14	2.35
GOLI4	Golgi integral membrane protein 4	86	87736	2	2.35
GANAB	Neutral alpha-glucosidase AB	68	116338	8	3.11
MIA3	Melanoma inhibitory activity protein 3	70	255118	6	3.45

54 unique proteins that were significantly changed ($p \leq 0.10$) in the fasted deficient mice compared to fasted wild type mice. They were identified with a minimum of 2 peptides. The table includes the significantly changed proteins with gene symbol, gene names, minimum peptides detected for each protein, minimum protein score, protein mass and averaged ratios of protein expression in deficient mice to those in wild type mice. *p*-values were not shown ($p \leq 0.10$, Student's *t* test). The protein was considered to be up-regulated or down-regulated if its expression ratio was over 1.25 or less than 0.75, respectively.

Analysis of the biological functions associated with differentially expressed proteins showed that the majority of the proteins with significant alterations were associated with the functional classifications of carbohydrate metabolism, lipid metabolism, molecular transport and small molecule chemistry. Protein degradation and synthesis were also uniquely altered with fasting in VLCAD deficient mice. (Figure 14 and Table 12). The protein networks of lipid metabolism with a score of 24 and cell function and carbohydrate metabolism with a score of 9 were merged as shown in Figure 15. In addition to the network of lipid metabolism, molecular transport and small molecule chemistry, which was identified as being the top-rated network in VLCAD deficient mice, the network of carbohydrate was also identified as one of the top-rated networks of altered proteins in VLCAD deficient mice reflecting the functional response to fasting in VLCAD deficient mice (Figure 15,18).

Examination of proteins with altered expression composing the merged network revealed that the majority of altered proteins in fasted VLCAD deficient mice differed from those changed in fed VLCAD deficient mice. Fewer proteins were included in the network of lipid metabolism identified in fasted VLCAD deficient mice than those included in the same network of lipid metabolism in fed VLCAD deficient mice. Only 2 proteins encoded by *SCP2* and *NUDT7* were decreased in VLCAD deficient mice in both the fed and fasted states. A sulfur dioxygenase encoded by *ETHE1* and located in the mitochondrial matrix was decreased when VLCAD deficient mice were fasted. Superoxide dismutase 2 encoded by *SOD2* was only decreased in the fasted state but maintained a steady level in the fed state.

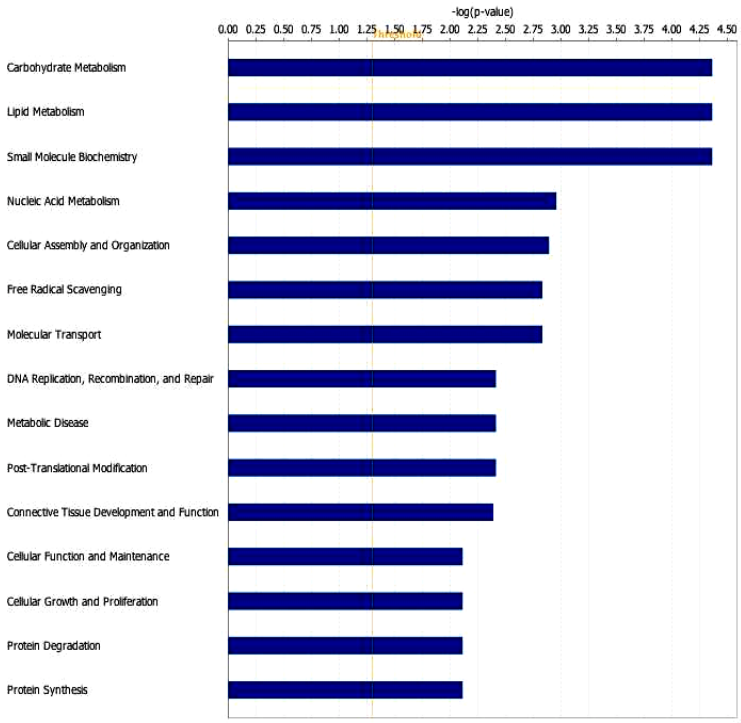

Figure 14. Molecular and cellular functions of altered proteins in fasted VLCAD deficient mice

The molecular and cellular functions associated with altered proteins in fasted VLCAD deficient mice were analyzed by IPA. Definitions of functions are provided in Appendix A. The Y-axis denotes the related functions. The X-axis represents the –log (p-value) of the association (Fisher's exact test). The altered proteins were those expressed differentially in fasted VLCAD deficient mice as compared to fasted wild type mice.

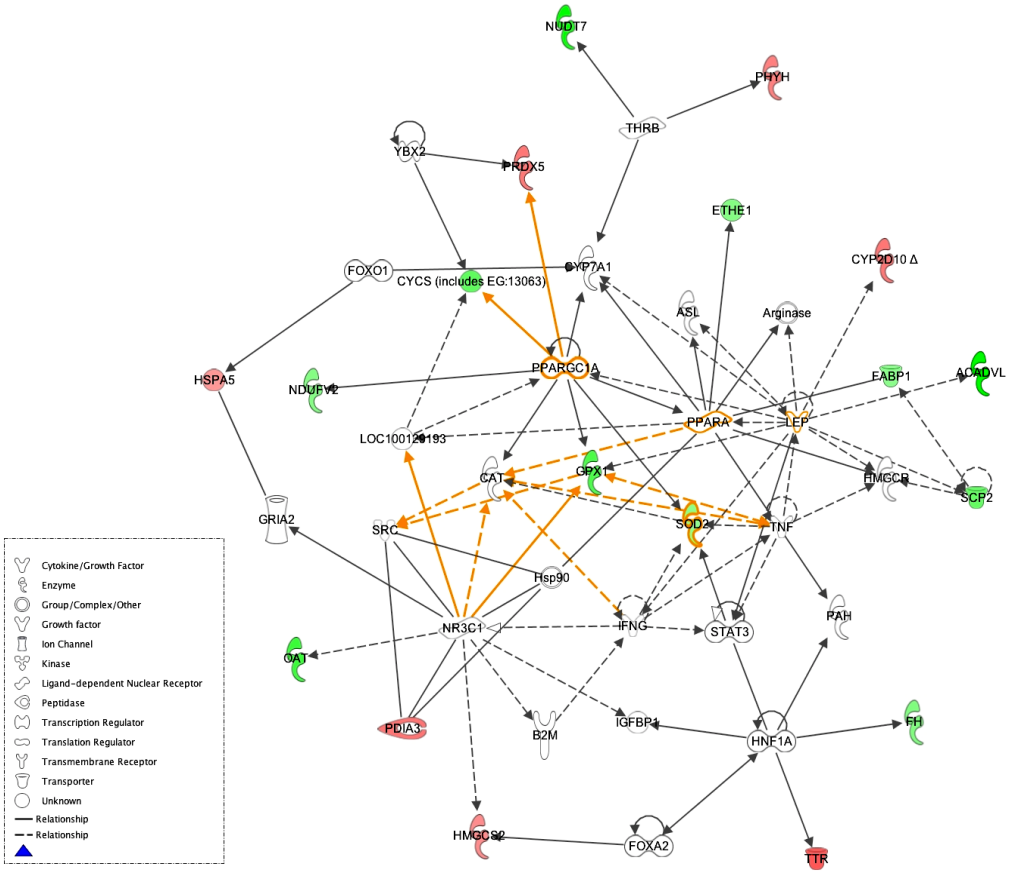

Figure 15. Top-rated networks of altered proteins in fasted VLCAD deficient mice

This network (lipid metabolism, molecular transport and small molecule chemistry, cell function and carbohydrate metabolism) was generated by IPA. Red nodes indicates that the protein is up-regulated in fasted VLCAD deficient mice compared to fasted wild type mice. Green indicates that protein is down-regulated in VLCAD deficient mice in the fasted state. The color intensity corresponds to the degree of abundance. Proteins in white are those inferred from the Ingenuity Pathways Knowledge Base. The shapes denote the molecular class of the protein. A solid line indicates a direct molecular interaction, and a dashed line indicates an indirect molecular interaction.

The most affected canonical pathways associated with quantitatively changed proteins in VLCAD deficient mice in the fasted state were pathways of valine, leucine and isoleucine metabolism, fatty acid metabolism and amino acid metabolism including arginine, proline, tyrosine, phenylalanine and ß-alanine. The citrate acid cycle and propionate metabolism were also significantly altered (Figure 16). Most of the affected pathways encompassed down-regulated proteins. Galactose metabolism was identified as a significantly associated pathway, showing a compensatory pattern associated with up-regulated enzymes including alpha-glucosidase encoded by GANAB and glucosidase II that catalyze the exohydrolysis of 1,4-alpha-glucosidic linkages with release of alpha-glucose.

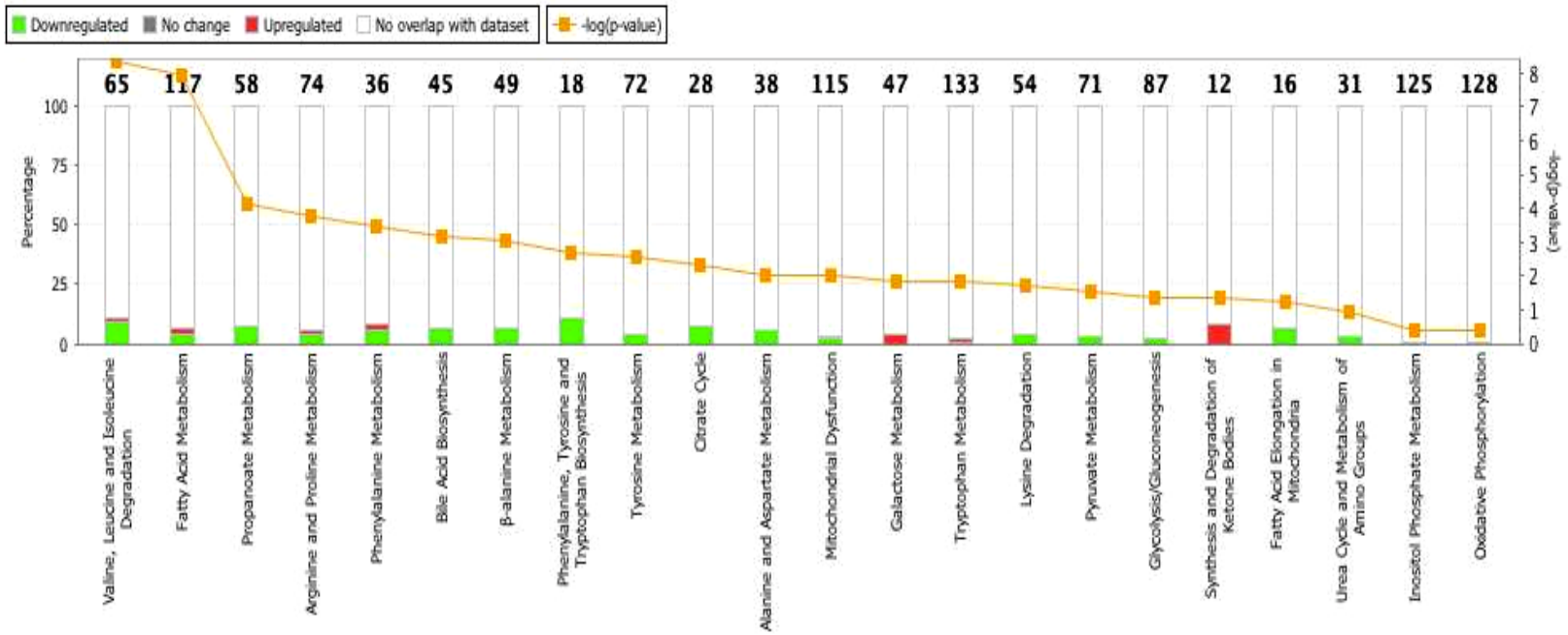

Figure 16. Affected canonical pathways in fasted VLCAD deficient mice

The canonical pathways associated with altered proteins in fasted VLCAD deficient mice compared to fasted wild type mice were generated by IPA Green indicates that the protein is down-regulated. Red indicates that the protein is up-regulated. Yellow dot represents the -log (p-value) of the association (Fisher's exact test). The X-axis denotes the associated functions. The Y-axis represents the percentage of altered proteins among all available molecules in Ingenuity Knowledge database associated with the functional group denoted by X-axis.

3.4.3 Comparison of differentially expressed proteins in VLCAD deficient mice between two feeding states

To evaluate global biological changes induced by fasting and VLCAD deficiency, altered mitochondrial proteins in fasted VLCAD deficient mice were compared with the altered proteins in fed VLCAD deficient mice. The altered proteins in VLCAD deficient mice as compared to wild type mice under the same feeding condition have been identified in the previous two experiments (Table 9 and Table 10). The majority of changed proteins in VLCAD deficient mice in the fasted state differed from those altered proteins identified in VLCAD deficient mice in the fed state, while only a few proteins were identified in both datasets. The *NUDT7* encoding protein was significantly decreased in both states. A non-specific lipid transfer protein encoded by *NLTP (SCP2)* with multiple functions of protein binding, lipid binding and sterol carrier was down regulated in deficient mice in both states. This suggests that non-specific lipid transportation was decreased due to the lack of availability of long-chain fatty acids related to the deficiency of VLCAD regardless of the feeding state. A sulfur dioygenase encoded by *ETHE1* and localized in the mitochondrial matrix functioning in sulfide catabolism was increased in VLCAD deficient mice in the fed while its expression was decreased in VLCAD deficient mice in the fasted state. The heat shock protein HSP60 was up-regulated in VLCAD deficient mice in the fed state, however, it lost its compensatory change in the fasted deficient animals showing no significant change with the protein expression in fasted VLCAD deficient mice. The up-regulation of HSP60 in VLCAD deficient mice in the fed state was consistent with the result from SCAD deficient mice in the fed state, in which, HSP60 was also up-regulated. These results suggest that changes in the functional group of protein binding, ATP binding and protein folding

in mitochondria were related to ACAD deficiencies and that fasting in VLACAD deficiency negated these changes.

The function of Comparison Analysis in IPA was used to further differentiate the effects of VLCAD deficiency and feeding state in deficient and wild type mice. Mitochondrial proteins in VLCAD deficient mice in one of the feeding states were compared to wild type mice in the same feeding state in the previous experiments. All altered proteins identified in each experiment were inputted into the software, and associated functions and canonical pathways altered in each dataset were then compared. Eleven common molecules were identified in the network of lipid metabolism, molecular transport and small molecule chemistry, which rated as the most altered network in both fed and fasted VLCAD deficient mice. This result suggests that lipid metabolism was likely affected by the VLCAD deficiency primarily rather than as a result of fasting as a stressor (Figure 17). It should be noted that altered proteins were defined as significantly changed in VLCAD deficient mice in one of the feeding states when compared to wild type mice in the same feeding state.

Comparison of the top-rated networks containing altered proteins between fasted and fed VLCAD deficient mice reveals that the function categories of cellular function and maintenance and carbohydrate metabolism involved more altered proteins in fasted than in fed VLCAD deficient animals. This unique network of carbohydrate metabolism that was assigned into its high-level functional categories (cellular function, cell maintenance, cell death and carbohydrate metabolism in IPA) was only identified in the fasted state in VLCAD deficient mice (Figure 18) was constructed based primarily on proteins decreased with expression. Functional analysis also demonstrates that carbohydrate metabolism was the most significantly associated functions in VLCAD deficient mice in the fasted state (Table 11, Table 12). This finding suggests that

deficient mice are more vulnerable to fasting stress than the wild type mice consistent with the observation that VLCAD-deficient mice demonstrated a milder phenotype and only developed hypoglycemia after prolonged fasting or cold-induced stress (Cox et al, 2001a).

A fasting induced difference was also seen in the associated functions group of protein degradation and synthesis and amino acid metabolism (Figure 19). However, the significance of global function of the lipid metabolism, small molecule chemistry and cellular assembly and molecular transport was not altered by fasting in VLCAD deficient mice (Figure 11, Figure 14, Table 11 and Table 12).

The significance of canonical pathways of valine, leucine and isoleucine degradation, fatty acid elongation in mitochondria, and oxidative phosphorylation associated to altered proteins in fasted deficient mice were altered in fed deficient mice (Figure 20). These results suggest that the significance differences in these pathways are likely dependant on the feeding status of VLCAD deficient mice (Figure 13, Figure 16 and Figure 20). Fatty acid metabolism, lipid metabolism, mitochondrial dysfunction pathways were altered in mutant animals in the fed state. Amino acid metabolism, especially branched chain amino acid metabolism and carbohydrate metabolism, as well as the fatty acid metabolism were more significantly altered in the fasted deficient mice than in the fed deficient mice. The oxidative phosphorylation pathway was significantly affected based primarily on increased proteins seen in the fed VLCAD deficient mice. However, this pathway was normalized by fasting in VLCAD deficient mice.

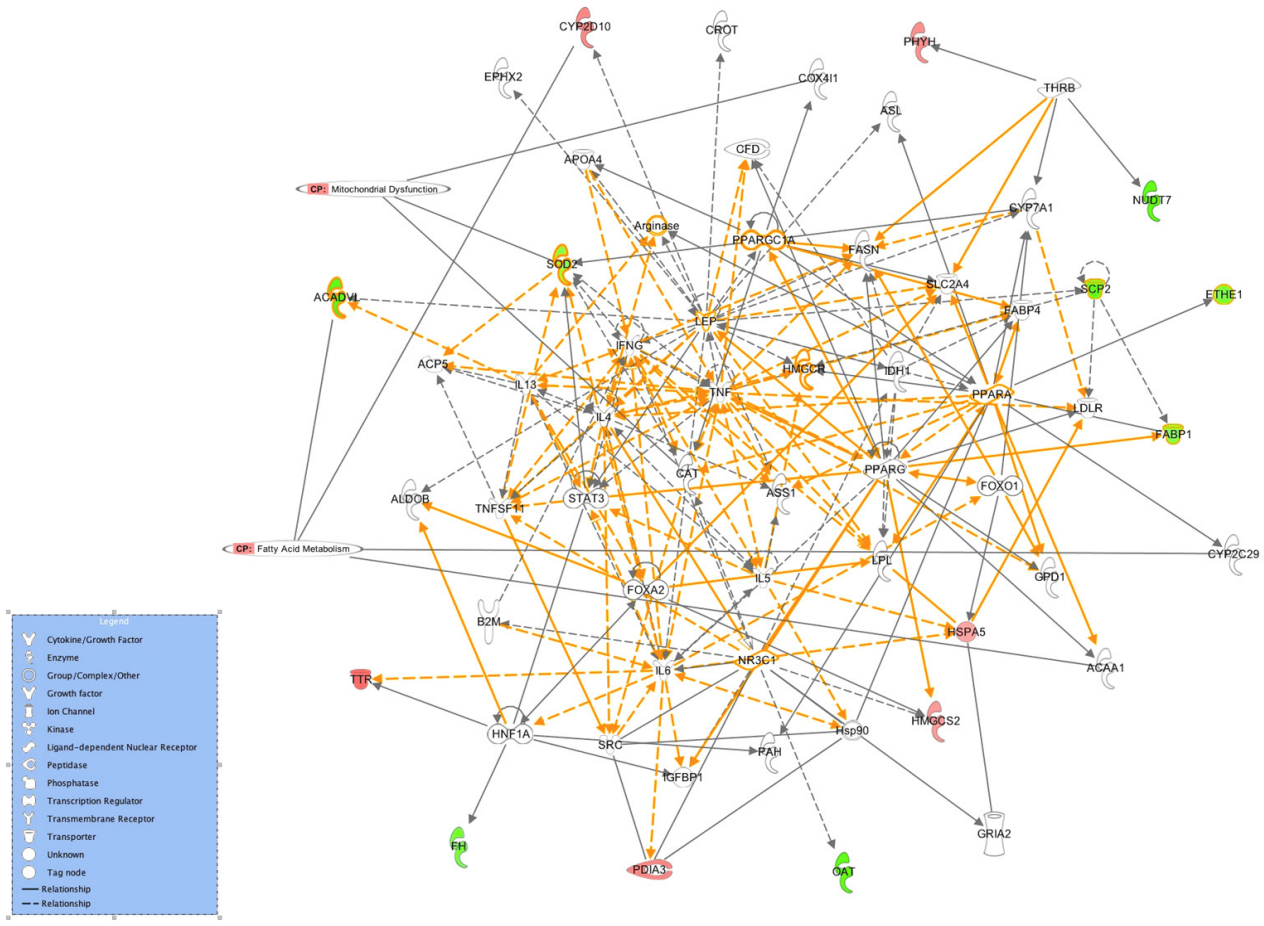

Figure 17. Comparison of the most significant networks associated with altered proteins in fed and fasted VLCAD deficient mice

The same named networks of lipid metabolism, molecular transport and small molecule chemistry associated with altered protein in fed and fasted VLCAD deficient mice were generated and merged by IPA. Red nodes indicate that the protein is up-regulated in VLCAD deficient mice compared to wild type mice. Green indicates that the protein is down-regulated. The color intensity corresponds to the degree of abundance. Proteins in white are those identified through the Ingenuity Pathways Knowledge Base. The shapes denote the molecular class of the protein. A solid line indicates a direct molecular interaction, and a dashed line indicates an indirect molecular interaction.

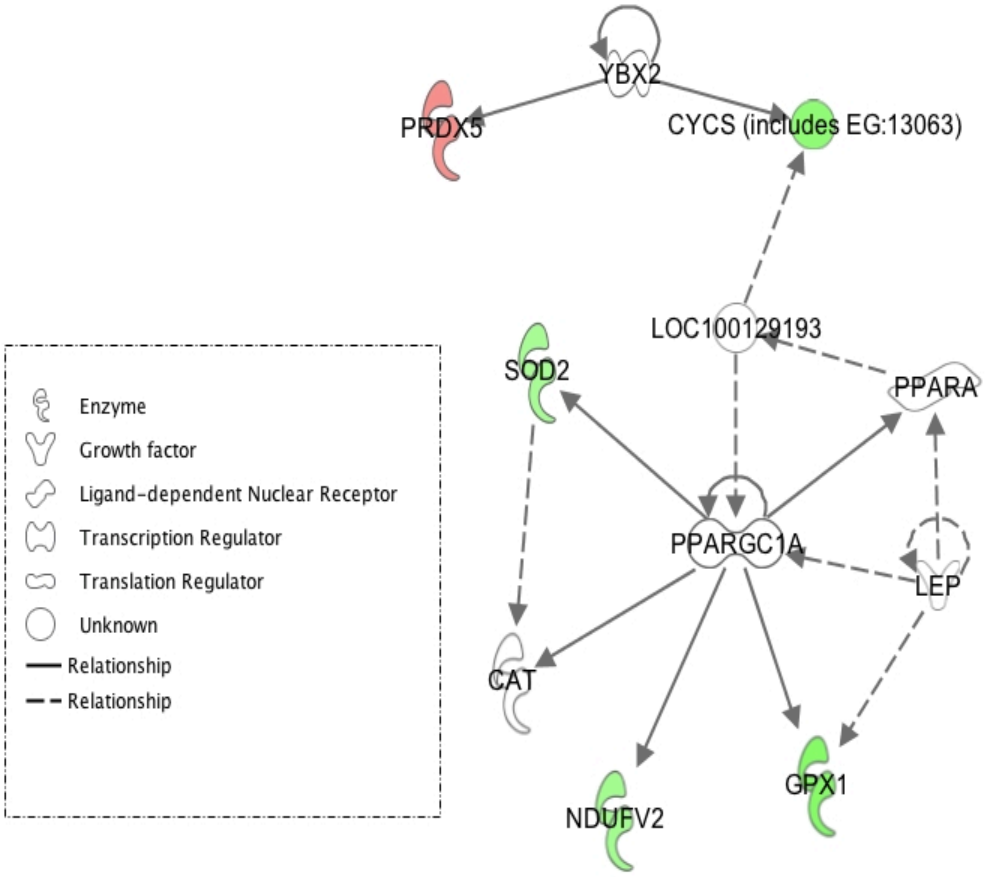

Figure 18. Carbohydrate metabolism (shown with its high-level functional category)

altered in fasted VLCAD deficient mice

This network of cellular function, cell maintenance, death and carbohydrate metabolism associated with altered proteins in fasted VLCAD deficient mice compared to fasted wild type mice was generated by IPA. Red nodes indicate that the protein is up-regulated in the fasted VLCAD deficient mice compared to wild type. Green indicates that protein is down-regulated. The color intensity corresponds to the degree of abundance. Proteins in white are those inferred from the Ingenuity Pathways Knowledge Base. The shapes denote the molecular class of the protein. A solid line indicates a direct molecular interaction, and a dashed line indicates an indirect molecular interaction.

The pathway of synthesis of ketone bodies was not significantly changed either in the fed VLCAD deficient or the fasted mutant mice, consistent with the clinically observation that patients with VLCAD deficiency are hypoketonic when fasted. However, 3-ketoacyl-CoA thiolase A (*ACAA1*), which is involved in the synthesis and degradation of ketone bodies in peroxisomes, was decreased in VLCAD deficient mice in the fed state. In the fasted state, 3-hydroxy-3-methylgutaryl-CoA synthase2 (*HMGCS2*), an enzyme that catalyzes the condensation of acetyl-CoA and acetoacetyl-CoA to form 3-hydroxy-3-methylglutaryl-CoA (HMG-CoA) was increased. Nevertheless, the pathway of ketone bodies production was not affected based on the significance of association in IPA analysis.

Overall, the fatty acid elongation pathway was not altered significantly in the fasting mutant animals despite the finding that several changes occurred in this pathway. The protein encoded by *ACAA2,* which catalyzes the last step of the mitochondrial FAOD, changed in the fasted deficient animals. Three enzymes encoded by *ACAA1, ACAA1b* and *PECR*, which are the acetyl-CoA acyltranserases, and peroxisomal trans-2-2-enoyl-CoA reductase encoded by *NADPH2* in the fatty acid elongation pathway were reduced in the VLCAD mutants in the fed state. However, these changes did not cause the pathway to be significantly altered.

Table 11. Molecular and cellular functions associated with changed proteins in VLCAD deficient mice in the fed state

Name	p-value	# Molecules
Lipid Metabolism	7.83E-06-4.87E-02	12
Nucleic Acid Metabolism	7.83E-06-2.16E-02	4
Small Molecule Biochemistry	7.83E-06-4.87E-02	14
Drug Metabolism	2.84E-05-4.58E-02	7
Molecular Transport	3.36E-04-4.87E-02	6

Table 12. Molecular and cellular functions associated with changed proteins in VLCAD deficient mice in the fasted state

Name	p-value	# Molecules
Carbohydrate Metabolism	4.31E-05-4.88E-02	3
Lipid Metabolism	4.31E-05-4.88E-02	8
Small Molecule Biochemistry	4.31E-05-4.88E-02	12
Nucleic Acid Metabolism	1.09E-03-1.53E-02	4
Cellular Assembly and Organization	1.27E-03-4.51E-02	6

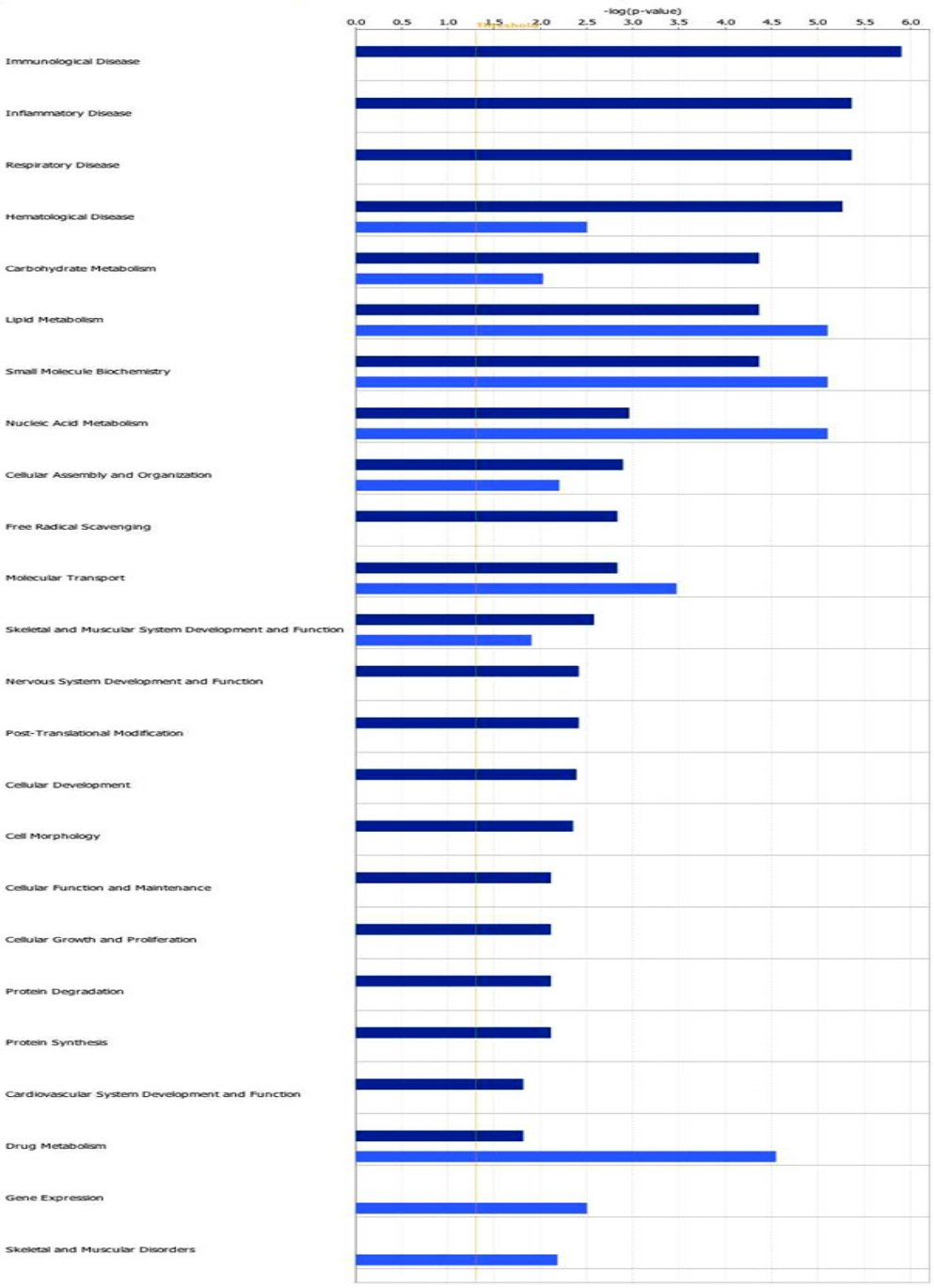

Figure 19. Functions associated with altered proteins in VLCAD deficient mice in fed and fasted states

The dark blue color shows functions associated with altered proteins in fasted VLCAD deficient as compared to fasted wild type mice. The light blue color shows functions associated with altered proteins in fed VLCAD deficient as compared to fed wild type mice. X-axis: significance of associations with observed changed molecules in a specific function (p=0.05).

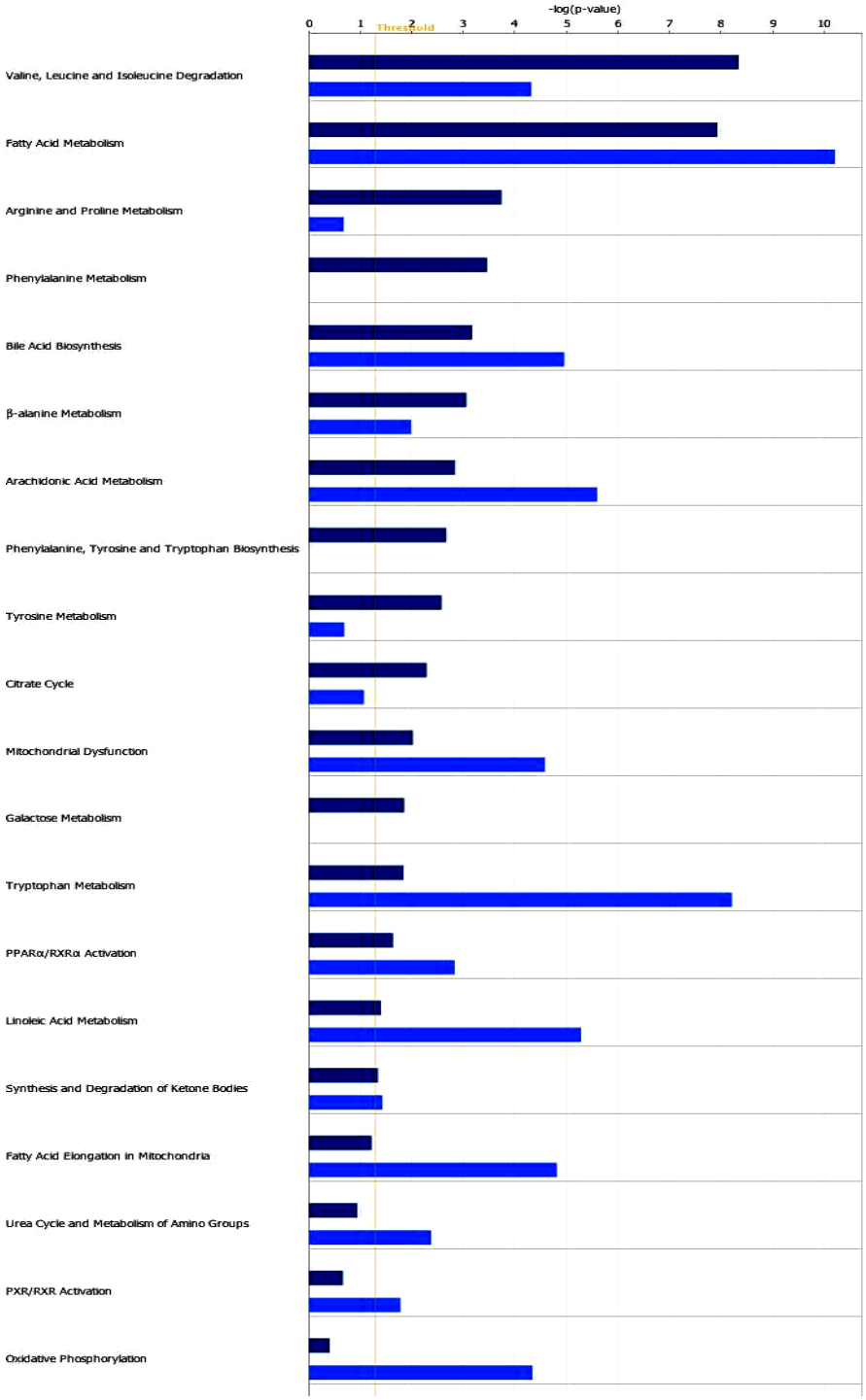

Figure 20. Canonical pathways associated with altered proteins in VLCAD deficient mice in fed and fasted states

The dark blue color shows functions associated with altered proteins in fasted VLCAD deficient as compared to fasted wild type mice. The light blue color shows functions associated with altered proteins in fed VLCAD deficient as compared to fed wild type mice. X-axis: significance of associations with observed changed molecules in a specific function ($p \leq 0.05$).

3.4.4 Fasting effects on deficient and wild type mice

To further explore the differential effect of fasting on wild type and VLCAD deficient mice, two additional experiments were performed comparing proteomic profiles in the mitochondria isolated from both genotypes between the fasting and fed states. One of experiments (Experiment 4 in Table 8) compared the proteomic profiles of mitochondria in VLCAD deficient mice in the fasted state to the profiles of deficient mice in the fed state. Another experiment (Experiment 5 in Table 8) was performed to compare the proteomic profiles of wild type animals in the fasted state to the profiles of wild type animals in the fed state.

Among the proteins that were differentially expressed in VLCAD deficient mice in the fasted state compared to those in the fed state, 35 were classified as significant ($p \leq 0.05$, Student's test, 1 side) with over 1.25-fold change or less than 0.75-fold change (Table 11). Using the same selection criteria, 41 proteins were classified as significantly changed in wild-type mice in the fasted state (Table 13). The detailed information on significantly altered proteins in each experiment was provided in Table 13 and Table 14. Most of altered proteins in both datasets were down-regulated, and the majority of altered proteins in fasted VLCAD deficient mice were different from those that were altered in fasted wild type animals. Few proteins were similarly altered with fasting in both genotype animals. One such protein was acetyl-CoA acyltransferase 2 encoded by *ACAA2*, which catalyzes the last step of mitochondrial fatty acid oxidation. It was up regulated in wild type and mutant mice with fasting. The data from previous experiments had showed that *ACAA2* was down-regulated in the deficiency of VLCAD in the fed state (Table 9).

Table 13. Statistically significant altered proteins in fasted VLCAD deficient mice compared to fed VLCAD deficient mice

Gene symbol	Gene Name	Protein score	Protein mass	Minimum peptides	Averaged ratio FKO: NKO
M2GD	Dimethylglycine dehydrogenase,	1678	113197	111	-2.97
PHB	Prohibitin	831	33803	5	-2.90
CP2F2	Cytochrome P450 2F2	357	62789	3	-2.39
SARDH	Sarcosine dehydrogenase, mitochondrial	875	110963	38	-2.39
CPSM	Carbamoyl-phosphate synthase [ammonia], mitochondrial	5588	196508	294	-2.26
CP2DQ	Cytochrome P450 2D26	78	64166	2	-2.13
NDUA4	NADH dehydrogenase [ubiquinone] 1 alpha subcomplex subunit 4	187	12059	8	-2.11
QCR1	Cytochrome b-c1 complex subunit 1	76	57546	9	-1.96
ABCD3	ATP-binding cassette sub-family D member 3	594	88929	21	-1.88
COX2	Cytochrome c oxidase subunit 2	419	27922	18	-1.82
ATPA	ATP synthase subunit alpha	9622	69542	265	-1.82
QCR2	Cytochrome b-c1 complex subunit 2	113	56769	5	-1.82
CISY	Citrate synthase	103	60451	3	-1.77
PYC	Pyruvate carboxylase	4282	148148	67	-1.74
PRDX5	Peroxiredoxin-5, mitochondrial	361	27027	8	-1.71
THIL	Acetyl-CoA acetyltransferase,	744	54798	24	-1.68
PCCB	Propionyl-CoA carboxylase beta chain, mitochondrial	1616	66164	8	-1.66
ECHA	Trifunctional enzyme subunit alpha	3713	103551	43	-1.6
KAD2	Adenylate kinase 2, mitochondrial	464	33070	21	-1.50
ECH1	Delta(3,5)-Delta(2,4)-dienoyl-CoA isomerase, mitochondrial	1494	43064	6	-1.42
HMGCL	Hydroxymethylglutaryl-CoA lyase	468	40895	2	-1.42
CY1	Cytochrome c1, heme protein	827	40052	19	-1.37
DLDH	Dihydrolipoyl dehydrogenase, mitochondrial	80	66516	11	-1.35
ALDH2	Aldehyde dehydrogenase, mitochondrial	2155	66346	72	-1.32
MDHM	Malate dehydrogenase, mitochondrial	27170	43866	380	1.36
CH10	10 kDa heat shock protein, mitochondrial	406	14606	43	1.38
PDIA1	Protein disulfide-isomerase	3853	72944	118	1.41
RT36	28S ribosomal protein S36, mitochondrial	239	14136	31	1.42
GRP78	78 kDa glucose-regulated protein	3498	91330	23	1.58
GPX1	Glutathione peroxidase 1	246	25238	8	1.65
THIM	3-ketoacyl-CoA thiolase, mitochondrial	12121	49804	185	1.67
SODC	Superoxide dismutase [Cu-Zn]	3257	19113	47	1.73
UK114	Ribonuclease UK114	224	17030	2	1.89

Table 13 Continued

MUP2	Major urinary protein 2	722	24835	75	2.38
LACB2	Beta-lactamase-like protein 2	64	38439	3	2.43

35 unique proteins that were significantly changed ($p \leq 0.10$, Student's t-test) in the fasted deficient mice compared to fed deficient mice. They were identified with a minimum of 2 peptides. The table includes the significantly changed proteins with gene symbol, gene names, minimum peptides detected for each protein, minimum proteins score, protein mass and averaged ratios of protein expression in fasted VLCAD deficient mice versus in fed VLCAD deficient mice (FKO: NKO). *p*-values were not shown ($p \leq 0.10$, Student's t test). The protein ratio was considered to be a significant up-regulation or down-regulation if its expression ratio was ≥ 1.25 or ≤ 0.75, respectively. FKO (protein expression in VLCAD deficient mice in the fasted state). NKO (protein expression in VLCAD deficient mice in the fed state).

Table 14. . Statistically significant altered proteins in fasted wild type mice compared to fed wild type mice

Gene symbol	Gene names	Protein score	Protein mass	Minimum peptides	Averaged ratio FWT:NWT
NUD12	Peroxisomal NADH pyrophosphatase NUDT12	144	61156	3	-2.54
ENPL	Endoplasmin	593	116072	21	-2.46
LICH	Lysosomal acid lipase/cholesteryl ester hydrolase	86	53052	4	-2.38
GANAB	Neutral alpha-glucosidase AB	62	116338	2	-2.37
CP2D9	Cytochrome P450 2D9	97	62968	3	-2.25
UD2A1	UDP-glucuronosyltransferase 2A1	69	73117	4	-2.24
UD2A2	UDP-glucuronosyltransferase 2A2	69	71552	4	-2.24
NDUA4	NADH dehydrogenase [ubiquinone] 1 alpha subcomplex subunit 4	115	12059	2	-2.23
MMSA	Methylmalonate-semialdehyde dehydrogenase [acylating],	700	67981	11	-2.21
UD2A3	UDP-glucuronosyltransferase 2A3	69	72933	3	-2.07
UDB17	UDP-glucuronosyltransferase 2B17	69	73444	3	-2.07
NDUA9	NADH dehydrogenase [ubiquinone] 1 alpha subcomplex subunit 9,	123	48963	2	-2.0
AL3A2	Fatty aldehyde dehydrogenase	214	64315	2	-1.80
PDIA3	Protein disulfide-isomerase A3	337	72829	28	-1.77
EFGM	Elongation factor G, mitochondrial	260	98392	14	-1.72
CP3AB	Cytochrome P450 3A11	300	72999	19	-1.72
BDH	D-beta-hydroxybutyrate dehydrogenase	216	45837	7	-1.63
NLTP	Non-specific lipid-transfer protein	2066	73587	43	-1.63
ECHA	Trifunctional enzyme subunit alpha,	554	103551	13	-1.60
THIKB	3-ketoacyl-CoA thiolase B, peroxisomal	1044	49857	36	-1.59
HYES	Epoxide hydrolase 2	1422	73582	14	-1.56
ALDH2	Aldehyde dehydrogenase,	1918	66346	64	-1.55
THIKA	3-ketoacyl-CoA thiolase A, peroxisomal	1460	49465	39	-1.55
CYB5	Cytochrome b5	1004	18578	13	-1.53
PAHX	Phytanoyl-CoA dioxygenase, peroxisomal	845	45339	18	-1.49
RPN1	Dolichyl-diphosphooligosaccharide--protein glycosyltransferase subunit 1	179	81400	7	-1.48
THTR	Thiosulfate sulfurtransferase	1827	38192	15	-1.44
RETST	All-trans-retinol 13,14-reductase	489	80565	13	-1.42
DHB4	Peroxisomal multifunctional enzyme type 2	2156	95056	12	-1.40
AL4A1	Delta-1-pyrroline-5-carboxylate dehydrogenase, mitochondrial	550	72482	13	-1.39
GRP78	78 kDa glucose-regulated protein	4429	91330	78	-1.38
TRI14	Tripartite motif-containing protein 14	213	55987	8	-1.36
PRDX3	Thioredoxin-dependent peroxide reductase, mitochondrial	111	32552	7	1.38

Table 14 Continued

ETHE1	Protein ETHE1, mitochondrial	695	30569	3	1.44
THIM	3-ketoacyl-CoA thiolase,	3925	49804	94	1.48
CBR1	Carbonyl reductase [NADPH] 1	198	37240	4	1.59
CH10	10 kDa heat shock protein	165	14606	14	1.65
MUTA	Methylmalonyl-CoA mutase,	343	98491	4	1.71
ACBP	Acyl-CoA-binding protein	146	14861	4	1.82
NDUV2	NADH dehydrogenase [ubiquinone] flavoprotein 2	1679	32107	11	1.90
BOLA1	BolA-like protein 1	102	16029	4	2.48

41 unique proteins that were significantly changed ($p \leq 0.10$, Student's *t*-test) in the fasted wild type mice compared to fed wild type mice. They were identified with a minimum of 2 peptides. The table includes the significantly changed proteins with gene symbol, gene names, minimum peptides detected for each protein, minimum proteins score, protein mass and averaged ratios of protein expression in fasted wild type mice versus in fed wild type mice (FWT: NWT). *p*-values were not shown ($p \leq 0.10$, Student's t test). The protein ratio was considered to be a significant up-regulation or down-regulation if its expression ratio was ≥ 1.25 or ≤ 0.75, respectively. FWT (protein expression in wild type mice in the fasted state). NWT (protein expression in wild type mice in the fed state).

Two mitochondrial chaperonin proteins were differently altered in these experiments (Experiment 4 and 5) and the previous ones (Experiment 1, 2 and 3). Chaperonin 10 (*HSPE1*) was up-regulated in both VLCAD deficient and wild type mice in the fasted state as compared to the fed state, but was down-regulated in fasted VLCAD deficient mice as compared to the fasted wild type mice. However, this protein was similarly expressed in fed VLCAD deficient and fed wild type mice. HSP60 (*HSPD1*), a HSP10(*HSPE1)* co-chaperonin, showed a different pattern of changes. HSP60 showed higher expressions in VLCAD deficient mice in the fed state compared to fed wild type animals but no changes in fasted VLCAD deficient mice as compared to fasted wild type mice. Its expression was unchanged in fasted animals of either genotype compared to the fed state.

HADHA encodes the alpha subunit of the mitochondrial trifunctional protein responsible for catalyzing the last three steps of mitochondrial ß-oxidation for long chain substrates. This enzyme of hydroxyacyl-CoA dehydrogenase is also a member of acetyl-CoA C-acetyltransferase family. It was down-regulated in both genotypic mice in the fasted state as compared to the fed state (Experiment 4 and 5). Further examination of the data in fasted VLCAD deficient mice showed that it was down-regulated in fasted VLCAD deficient mice (averaged ratio=0.75) as compared to fasted wild type animals, but that this change (*p*-value=0.08) didn't meet the criteria for significance. *HADHA* expression level was unchanged in VLCAD deficient mice in the fed state compared to fed wild type animals, indicating that the down-regulation of this enzyme was due to fasting rather than VLCAD deficiency. A similar pattern of change was seen in *ALDH2*, which was down-regulated in fasted animals as compared to normal fed animals regardless of the genotypes. Its down-regulation was also observed in fasted VLCAD deficient mice compared to the fasted wild type mice. However, there is no change observed in fed VLCAD deficient mice

as compared to the fed wild type mice. Therefore, fasting had effects on the down-regulation of this enzyme in either type of animals but it is difficult to clarify if it had the same degree of effects on deficient animals as it did on the wild type animals.

The merged networks of altered proteins from two datasets (Experiment 4 and 5) are shown in Figure 9 and 10. The top rated network of lipid metabolism and molecular transport was identified in each data set. A few common molecules including proteins encoded by *HSPA5*, *HADHA* and *GPX1* were shared in two dataset. However, in merged networks, the majority of these common molecules were inferred from the Ingenuity knowledge database that linked the connections between the changed proteins. They include the nuclear receptor *PPARA*, the transcription regulator *PPARGC14*, the transporter *APOA4* and the growth factor leptin. Several of these linkers were also inferred from the top-rated network of altered proteins in fasted VLCAD deficient mice and fed VLCAD deficient mice (Figure 12 and Figure 15). The results from both datasets clearly showed that fasting have significant effects on fatty acid elongation in the mitochondria and synthesis and degradation of ketone bodies.

The toxic analysis function of the IPA software was designed to characterize specific organ system changes related to exposure to suspected toxins. This analysis was utilized to identify patterns of altered protein expression in VLCAD deficient mice suggestive of pathologic changes resulting from primary VLCAD deficiency or induced secondary abnormalities. The prediction of toxicity based on the pattern of altered proteins in fed VLCAD deficient mice and in the fasted VLCAD deficient mice is shown in Figure 23. Interestingly, a pattern of protein changes indicative of cardiac damage was more pronounced in fasted VLCAD deficient mice than in fed deficient animals, consistent with the known risk for development of cardiomyopathy in VLCAD deficient patients under metabolic stress. A pattern of protein changes consistent with

liver steatosis was present in fed VLCAD deficient mice and did not change with fasting suggesting that avoidance of fasting may not alter liver dysfunction in these patients. Of note, fasting effects on liver and heart were slightly seen in the patterns of protein expression in mice of both genotypes, but were more significantly associated with liver steatosis in deficient mice (Figure 24). The pattern of protein changes suggesting liver steatosis was slightly more exaggerated in fasted VLCAD deficient mice than in fasted wild type, and a greater protective response to fasting was seen in the liver of wild type animals.

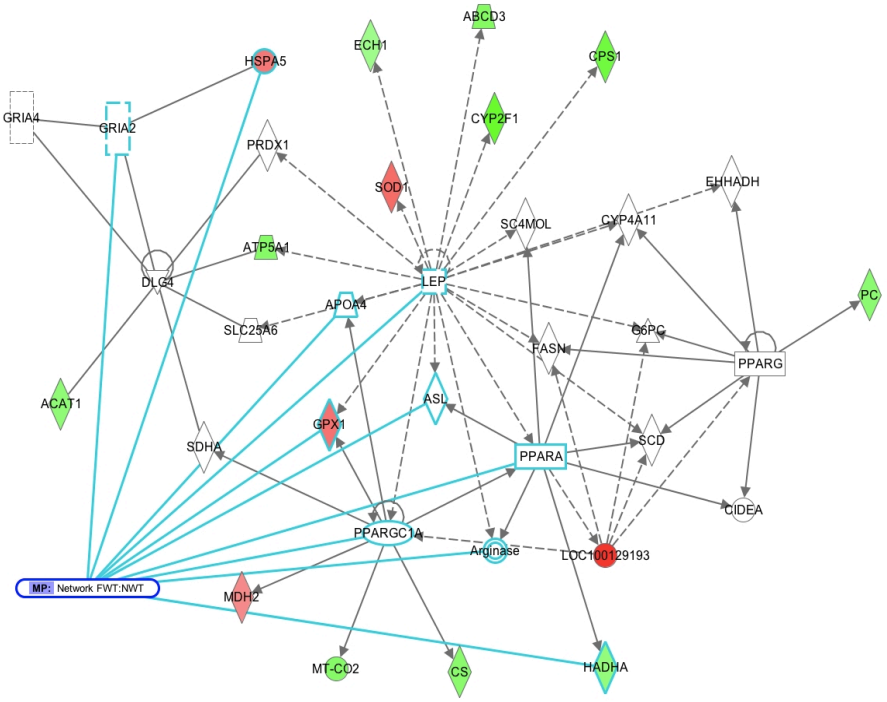

Figure 21. Merged networks of altered proteins with fasting

The network of altered proteins with fasting on VLCAD deficient mice (proteome profile in fasted VLCAD deficient mice was compared to that in fed VLCAD deficient mice) was overlaid with the effects of fasting on wild type mice (proteome profile in fasted wild type mice was compared to that in fed wild type). Red nodes indicate that the protein is up-regulated in the fasted VLCAD deficient mice as compared to fed deficient mice. Green indicates that the protein is down-regulated in the fasted VLCAD deficient mice. The color intensity corresponds to the degree of abundance. Proteins in white are those inferred from the Ingenuity Pathways Knowledge Base. The shapes denote the molecular class of the protein. A solid line indicates a direct molecular interaction, and a dashed line indicates an indirect molecular interaction. Solid blue line highlights the molecules shown in the network of altered proteins in fasted deficient mice as compared to fed deficient mice.

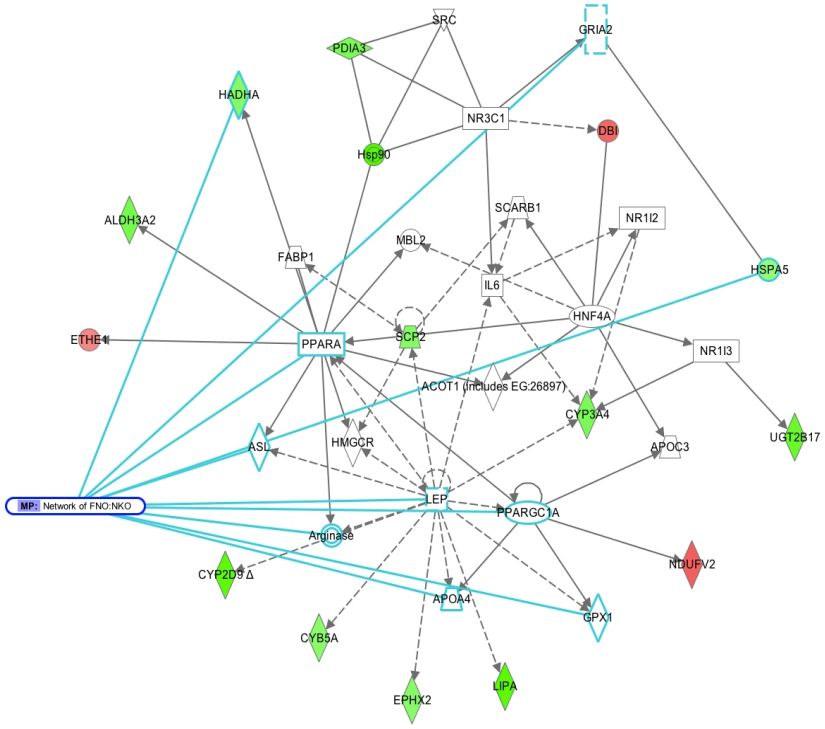

Figure 22. Merged networks of altered proteins with fasting

The network of altered proteins with fasting on wild type mice (proteome profile in fasted wild type mice was compared to that in fed wild type) was overlaid with the effects on VLCAD deficient mice (proteome profile in fasted VLCAD deficient mice was compared to that in fed VLCAD deficient mice). Red nodes indicate that the protein is up-regulated in the fasted wild type as compared to fed wild type mice. Green indicates that the protein is down-regulated. The color intensity corresponds to the degree of abundance. Proteins in white are those inferred from the Ingenuity Pathways Knowledge Base. The shapes denote the molecular class of the protein. A solid line indicates a direct molecular interaction, and a dashed line indicates an indirect molecular interaction. Solid blue line highlights the molecules shown in the network of altered proteins in fasted wild type mice as compared to fed wild type mice.

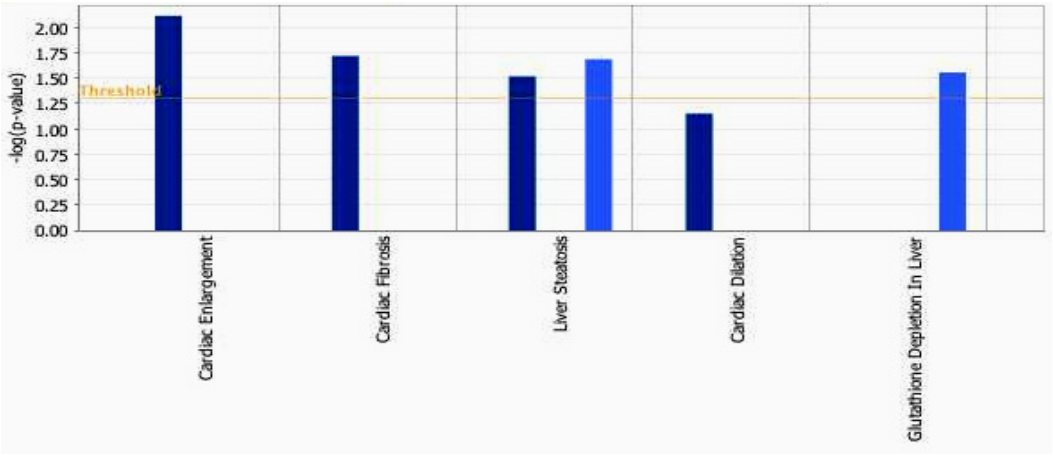

Figure 23. Prediction of toxicity of altered proteins in VLCAD deficient mice in fasted and fed states

Toxicity analysis was performed in IPA based on the pattern of altered proteins in VLCAD deficient mice in both fasting and fed states. Dark blue color denotes toxicity predicted by changed proteins in fasted VLCAD deficient mice compared to fasted wild type mice. Light blue shows toxicity predicted by changed proteins in fed VLCAD deficient mice compared to fasted wild type mice. Y-axis: significance of toxicity arising from the changed proteins($p \leq 0.05$).

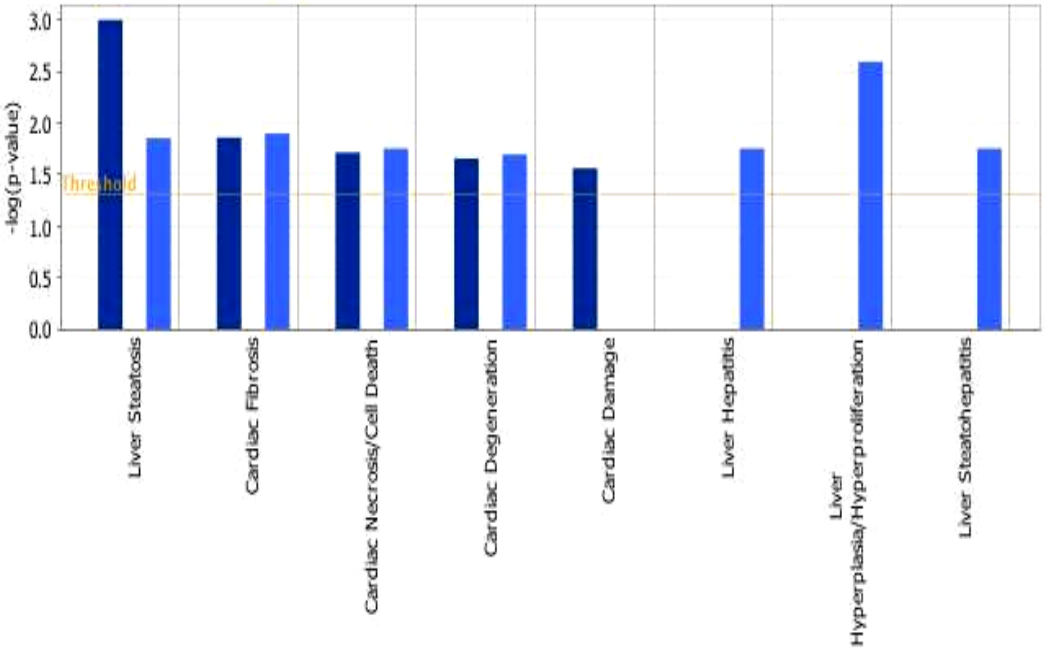

Figure 24. Prediction of toxicity of altered proteins due to fasting in VLCAD deficient and wild type mice

Toxicity analysis was performed in IPA based on the pattern of altered proteins due to fasting in VLCAD deficient mice and wild type mice. Light blue shows toxicity predicted by changed proteins in VLCAD deficient mice due to fasting. Dark blue color denotes toxicity predicted by changed proteins in wild type mice due to fasting.

3.5 DISCUSSION

The underlying mechanism of clinical and genetic heterogeneity in VLCAD deficiency is unknown, and likely includes genetic and environmental factors, as well as their interaction. To explore the biological effects of these factors and their relationships to the disease manifestation, proteomic changes in mitochondria in VLCAD deficient mice in the fasting and fed states and changes in mitochondrial protein profiles induced by fasting in mutant and wild type animals were quantitatively measured. The novelty of this study lies in the use of animal models to screen for global biological changes related to genotypic and environmental changes and to explore the relevance of alterations in specific functions and pathways using well defined control groups. It is the first large scale quantitative proteomics profiling of VLCAD deficient animals, and as such it has allowed us to characterize the molecular impact of physiologic stress in these animals and investigate genetic-environmental interactions at a global level. The mitochondrial proteome of wild type and VLCAD deficient mice while fed and fasted, and each type of mice in the fed state to the fasted stated were compared. The results revealed expression changes in numerous proteins associated with lipid metabolism in both the fed and fasted states and with deficiency regardless of feeding state. In the fed state, the most significantly changed proteins in VLCAD deficient mice were those involved in fatty acid metabolism, while alterations in amino acid metabolism and fatty acid metabolism predominated in the fasted mutant mice. The proteins that were altered only with fasting induction and those that were modified with the deficiency of *ACADVL* alone were identified by comparing altered proteins from different pair-wise experiments. The evaluation of fasting effects on VLCAD deficient and wild type mice within independent experiments offers a better understanding of these genotype specific

environmentally induced changes, which will provide greater insight into the mechanism and possible points of therapeutic intervention in this disorder.

The network of lipid metabolism, molecular transport and small molecule chemistry was identified as altered in SCAD deficient mice (Chapter 2). The same named network was shown to be the top-rated network associated with altered proteins in VLCAD deficient mice as compared to wild type mice. However, more down-regulated proteins were detected in VLCAD deficiency than in SCAD deficiency. This observation implies a more severe physiologic impact caused by deficiency of VLCAD than SCAD, in keeping with the more severe clinical phenotypes seen in patients with VLCAD deficiency. The diverse changes in canonical pathways of energy metabolism in VLCAD deficiency highlight the alterations of fatty acid metabolism in this disorder, while changes in the mitochondrial proteome in fasted deficient mice identify secondary changes that occur due to fasting. *NLTP* (SCP2), encoding a non-specific lipid transfer protein with multiple functions of protein binding, lipid binding and sterol carrier, was decreased in VLCAD deficient mice in the fed and fasted states suggesting that lipid transport was decreased due to the derangement of metabolism of long-chain fatty acids arising from the deficiency of VLCAD. However, the same protein was up-regulated in SCAD deficient mice indicating that it was responding to a different, unknown metabolic signal.

HSP60, a mitochondrial chaperonin protein encoded by *HSPD1*, was up-regulated in fed VLCAD and SCAD deficient mice suggesting that mitochondrial protein folding is affected in both deficiencies. However, no changes were identified in fasted deficient animals as compared to fasted wild type animals. It did not alter in either VLCAD deficient animals or wild type animals with fasting when compared to their non-fasted counterparts suggesting the physiologic stress (fasting) is unrelated to its change. Therefore, the disappearance of compensatory change

of HSP60 in fasted deficient animals indicates that interaction of gene (*ACADVL*) and environment (fasting) may exist in the expression of HSP60. It should be noted that lack of significant changes identified in the fasted animals might simply be due to the difficulty in detecting of proteins with low levels of expression in the fasted samples. In contrast, chaperonin 10 (*HSPE1*), another mitochondrial chaperonin protein, was up-regulated in the fasting state in both VLCAD deficient and wild type animals as compared to the fed state indicating that fasting impacts the expression of chaperonin 10. However, it was down-regulated in fasted VLCAD deficient mice as compared to the fasted wild type mice, again indicating the interaction of gene (*ACADVL*) and environment (fasting) in the expression of *HSPE1*. Thus, mitochondrial folding appears to adjust to the environmental conditions (i.e., fasting) and may provide another secondary pathway for modulation of phenotype in various disorders under different conditions.

Comparison of the findings with alterations of proteins or encoding genes altered in other diseases with changes seen in VLCAD deficient mice helps provide some insight into the pathophysiology of VLCAD deficiency. *ASS1* (argininosuccinic acid synthase 1) and *PIPOX* (with a synonymous name of *SOX*, peroxisomal sarcosine oxidase) have been shown to have changes associated with skeletal and muscular diseases. Defects in *GPD1* (glycerol-3-phoshate dehydrogenase 1) and *PHYH* (phytanoyl-COA hydroxylase 2) and *SOD2* (superoxide dismutase 2) have been associated with systemic hepatic disease. Mice mutant for *GPD1* gene (homozygous knock out) and a mutant *Slc25a13* gene showed increased hyperammonemia, hepatic steatosis and hypoglycemia (Saheki et al, 2007). Homozygosity for a *PHYH* knock out allele increased hepatic steatosis in mouse, which was increased by Phytol-enrich diets (Ferdinandusse et al, 2008). Similarly, the mutant *SOD2* animals had increased hepatic steatosis (Begriche et al, 2006). In fed VLCAD deficient mice, proteins encoded by *GPD1* and *PHYH*

were decreased, whereas in the fasted VLCAD deficient mice, the protein encoded by *PHYH* was increased. Superoxide dismutase 2 was down-regulated in VLCAD deficient mice in the fasted state. These findings may provide insight into the myopathic and hepatic phenotypes seen in VLCAD deficiency. 4-Aminobutyric transaminase (*ABAT*), which catalyzes the conversion of 4-aminobutyric acid (GABA) and 2-oxoglutarate into succinic semialldehyde and glutarate in mitochondria, was increased in VLCAD deficient mice, but decreased in SCAD deficient animals. *ABAT* deficiency presents with prominent neurologic symptoms(Gibson et al, 1985), and may reflect the complicated reported pattern of neurologic symptoms in SCAD deficient patients, but rarely seen in VLCAD deficiency. Thus, *ABAT* encoding protein may prove to be a risk marker for development of a neurological phenotype in FAODs.

Proteins in the most significantly altered constructed network in fed and fasted VLCAD deficient mice were linked by several well described transcription factors inferred from the IPA knowledge database. They included nuclear receptors of *PPARA*, *PPARG*, *PPARGC1A*, and *NR3C1* (nuclear receptor subfamily 3, group C) highlighting the importance of nuclear receptors in the molecular response to VLCAD deficiency. A similar relationship has been demonstrated in one previous study that showed that expression of the *PPARA* and *PPARG* genes were increased in VLCAD deficient mice in the fasted state, but was unchanged or slightly reduced in the fed state (Goetzman et al, 2005). 3-hydroxy-3-methylglutaryl-CoA reductase (*HMGCR*) is the rate-limiting enzyme for cholesterol synthesis and is regulated via a negative feedback mechanism mediated by sterols and non-sterol metabolites. Leptin (*LEP*) is secreted by white adipocytes and plays a major role in the regulation of body weight. These molecules were inferred on the basis of relationships with other molecules incorporated in the IPA knowledge database to participate

in regulating changes in the function of lipid metabolism in VLCAD deficient mice. Further studies are needed to demonstrate their roles in determining clinical symptoms in FAODs.

Multiple proteins are altered in fasted VLCAD deficient mice as compared to fasted wild type mice, consistent with an earlier report that mutant animals express some specific pathological and biochemical phenotype symptoms under this condition(Cox et al, 2001b). However, the relative effects of fasting vs. *ACADVL* gene deficiency were not well delineated in that study. To further define the altered proteins and pathways responsible for abnormal response to fasting, independent comparisons between fasted animals of both genotypes and fed animals were conducted. The analyses revealed that fasting had significantly different effects in wild type animals than VLCAD deficient ones, and, furthermore that gene-environment interactions existed, which were indicative by the observations on several proteins and some associated functional groups and canonical pathways. Acetyl-CoA acyltransferase 2 (*ACAA2*), which catalyzes the last step of mitochondrial fatty acid oxidation, was up regulated in wild type and mutant mice with fasting. However, it was down-regulated in fed VLCAD deficient as compared to fed wild type mice (Table 9). It is suggestive that the fasting resulted in a compensatory change in this enzyme for the release of acetyl CoA for Krebs cycle activity when the energy was depleted in the fasting state. The alteration of its expression from down-regulation in VLCAD deficiency to up-regulation due to fasting indicated that the effect of fasting counteracted with the effect of gene deficiency leading to the unchanged expression in the fasted VLCAD deficient mice. A similar phenomenon was seen in *ACAA2* expression in fasted VLCAD deficient mice to fasted wild type mice, in which *ACAA2* did not show changes. An apparent gene-environment interaction was also demonstrated in the expression of chaperonins HSP60 and HSP10 as discussed earlier.

While lipid metabolism was the predominant change seen in fed mutant animals and both differed compared to wild type mice, the carbohydrate metabolism with its assigned higher-level functional category with cellular function, cell maintenance and cell death was most altered in fasted VLCAD deficient mice. However, most altered proteins that were grouped into the carbohydrate metabolism include proteins encoded by *SCP2* with down-regulation and *GANAB* and *PRKCSH* with up-regulation in VLCAD deficient mice with fasting. Comparison between altered proteins in fasted VLCAD deficient mice and those changed in fed VLCAD mice (as both compared to wild type mice in each feeding condition) support this finding. The decrease in proteins associated with carbohydrate metabolism is not likely related to the observation that VLCAD deficient mice are well in the fed state and develop hypoglycemia only after prolonged fasting (Cox et al, 2001a). Rather, identification of altered carbohydrate metabolism was related to up-regulation of *GANAB* and *PRKCSH*, two proteins related to galactose metabolism (Figure 16). In addition, SOD2 was down-regulated in fasted VLCAD deficient mice and is related to carbohydrate metabolism indirectly through other molecules. Significant differences were also seen in the functions of protein degradation, synthesis and amino acid metabolism (Figure 19). Overall, findings in this study identify an environmental effect specific to the VLCAD deficient genotype, leaving mutant animals more vulnerable than wild type mice to the stress of fasting.

Canonical pathway analysis identified significant changes in fasting animals of both genotypes, including alterations in proteins involved in branched chain amino acid metabolism, fatty acid metabolism, pyruvate metabolism, and the synthesis and degradation of ketone bodies. In contrast, fewer differences in the significance was seen between the changes in deficient mice and in wild type mice, indicating that the changes in these pathways were related to fasting but not genotype. In response to energy demands during fasting, fatty acids stored as triacylglycerols

in the body are mobilized for use by peripheral tissues. The results from this proteomic study confirm that the normal physiologic response to fasting remains intact in the face of VLCAD deficiency.

It is noteworthy that well characterized biochemical abnormalities seen in individuals with fatty acid oxidation defects are reflected in changes in the protein profiles in VLCAD deficient mice. Although expression of some individual proteins changed, association analysis showed that in total, the pathway of ketone bodies production was not significantly up regulated in fasting as in wild type animals. Alteration of other pathways is more difficult to interpret. The pathways of amino acid metabolism, especially branched chain amino acid metabolism, as well as carbohydrate and fatty acid metabolism were more significantly altered in the fasted state than in the fed state in mutant mice suggesting a more global derangement in cellular metabolism in fasting mutant animals. The greatest differences were in the oxidative phosphorylation and citric acid cycle pathway and bile acid synthesis. An increased pattern in oxidative phosphorylation identified in fed VLCAD deficient mice disappeared when they were fasted. The oxidative phosphorylation pathway was unchanged when wild type mice were fasted. However, fasting induced the down-regulation of several proteins in OXPHOS in mutant animals. Thus a presumed compensatory change in the mutant animals appears to be negated during fasting, and may play a role in the development of symptoms.

The global changes on protein expression resulting from fasting and gene deficiency were investigated. The clinical relevance to secondary changes associated with *ACADVL* gene deficiency was further evaluated through the toxicity analysis function in the IPA software to provide additional insight into the pathologic alterations induced by *ACADVL* gene deficiency and fasting. Mice deficient for VLCAD develop hepatic steatosis upon fasting (Cox et al,

2001b). They also accumulate microvesicular lipids and demonstrate marked mitochondrial proliferation in heart (Exil et al, 2003). Both phenotypes are seen in the human deficiency to some extent. In one study, 12 of 15 patients with VLCAD deficiency showed dilated or hypertrophic cardiomyopathy (Mathur et al, 1999). Toxicity analysis using the IPA software indeed identified a pattern of protein changes predictive of liver damage (steatosis) in VLCAD deficient mice under both feeding states and the liver changes were slightly exacerbated in VLCAD deficient mice with fasting. A pattern of protein changes predictive of significant cardiac effects of fibrosis, enlargement and dilation) was identified in fasted deficient mice suggesting that fasting may play more of roles in the development of cardiac than liver symptoms in affected patients. It has been hypothesized that the myocardial damage may be due to the accumulation of toxic metabolites during starvation (Strauss et al, 1995). We propose that the cardiac effects of VLCAD deficiency are a consequence of a combination of the primary acute stress combined with resultant secondary physiologic manifestations in the genetic deficiency.

Proteomic experiments in this study benefited from the sensitivity and quantitation of LC-MS/MS, but considerable challenges remained. First, experiments were performed and all samples were collected over time, thus, variability in sample handling and storage were introduced into experiments, which is a significant issue in light of the high sensitivity of this technique. Much of the assay variability can be attributed to the inherent limitations arising from the efficiency of commercially available reagents and approaches, variability of biological replicates, the data analysis tools and database used for mass spectra and pathway analysis. For examples, IEF was used for the separation of peptides. Most, but not all, of the peptides could further be separated and captured by MS, which include those having pKa around 3.5-4.5,

leading to inefficiency of separation. Columns used for the purification and elution of peptides introduced additional reproducibility issues. Second, changes in the level of low abundance proteins are difficult to quantitate, and thus, alterations induced by the primary gene defect and its interaction with the environment (fasting) are likely to be under recognition. It should be noted that while few proteins were altered with the same pattern in deficient mice in both feeding states, this might be due to that fewer proteins in the fasted deficient mice were under detection. Fewer proteins were identifiable in deficient mice than in wild type mice when they were fasted. This issue may be arisen from the unfavorable reproducibility rather than that fewer proteins were present. It is also important to note that alterations of some low level proteins identified in only one experiment could be real even though it is not reproducible in repeat experiments. Additional experiments will be necessary to validate such changes if they are of interest. Identifying more differentially expressed proteins was of particular interest in this study. To maximize the identification of significantly changed proteins for further comparisons among datasets, the selection criterion of significance was set to be at $p \leq 0.05$ (1 side), which was under the assumption that one specific protein was significantly changed as either up-regulated or down-regulated. However, this approach did not negate the levels of changes in abundant proteins in the fasted animals.

Finally, these proteome studies on VLCAD deficient mice focused on mitochondria and thus are limited to proteins whose genes are located either on the mitochondrial chromosome or are nuclear encoded but imported into mitochondria after translation. A broader examination of changes in other cellular compartments may provide additional evidence for secondary derangements caused by and important to this deficiency.

In conclusion, the mitochondrial proteome changes in VLCAD deficient mice were quantitatively characterized and effects related to fasting in both mutant and wild type animals were identified in this study. Some of these changes reflect known physiologic and pathologic alterations previously characterized in VLCAD deficiency and fasting. Others provide novel insights into possible new secondary effects of the defect and mechanisms for disease heterogeneity. The results from this study identify an aberrant fasting response in VLCAD deficient mice and provide possible physiologic explanations for the diversity of disease severity in patients with VLCAD deficiency. The secondarily altered proteins in mutant animals define interactions of both genes and specific environmental interactions with the *ACADVL* gene. These experiments demonstrate the power of the system in this study to examine altered responses to environmental factors related to a primary genetic deficiency and offer the possibility of identifying new strategies for treatment of acute symptoms and long-term sequelae. Further exploration with this system and subsequent functional studies suggested from this study will allow elucidation of the mechanisms that underlie the phenotypic complexity in VLCAD deficiency.

4.0 ENVRIRONMENTAL EFFECTS AND GENE INTERACTION IN TWO FATTY ACID BETA OXIDATION DISORDERS

4.1 INTRODUCTION

It has become increasingly recognized that many common diseases arise as a result of both genetic and environmental factors, as well as the interactions between them. It is not hyperbole to suggest that virtually all-human diseases could be viewed as being the result of the interaction of genetic susceptibility factors and modifiable environmental factors. Even the phenotype of Mendelian disorders is subject to modulation by expression of other genes interacting with the environment. However, few of the modifying factors in this situation have been identified. Disorders of fatty acid oxidation (FAODs) exemplify these issues. Patients with disorders of FAODs often present with recurrent rhabdomyolysis and hypoglycemia but the clinical spectrum is pleiotropic and variable. For example, the severity of symptoms in patients with deficiencies of the acyl-CoA dehydrogenases (ACADs) that catalyze the first intra-mitochondrial step of fatty acid oxidation varies from asymptomatic to life threatening metabolic crisis. Symptoms are often induced by fasting or physiologic stress, illustrating the importance role of environmental factors in the pathophysiology of these disorders. Carriers for a mutation

on one allele in one of the ACADs are usually asymptomatic, but individuals heterozygous for mutations in more than one gene involved in energy metabolism can become symptomatic, a phenomenon termed “synergistic heterogeneity” (Vockley et al, 2000). In total, these observations demonstrate the complexity of gene-gene and gene-environment interactions that define genetic disease.

The ACADs are a family of related enzymes that consists of at least 9 members. DNA sequencing studies show that the amino acid sequences of the various ACADs share 30-35% identical residues but sequencing identities between species approach 90%, indicative of evolutionary divergence of a common ancestral gene (Matsubara et al, 1989b; Su et al, 2002; Swigonova et al, 2009). ACADs catalyze the β-dehydrogenation of acyl-CoA esters in the mitochondrial matrix but differ in their substrate specificity. VLCAD is most active against acyl-CoA substrates of chain length of 14-20 carbons, and SCAD is optimally active with C4 and C6-CoA substrates. In Chapters 2 and 3, I have used global analysis of the mitochondrial proteome to identify proteins secondarily altered in mice with genetic defects in SCAD and VLCAD deficiency. Proteomic changes induced by fasting in VLCAD deficient mice were likewise globally surveyed to systemically evaluate the biological response to this physiologic stress. Extending these analyses to define consensus proteins altered in both animal models would help delineate the common mechanisms of molecular changes induced by both deficiencies, providing insight into common potential opportunities for therapeutic intervention. In contrast, identification of the proteins changes unique to each genetic variant would allow targeted intervention optimized to each disorder and provide new biomarkers to confirm diagnosis and monitor therapy.

The effect of environmental factors on phenotype and identification of gene-environment interactions are usually measured in epidemiological studies on individuals who are genetically susceptible to an environmental exposure. However, genetic variation and inconsistent environmental exposure make such studies challenging. Restricting the search for gene–environment interactions to well defined genetic models that interact in the same or related biological pathways offers an attractive option to better dissect the relative roles of genes and environment in the development of disease. In this chapter, proteome changes in VLCAD and SCAD deficient mice are compared to define the secondarily altered proteins unique to and shared by these disorders. Network analysis allowed comparison of the annotated functions and canonical pathways associated with the changed proteins in the two models. Ultimately, defining alterations related to the primary genetic defects, environmental effects on them, the relationship of the two defects, and interactions of secondarily altered proteins due to each defective gene will provide insight into the pathogenesis of these disorders and allow the development of appropriate interventions for high-risk individuals.

4.2 METHODS

4.2.1 Pathway and Network Analysis

All changed proteins in fed VLCAD deficient mice, fed SCAD deficient mice, and fasted VLCAD deficient mice were individually compared to changes in wild types (Chapter 2 and Chapter 3). The differentially expressed proteins in each dataset were then subjected to the comparison analysis incorporated in IPA. Filters and general settings were set as for previous

analyses. Comparison analysis in IPA allows direct comparison of changes in biological states across a set of observations. I utilized this function to assess the functional annotations, canonical pathways and relevant pathological endpoints from the changed proteins/genes across the genotypes (SCAD and VLCAD) and stresses (fasted and fed) states within VLCAD.

4.2.2 Regression model

To assess the associations between VLCAD gene knock-out, fasting effects and changed genes/proteins and explore better biomarkers in the predication of *ACADS* gene changes, a simple regression analysis was used to describe their relationships. The genetic factor VLCAD and fasting stress were defined as explanatory variable X, while the proteins that were significantly altered were considered as response variables. The relationship is described as the equation: $y = \alpha + \beta 1x + \beta 2x + \varepsilon$, where the component ε is comprised of factors that are unobservable, or at least unobserved. The protein values in biological experimental replicates were log2-transformed (Chapter 3). In this analysis, the protein value relative to 113 labeled one was the response variable y in each independent calculation. The SCAD or VLCAD variable was assigned to have two values, 0 and 1, in the regression analysis, based on the absence or presence of the deficient gene. Fasting was assigned to have two values 0 and 1 depending on the feeding status of mice. A protein was to have a changed value of folds change when VLCAD-/- or SCAD -/- had a value of 0 in deficient mice, and a value of 1 in wild type. Parameter α, β and ε were computed from the equation using the software package Stata (College station, Texas). β was used to test the significance of associations.

4.3 RESULTS

To characterize the changes in the mitochondrial proteome related to SCAD deficiency, I utilized DIGE analysis with MALDI-TOF/TOF for protein identification and quantification (Chapter 2). iTRAQ labeling followed by peptide separation and identification with LC-MALDI-TOF/TOF was performed to evaluate the proteomic changes resulting from VLCAD deficiency as well as fasting stress on the animals (Chapter 3).

4.3.1 Consensus and inconsistently altered proteins

An overview of the consensus proteins that were changed in both deficient animal models is shown in Table 15. Six proteins were consistently identified in both SCAD deficient and VLCAD deficient mice in the fed state. However, only one of them, HSP60 *(HSPD1)* was altered in the same direction. In contrast, 5 proteins were identified as altered in both SCAD deficient mice and VLCAD deficient mice but with different patterns of changes. 4-aminobutyrate aminotransferase encoded by *ABAT* was decreased in SCAD deficiency but increased in VLCAD deficiency. SCP2, a non-specific lipid transfer protein was increased in SCAD deficient mice but decreased in VLCAD deficient mice. Down-regulation of SCP2 did not occur in fasted VLCAD deficient mice. IMMT, an inner membrane protein mitofilin, was down-regulated in SCAD deficiency but increased in VLCAD deficiency regardless of the feeding status.

Several proteins, including aldehyde dehydrogenase, 2-oxoglutarate dehydrogenase complex, electron transfer flavoprotein, fumarate hydratase 1 precursor, and ornithine aminotransferase, were up-regulated in SCAD deficient mice but down-regulated in VLCAD

deficient mice only when they were fasted. Examination of fasting effects on both wild type and VLCAD deficient mice showed that expression of ALDH2 (aldehyde dehydrogenase) was decreased in both animals. However, no expression differences were detected in other proteins, including ornithine aminotransferase and electron transfer flavoprotein, in response to fasting in either VLCAD deficient or wild type mice.

Table 15. Consensus proteins changed in SCAD deficient and VLCAD deficient mice

Gene symbol	Gene names	Ratio of protein expression fed SCAD -/-: fed SCAD+/+	Ratio of protein expression fed VLCAD-/-: fed VLCAD+/+	Ratio of protein expression fasted VLCAD-/- : fasted VLCAD+/+
ABAT/GABT	4-aminobutyrate aminotransferase	-1.47	1.329	
ALDH2	Aldehyde dehydrogenase, mitochondrial	3.11		-2.351
CATA	Catalase	1.59	-1.689	
CYP2d26	Cytochrome P450 2D26		-1.498	1.873
DLST/ODO2	Component of 2-oxoglutarate dehydrogenase complex	2.42		-2.034
ETHE1	Protein ETHE1		1.393	-1.557
ETFA	Electron transfer flavoprotein subunit alpha	1.980		-1.357
FH/FUMH	Fumarate hydratase 1 precursor	1.490		-1.594
HSPD1/CH60	60 kDa heat shock protein	1.65	1.332	
IMMT	Mitochondrial inner membrane protein	-1.493	1.48	2.161
PHYH/PAHX	Phytanoyl-CoA dioxygenase, peroxisomal		-1.957	1.746
NUDT7	Peroxisomal coenzyme A diphosphatase		-2.286	-2.486
OAT	Ornithine aminotransferase, mitochondrial	2.100		-2.212
RRBP1	Ribosome-binding protein 1	1.74		1.945
SCP2/NLTP	Non-specific lipid-transfer protein	1.92	-1.932	-1.874

4.3.2 Comparison of annotated functions

The biological functions associated with differentially expressed proteins were compared among animals with SCAD deficiency, VLCAD deficiency in the fed state, and VLCAD deficiency in the fasted state. The difference of associated functions with top significance ($p \leq 0.05$) is shown in Figure 25. Differences in associated functions included immunological disease, inflammatory disease, respiratory disease and hematological disease, which were only discovered in VLCAD deficient mice when they were fasted. Proteins that implicate these functions include *ALDH2, P4HB, PDIA3, MYH9, HSPA5, SOD2*, and *SCP2*, most of them with overlapping in associations. However, most of them were up regulated rather than down regulated in fasted VLCAD deficient animals.

Proteins associated with carbohydrate metabolism were more significantly altered in fasted VLCAD deficient mice than in fed VLCAD deficient mice and fed SCAD deficient mice. Comparison analysis also showed altered proteins in SCAD deficiency associated with neurological disease and amino acid metabolism, but there was no clear associations between neurological disease and altered proteins in VLCAD deficiency in the fed state. Altered proteins associated with neurological disease are shown in Table 16. They include SOD2 (down-regulated) and aspartylglucosaminidase (up-regulated), both of which were identified in fasted VLCAD deficient mice as compared to fasted wild type mice. SOD2 was only reduced in VLCAD deficient animals in the fasted status. This protein was unchanged in fed VLCAD or fed SCAD deficient mice. Prominent effects associated with neurological disease were found in SCAD deficiency involving 6 altered proteins with encoding genes of OTC, *NDUFS7, ABAT, GLUD1, HSPD1*, and *MDH2* (Chapter 2). All except HSP60 (*HSPD1*) were decreased in SCAD

deficiency. No proteins associated with neurological disease were identified in fed VLCAD deficient mice.

Less difference in association significance was seen in the functions of lipid metabolism, small molecule chemistry and metabolic disease between SCAD and VLCAD deficiencies (Figure 25). More similarities of these functions were found between fed and fasted VLCAD deficient mice than between SCAD and VLCAD deficiency. In general, changes in fed and fasted VLCAD deficient mice were more closely related to each other than to SCAD deficiency.

Table 16. Altered proteins associated with neurological disease

Deficiency	Altered proteins	Associated functions/diseases
VLCAD deficiency in the fasted state	SOD2(-), AGA(+)	Neurological disease
SCAD deficiency	OTC(-), NDUFS7(-), ABAT(-), GLUD1(-), HSPD1(+), MDH2	Neurological disease

(-) denotes the up-regulation, (+) denotes the down-regulation

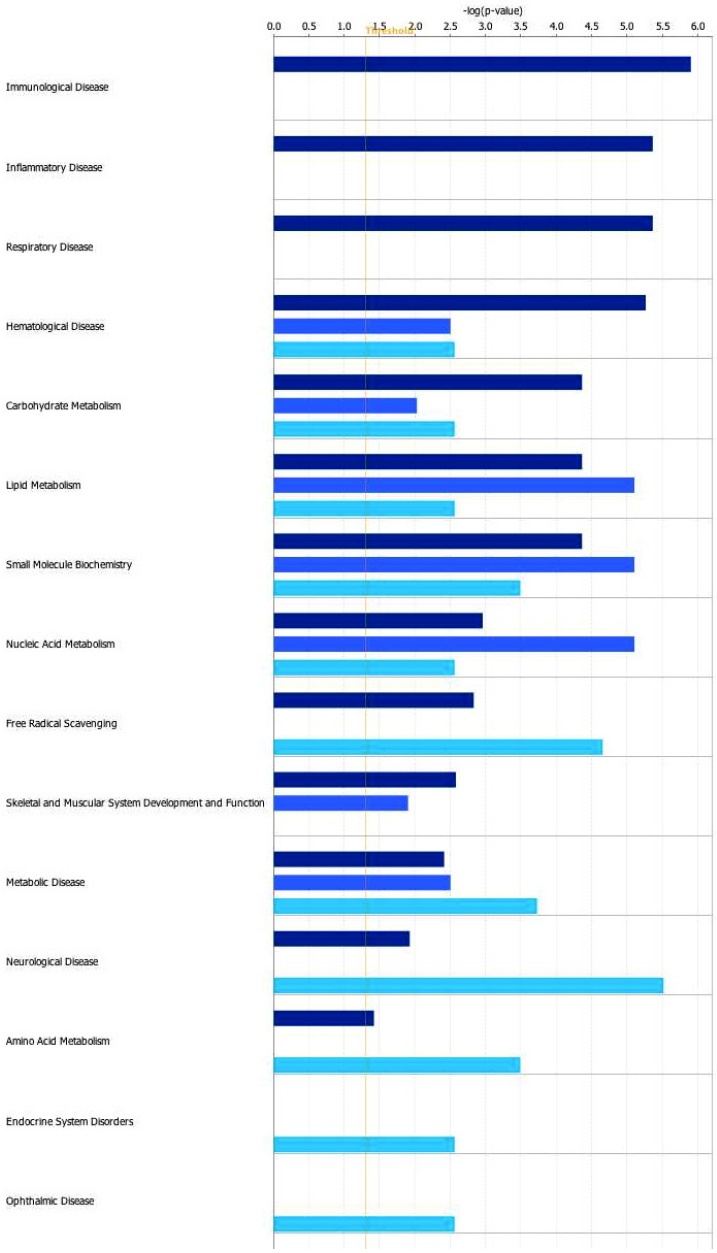

Figure 25. Comparison of annotated functions associated with altered proteins

Comparison of functions associated with differentially expressed proteins in deficient mice when compared to corresponding wild type mice. Light blue- SCAD deficiency. Mild blue-VLCAD deficiency in the fed status. Dark blue-VLCAD deficiency in the fasted status. *p*-value: Fisher's exact test (threshold $p=0.05$).

4.3.3 Comparison of involved canonical pathways

Most of the canonical pathways associated with secondarily altered proteins differed between VLCAD deficiency and SCAD deficiency (Figure 26). The amino acid metabolism related pathways such as arginine and proline metabolism, glutamate metabolism, histidine metabolism, and ß-alanine metabolism were more significantly altered in SCAD deficiency. Fatty acid metabolism was almost equivalently altered in SCAD deficiency and VLCAD deficiency in the fed states. Though few overlapping molecules involved in this fundamental pathway in ACADD were identified in the three datasets, most of them were of similar function (Table 17). For example, proteins encoded by *ACAA1* and *ACAA2* performed the same enzymatic (acetyl-CoA acyltransferase) activity but with different substrates. Enoyl-CoA delta isomerase 1 encoded by *ECI1* is a member of the hydratase/isomerase superfamily involved in □-oxidation of unsaturated fatty acids. *ECI2* (*PECI*) is an auxiliary enzyme that catalyzes an isomerization step required for the beta-oxidation of unsaturated fatty acids.

More significant changes in protein expression were involved in mitochondrial dysfunction and oxidative phosphorylation in SCAD deficiency than in VLCAD deficiency (Figure 26), with the majority of proteins involved in mitochondrial dysfunction being included in the oxidative phosphorylation pathway (Table 17). Moreover, the changes in SCAD deficiency differed remarkably from those seen in VLCAD deficiency. Multiple complex I, III, and IV subunits were decreased in SCAD deficiency, but fewer of them were altered in VLCAD deficiency (fed), and those that were altered, were increased. Only ATP synthase (complex V) was increased in both SCAD deficiency and VLCAD deficiency in the fed state.

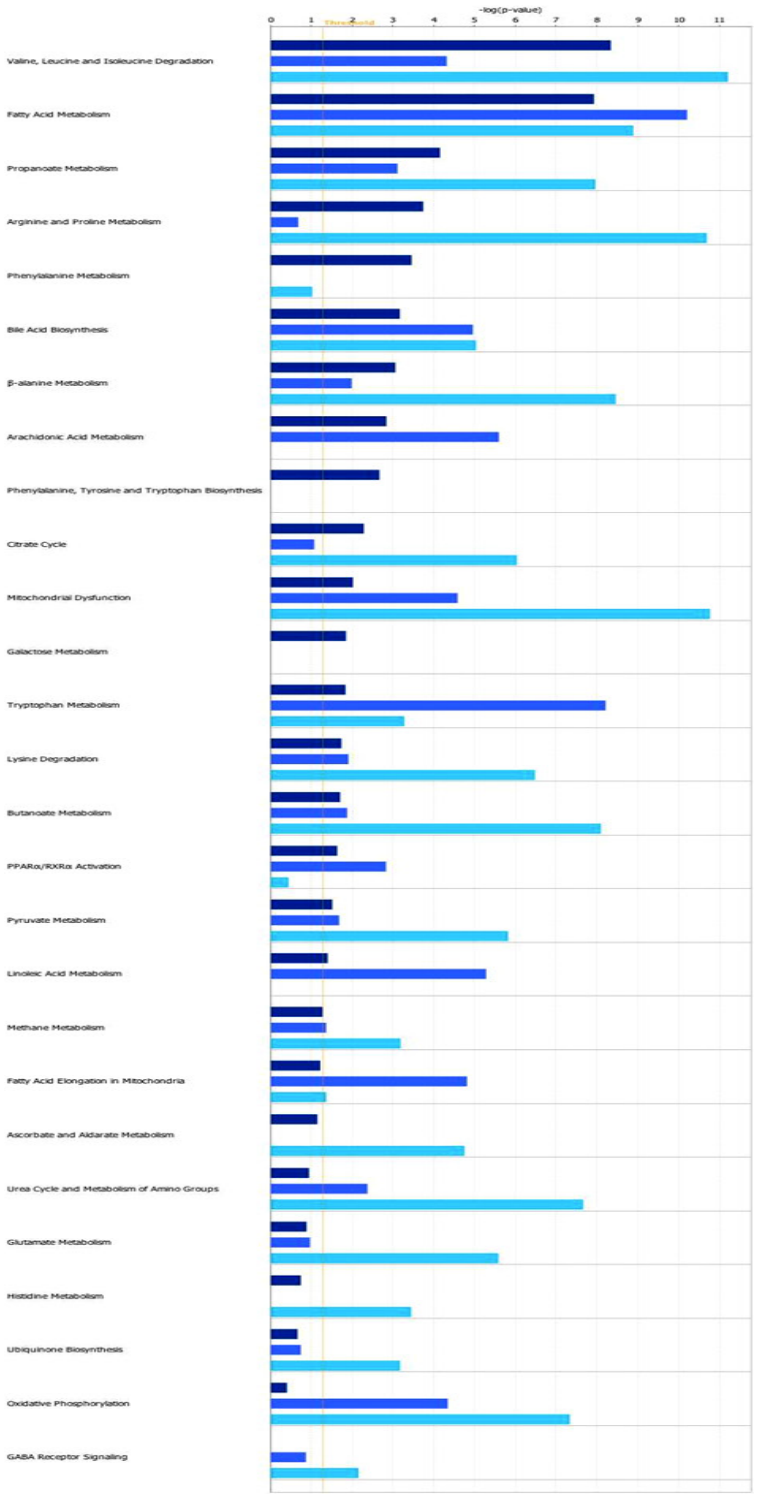

Figure 26. Comparison of canonical pathways associated with altered proteins

Comparison of canonical pathways associated with differentially expressed proteins in deficient mice compared to corresponding wild type mice. Light blue- SCAD deficiency. Mild blue-VLCAD deficiency in the fed state. Dark blue-VLCAD deficiency in the fasted state. p-value: Fisher's exact test (threshold p=0.05).

Table 17. Altered proteins and their involved canonical pathways

in SCAD deficiency (fed state)and VLCAD deficiency (fed state, fasted state)

Deficiency	Altered proteins	Pathway	-log(p-value)
VLCAD deficiency in the fasted state	ALDH2 (-), Cyp2d26 (+), CYP2D10 (+), ACADVL (-), ECI2 (+), IVD (-), ACAA2 (-), DHRS4 (-)	Fatty acid metabolism	7.93E00
VLCAD deficiency in the fed state	Acaa1b (-), Cyp2d26 (-), ACAA1 (-), ACADVL (-), CYP3A4 (-), PECR (-), Cyp2c29 (-)	Fatty Acid Metabolism	1.02E01
SCAD deficiency in the fed state	ALDH4A1 (+), ALDH2 (+), ACADL (+), CPT2 (-), ALDH9A1 (+), ACAA2 (+), ECI1 (+), ACADS (-)	Fatty Acid Metabolism	8.89E00
VLCAD deficiency in the fasted state	SOD2 (-), NDUFV2 (-), PRDX5 (+)	Mitochondrial Dysfunction	2.02E00
VLCAD deficiency in the fed state	NDUFV1 (+), ATP5B (+), CAT (-), UQCRC1 (+), COX4I1 (+)	Mitochondrial Dysfunction	4.59E00
SCAD deficiency in the fed state	COX6B1 (-), NDUFS7 (-), ATP5A1 (+), NDUFB7 (-), UQCRC2 (-), CAT (+), UQCRFS1 (-), NDUFA7 (-), AIFM1 (-)	Mitochondrial Dysfunction	1.08E01
VLCAD deficiency in the fasted state	NDUFV2 (-)	Oxidative Phosphorylation	4.09E-01
VLCAD deficiency in the fed state	NDUFV1 (+), UQCRHL (+), ATP5B (+), UQCRC1 (+), COX4I1 (+)	Oxidative Phosphorylation	4.35E00
SCAD deficiency in the fed state	COX6B1 (-), NDUFS7 (-), ATP5A1 (+), NDUFB7 (-), UQCRC2 (-), UQCRFS1 (-), NDUFA7 (-)	Oxidative Phosphorylation	7.33E00

(-) denotes the up-regulation, (+) denotes the down-regulation

4.3.4 Comparison of clinical relevance

The toxic function analysis incorporated in the IPA software attempts to assess the toxicity of small molecules on organs such as liver, heart and kidney. I instead used it to flag potentially clinically relevant changes induced in these organs by SCAD and VLCAD deficiency. In this analysis, the SCAD or VLCAD gene deficiency and secondary changes identified in the proteome were defined as a "toxins" and assigned to functional pathways as with more traditional small molecule studies (Figure 27). The toxicity results and their related proteins used in the analysis are shown in Table 18. The analysis identified a pattern of protein changes associated with cardiac enlargement, fibrosis and dilation only in fasting VLCAD deficient animals including the proteins encoded by *SOD2* and *GPX1*. The liver steatosis in VLCAD deficiency was predicted on the basis of changes in expression of *SOD2* and P*HYH*. However, the prediction of liver steatosis in SCAD deficiency was based on only one molecule LCAD, which has been previously demonstrated to cause hepatic steatosis (Beattie et al, 2008; Zhang et al, 2007).

Biomarker comparison analysis revealed that several potential biomarkers were unique to one dataset with no identified potential biomarkers common to all three datasets. The predicted biomarkers as well as their biofluid or tissue locations are summarized in Table 19. Specifically, there were no common biomarkers identified between SCAD deficiency and VLCAD deficiency, and only two enzyme biomarkers were shared between fed and fasting VLCAD deficient mice. The majority of enzyme biomarkers were unique to one feeding state in VLCAD deficient mice (Table 20). A simple linear regression analysis did not return a presumably significant assessment for the association test.

(Table 20). A simple linear regression analysis did not return a presumably significant assessment for the association test.

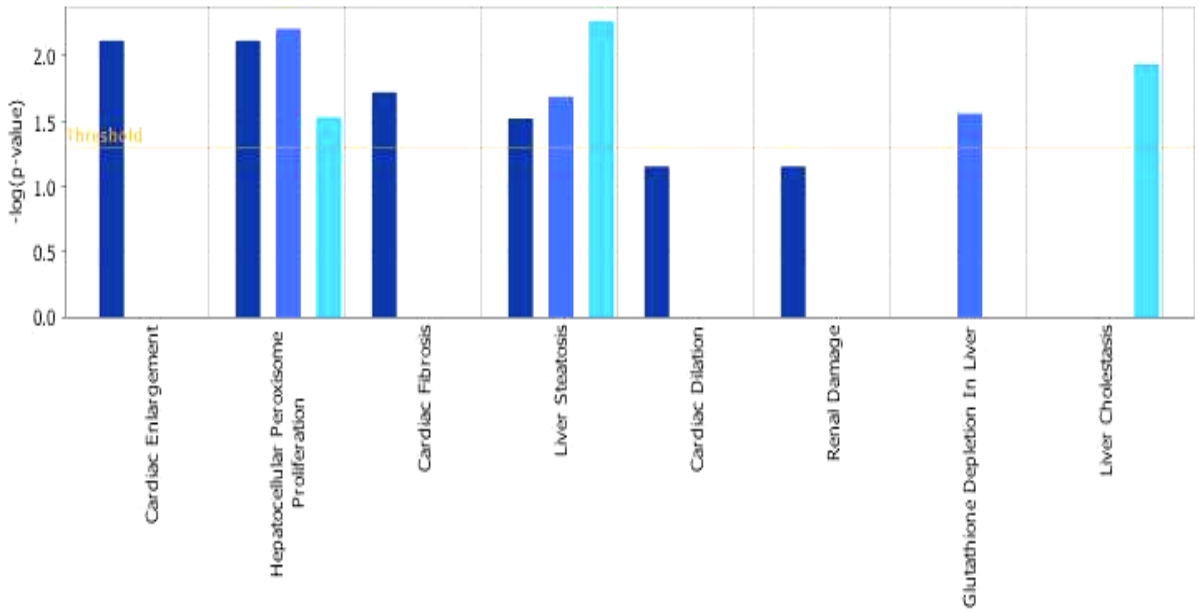

Figure 27. Clinically relevant changes associated with altered proteins

Prediction of pathological alterations from secondarily changed proteins and defective genes. Dark blue - VLCAD deficiency (fasted state). Mild blue- VLCAD deficiency (fed state). Light blue-SCAD deficiency(fed state) Y-axis: significance of toxicity arising from the changed proteins (p=0.05).

Table 18. Molecules used in the assessment of related toxic functions

Category	Analysis Name	Molecules
Cardiac Enlargement	VLCAD deficient (fasted)	SOD2
Hepatocellular Peroxisome Proliferation	VLCAD deficient (fasted, fed), SCAD deficient (fed)	SCP2
Cardiac Fibrosis	VLCAD deficient (fasted)	GPX1
Liver Steatosis	VLCAD deficient (fasted, fed)	SOD2, PHYH
Liver Steatosis	SCAD deficient (fed)	ACADL
Cardiac Dilation	VLCAD deficient (fasted)	SOD2, GPX1

Table 19. Unique biomarkers in SCAD deficiency or VLCAD deficiency

Gene Deficiency	Symbol	Entrez Gene Name	Family	Fold Change	Species	Tissues/Biofluid
VLCAD deficiency (fed)	ACP5	Acid phosphatase 5, tartrate resistant	phosphatase	-1.752	Human, Mouse	Blood, plasma/serum, B lymphocyte, liver
VLCAD deficiency (fed)	AMACR	alpha-methylacyl-CoA racemase	enzyme	-1.531	Human, Mouse	Not detected in biofluid but in macrophages, monocytes, liver.
VLCAD deficiency (fed)	CYP3A4	cytochrome P450, family 3, subfamily A, polypeptide 4	enzyme	-1.646	Human, Mouse	urine,B lymphocyte, liver.
VLCAD deficiency (fed)	EPHX2	epoxide hydrolase 2, cytoplasmic	enzyme	-1.626	Human, Mouse	urine,liver.
VLCAD deficiency (fed)	GPD1	glycerol-3-phosphate dehydrogenase 1 (soluble)	enzyme	-1.799	Human, Mouse	urine, Bronchoalveolar Lavage Fluid, liver
VLCAD deficiency(fasted)	FABP1	fatty acid binding protein 1, liver	transporter	-1.486	Human, Mouse	Blood,Plasma/Serum,urine, liver
VLCAD deficiency(fasted)	GPX1	glutathione peroxidase 1	enzyme	-2.126	Human, Mouse	Blood,Plasma/Serum,liver
VLCAD deficiency (fasted)	HMGCS2	3-hydroxy-3-methylglutaryl-CoA synthase 2 (mitochondrial)	enzyme	1.613	Human, Mouse	Not detected in biofluid,liver.
VLCAD deficiency (fasted)	HSPA5	heat shock 70kDa protein 5 (glucose-regulated protein, 78kDa)	other	1.443	Human, Mouse	Blood,Plasma/Serum,Urine, liver.
VLCAD deficiency (fasted)	NUCB1	nucleobindin 1	other	1.856	Human, Mouse	liver
VLCAD deficiency(fasted)	PDIA3	protein disulfide isomerase family A, member 3	peptidase	1.905	Human, Mouse	Blood,Urine,liver
VLCAD deficiency (fasted)	SOD2	superoxide dismutase 2, mitochondrial	enzyme	-1.467	Human, Mouse	Blood,Plasma/Serum,Urine, liver
SCAD deficiency(fed)	ACADL	acyl-CoA dehydrogenase, long chain	enzyme	2.000	Human, Mouse	Not detected in biofluid,liver
SCAD deficiency(fed)	ACADS	acyl-CoA dehydrogenase, C-2 to C-3 short chain	enzyme	-3.580	Human, Mouse	Not detected in biofluid,liver
SCAD deficiency(fed)	CPT2	carnitine palmitoyltransferase 2	enzyme	-2.703	Human, Mouse	Blood,Plasma/Serum,liver
SCAD deficiency(fed)	EPHX1	epoxide hydrolase 1, microsomal (xenobiotic)	peptidase	1.500	Human, Mouse	Not detected in biofluid,liver
SCAD deficiency(fed)	GLUD1	glutamate dehydrogenase 1	enzyme	-2.041	Human, Mouse	Blood,liver etc.
SCAD deficiency(fed)	PC	pyruvate carboxylase	enzyme	1.560	Human, Mouse	Not detected in biofluid,liver
SCAD deficiency(fed)	PHB	prohibitin	transcription regulator	-1.786	Human, Mouse	Blood, liver

*These candidate biomarkers were predicted by IPA.

Table 20. Common biomarkers in VLCAD deficiency in the fed state and fasted state

Symbol	Entrez Gene Name	Family	Fold Change in VLCAD deficiency (fed)	Fold Change in VLCAD deficiency (fasted)
ACADVL	acyl-CoA dehydrogenase, very long chain	enzyme	-4.033	-3.416
NUDT7	Nudix (nucleoside diphosphate linked moiety X)-type motif 7	enzyme	-2.286	-2.486
PHYH	phytanoyl-CoA 2-hydroxylase	enzyme	-1.957	1.746

4.4 DISCUSSION

Mitochondrial fatty acids β-oxidation proceeds via a series of enzymatic reactions in which an acyl-CoA ester is oxidized, hydrated, and oxidized again, with a final thiolytic cleavage to remove a two carbon acetyl-CoA moiety. Electrons are then channeled to oxidative phosphorylation through complex I of the respiratory chain by the electron transfer flavoprotein (ETF) (Figure 1). Multiple enzymes function at each step, depending largely on the chain length of the substrate. Genetic disorders in humans exist in nearly every enzyme in the pathway and patients can present with a bewilderingly wide array of symptoms. The mechanism for this clinical variability is completely unknown. Secondary changes in other pathways in energy production may, in part, explain some of this variation as well as an individual's response to environmental stimuli. In this study, I have attempted to clarify these issues through examination of the mitochondrial proteomic profile changes in models of VLCAD and SCAD deficiency under different environmental conditions. Secondarily altered proteins induced by these genetic deficiencies as well as their associated functions and involved pathways were compared to identify differences of potential import to determining phenotypic variation. Importantly, the majority of altered proteins differed in the two different deficiencies, implicating fundamentally different mechanisms of pathophysiology in the two disorders. Of note, even those proteins that were altered in both deficiencies showed different patterns of alterations. Thus, the very different phenotypes seen in patients with defects in these two ACADs are likely to at least in part be explained by the divergent changes induced by the primary gene defects.

Changes observed in chaperonin proteins provide some insights into secondary effects of these deficiencies on the process of protein folding or binding in the mitochondrial matrix. HSP60 was up-regulated in both deficient mice, suggesting that these functions represent a

compensatory mechanism related to disruption of fatty acid ß-oxidation in general rather than one specific to either defect. HSP60 encoded by *HSPD1* is involved in mitochondrial protein folding, and the accumulation of unfolded protein within the mitochondrial matrix results in the transcriptional up-regulation of chaperonin 60 and chaperonin 10 (Martin, 1997; Zhao et al, 2002). Fibroblasts with point mutations from patients with SCAD deficiency have been shown to have increased levels of HSP60 chaperonin presumably due to the accumulation of abnormal SCAD protein (Bross et al, 2007). It should be noted, however, that both of the mouse models of SCAD deficiency and VLCAD deficiency used in this study are null, so the effect in chaperonin function is not a result of the presence of abnormal or mutant protein. Up-regulation of HSP60 in VLCAD deficient mice suggests a compensatory response *in vivo* when fatty acids are not being used as the major energy resource. In normal individuals, FAO functions primarily as an endocrine mediated response to fasting and increased energy demands due to glycogen depletion. However, alteration of HSP60 in VLCAD deficient animals was not linked to fasting, suggesting a non-energy based stimulus for this change. In contrast, HSP10, which binds HSP60 to form a symmetric functional heteromer enhancing protein folding in an ATP-dependent manner (Burns et al, 1992), was down-regulated in VLCAD deficient mice in the fasted state, suggesting that this molecule change was energy induced. Considering these apparently divergent results, I hypothesize that protein folding is initially compensatory in the face of ACAD deficiency, but that this rescue mechanism is compromised with the more dramatic energy deficit caused by VLCAD deficiency, especially during fasting.

SCAD was originally characterized in children and adults with a wide variety of symptoms but is now most frequently identified in asymptomatic children through newborn screening. The preponderance of asymptomatic individuals is very different from other FAO

deficiencies. In this study, the pattern of altered mitochondrial proteins differed markedly between SCAD and VLCAD deficient mice. Specifically, 4-aminobutyrate aminotransferase involved in the conversion of 4-aminobutanoic acid (GABA) was decreased in SCAD deficiency but increased in VLCAD deficiency. GABA is the primary inhibitory neurotransmitter in the central nervous system. The down-regulation of this enzyme and other related enzymes may explain the preponderance of neurological symptoms reported in patients with manifesting SCAD deficiency. Additionally, the up-regulation level of this enzyme in VLCAD deficient mice suggests a compensatory response and may relate to the paucity of neurologic symptoms seen in this disorder. Interestingly, this potential protective response in this enzyme disappeared in VLCAD deficient mice when they were exposed to fasting suggesting that patients with this disorder may face added risk for neurologic dysfunction during fasting.

SCP2, a non-specific lipid transfer protein, was increased in SCAD deficient mice but decreased in fed and fasted VLCAD deficient mice as compared to the wild type mice in the same feeding state. This protein was decreased by fasting in wild type mice but was not altered further by fasting in VLCAD deficient mice. The discrepancy of SCP2 expression in two different defects of ACADs further demonstrated the distinctive features in patients with two deficiencies. It is illustrative that a defect of short chain fatty acids ß-oxidation induced the functions of lipid binding, and transferase activities as a compensatory response, while defective long-chain fatty acids ß-oxidation resulted in the reduction of these functions. The significance of reduction of SCP2 in VLCAD deficient mice compared to wild type mice in both feeding states likely reflects reduced needs for the lipid binding and transferase activities due to the accumulation of long chain fatty acids. Changes in fed VLCAD deficient mice are analogous to those seen in fasting wild type animals, leaving no room for further response during fasting in

VLCAD deficient mice. Opposite changes were seen in IMMT, an inner membrane protein mitofilin with critical functions in mitochondrial morphology and mitochondrial fusion and fission. This protein was down-regulated in SCAD deficiency but up-regulated in VLCAD deficiency regardless of the feeding status. The functional significance of these changes remains to be determined.

Aldehyde dehydrogenase encoded by *ALDH2* was decreased in both wild type and VLCAD deficient animals. Thus, the expression difference in aldehyde dehydrogenase in fasted VLCAD deficient mice is likely dictated by fasting rather than the genetic defect. However, expression differences in other proteins including ornithine aminotransferase and electron transfer flavoprotein can not be explained solely by fasting effects as changes were not seen in fasted VLCAD deficient mice. Thus, in contrast to SCAD deficiency, the environmental factor fasting and the genetic effect of VLCAD deficiency played synergistic roles in down-regulating these proteins.

As discussed in chapter 3, proteins involved in carbohydrate metabolism were mostly up-regulated in VLCAD deficient mice upon fasting rather than down-regulated as in wild type animals, thus representing a compensatory response specific to stressed VLCAD deficient animals. However, changes in SCAD deficient mice in proteins related to neurological disease and amino acid metabolism were not reflected in VLCAD deficiency in the fed state. It seems like that fasting induce alterations in these functions with milder significance. However, these alterations in SCAD deficiency include up-regulated aspartylglucosaminidase (*AGA*) and down-regulated SOD2, leaving the consequence of this association uncertain.

Examination of the literature on the neurologic disease related proteins altered in SCAD but not VLCAD deficient animals provides some potential insights into the mechanism of

neurologic damage in the former condition. Six proteins associated with neurological disease are altered in SCAD deficiency including proteins encoded by the *OTC, NDUFS7, ABAT, GLUD1, HSPD1* and *MDH2* genes. Of these proteins, all except heat shock protein 60 were decreased in SCAD deficiency. These proteins remain unchanged in VLCAD deficiency. In contrast, superoxide dismutase 2 (SOD2) and aspartylglucosaminidase (*AGA*) were both altered in fasted VLCAD deficient mice. AGA, involved in the catabolism of N-Linked oligosaccharides of glycoproteins, has been found to be associated with gliosis, aspartylgulcosaminuria and schizophrenia. This enzyme was up-regulated rather than down-regulated in VLCAD deficient mice only upon fasting. SOD2 appears to protect against reactive oxygen species and its dysfunction has been linked to a variety of neurological diseases. It was reduced in fasted but not fed VLCAD deficient animals. Thus, it is difficult to link them to significant deleterious effects in VLCAD deficiency.

It is perhaps not surprising that while some alterations in protein profiles differed in SCAD and VLCAD deficient mice, changes in proteins related to such major functions as lipid metabolism, small molecule chemistry, and metabolic disease were similar in both mouse models (Figure 25), especially comparing fasted VLCAD with fed SCAD deficient mice. More similarities of these functions were between VLCAD deficiency in the fasted status and in the fed status rather than between SCAD deficiency and VLCAD deficiency. Overall, changes reflecting defects in fatty acid metabolism displayed almost the same significance in the canonical pathway analysis (Figure 26). Although there is no doubt that the two deficiencies altered the same canonical pathway of fatty acid metabolism, the pattern of proteins altered in the two deficiencies showed some divergence. Further studies of these differences should provide

insight into the divergent pathophysiologic changes resulting from mutations in these evolutionarily and functionally conserved enzymes.

Dramatic alterations in the oxidative phosphorylation pathway observed in both VLCAD deficient and SCAD deficient likely reflect relative energy adjustments in response to defective fatty acid ß-oxidation. However, changes of protein expression in the OXPHOS pathway in SCAD deficient mice differed remarkably from those seen in VLCAD deficient animals. Specifically, multiple subunits in complex I, III and IV were decreased in SCAD deficiency, while fewer (but not the same) subunits were increased in fed VLCAD deficiency. This apparent compensatory response in VLCAD animals was lost with fasting, a situation that would exacerbate energy deficiency in these animals. In contrast, defects in this pathway in fed SCAD deficient animals identify reduced OXPHOS even when fed, and may be important in the development of clinical symptoms in this disorder. These opposite findings further highlight the distinctive features of SCAD and VLCAD deficiency and the significant effects of fasting imposed on VLCAD deficiency.

The toxic function analysis incorporated in the IPA software, which aims to assess the toxicity of small molecules on organs such as liver and heart in humans, was utilized in this study to help provide additional insight into the pathologic alterations induced by SCAD and VLCAD deficiency (Figure 26). The results identified a pattern in fasted VLCAD deficient animals associated with cardiac enlargement, fibrosis and dilation, particularly involving the proteins SOD2 and GPX1. This is in keeping with the identification of VLCAD deficiency as a cause of cardiomyopathy and sudden death in humans. A pattern of liver steatosis was seen in SCAD deficient mice. Of note, steatosis has previously been demonstrated in LCAD but not SCAD deficient animals (Zhang et al, 2007). However, microvesicular fatty changes in

hepatocytes from SCAD mutant mice have been reported (Wood et al, 1989), and SCAD deficient BALB/cBy mice have been shown to develop a fatty liver upon fasting or dietary fat challenge (Armstrong et al, 1993). In VLCAD deficient animals, liver steatosis may be due to or exacerbated by alterations in SOD2 and PHYH. Alterations in human SOD2 have been reported in association with a decrease of hepatocytes apoptosis induced by ethanol (Wheeler et al, 2001) and has been proposed as a biomarker for diagnosis of steatohepatitis (Iacobellis et al, 2006). Finally, mitochondrial SOD2 has been found to be associated with dilation and enlargement of heart (Lebovitz et al, 1996). It is possible that SOD2 played important roles in both the development of fatty changes in liver and cardiac damage with fasting in VLCAD deficiency.

Systematic natural history and pathophysiologic studies of patients with FAODs are difficult. Patients identified through newborn screening are often clinically asymptomatic, and the immediate need of correction of metabolic crises does not allow careful study of the patients in the symptomatic state. Although mouse models of genetic disease do not always completely or accurately reflect their human counterparts, the findings in the current studies suggest strong parallels. However, findings with the mouse models will ultimately require confirmation in human patients. Despite the significant advantages gained from incorporating MS/MS into proteomic studies, there are considerable challenges in interpretation of the accumulated data. Chief among these is the fact that some experiments were performed at different times in mice with different genetic backgrounds. Additionally assay variability can be introduced by inherent limitations arising from the efficiency of commercially available reagents and approaches, variability of biological replicates, and the data analysis tools and database used for mass spectra and pathway analysis.

It should be noted that mitochondria are multifunctional organelles in eukaryotic cells and play a critical role in energy metabolism. Several recent proteomic studies have focused on the characterization of global survey of this organelle. However, the detection of mitochondrial proteins with different proteomic approaches is variable (Kislinger et al, 2006; Mootha et al, 2003). The annotation of identified proteins has largely relied on additional computational methods to account for systematic or spurious noise. It is not surprising, therefore, that the number of proteins in mouse liver mitochondria identified in these studies differs from other published reports and the number of predicted mitochondrial proteins. This is especially true of the fasted animals, as all other reported studies were performed on fed animals, In addition, incomplete coverage of mitochondrial proteins may be related to technical variables such as peptide fractionation and analyzing only peptides with pI‘s of 3.5-4.5. Nevertheless, mitochondrial data obtained from these mouse studies augment information in the current mitochondrial proteome database.

The recognition that many proteins shuttle between cellular compartments performing multiple roles in the cell, as well as probable cross-contamination during fractionation, highlight the ongoing challenges of rigorously defining subcellular localization of proteins (Phizicky et al, 2003), and caution is justified in interpretation of data on proteins supposedly restricted to the mitochondria. For example, Nudix (nucleoside diphosphate linked moiety X-type motif 7)is a member of acetyl-CoA hydrolase family originally localized to peroxisomes. However, the Nudix 7 protein was subsequently identified in liver mitochondria from 12 week old male mice through LC-MS studies (Douette et al, 2005), The exact role of this protein in mitochondria is still unclear but the finding illustrates the potential for new discoveries through non-directed proteomic analyses and the need for further validation to discern real variation.

Any inconsistencies if observed between proteomic patterns in this dissertation and the literature could reflect several factors including inaccurate existing annotations and shuttling of certain proteins between compartments. In this regard, our IPA analysis sometimes flagged pathways and cellular functions as being altered that are not consistent with known pathophysiology. For example, carbohydrate metabolism is primarily based in cytosol, however, IPA analysis inferred an alteration in carbohydrate metabolism based on changes in expression of *GNANB* and *PRKCSH*, which are categorized as having multiple or unknown locations. It is also important to note that the significance of functional annotations or prediction was sometimes inferred from a limited number of entries in the IPA knowledge base or indirectly from changes in other predicted protein interactions. For example, DNA replication, recombination and repair was a flagged as a functional category of higher level by IPA (Appendix A). However, this assignment was based on changes in only 2 proteins belonging to the disulfide isomerase family A, *PDIA3* and *SOD2 encoding proteins* with the p-value calculated by considering the number of molecules that participate in that function and the total number of molecules that are known to be associated with that function in the Ingenuity Knowledge Base (Appendix A). It is not yet clear if this is in fact a real variation, and highlights the need to understand the basic concepts of biostatistical possibility utilized the IPA software.

The change in carbohydrate metabolism in fasted VLCAD deficient mice identified in the IPA analysis was based on the differential expression of *SCP2* (down-regulation) and *GANAB* and *PRKCSH* (up-regulation). *GANAB* encodes an alpha-glucosidase that participates in galactose metabolism. The ß-subunit of glucosidase II (PRKCSH) may bind GANAB but is of unknown function(Arendt & Ostergaard, 1997; Arendt & Ostergaard, 2000). Both proteins are predominantly localized in cytoplasm, endoplasmice recticulum and pre-Golgi intermediate

vesicles (Zuber et al, 2001). However, the human glucosidase 2 complex has also been reported in mitochondria from HepG2 cells (Lehr et al, 2005). SOD2, which has a variety functions in mitochondria and is localized in multiple subcellular organelles including mitochondria inner membrane, matrix, cytoplasm and others, influences carbohydrate metabolism through *PPARGC, LEP* and other molecules (Figure 30) related to carbohydrate metabolism uptake, transport, turn over, modification and production of D-glucose (Nishikawa et al, 2000).

Finally, proteomic screening methods are known to preferentially detect higher-abundance proteins (Ghaemmaghami et al, 2003). The limited number of fractions were collected in these studies, not all of the subunits of well-established multimeric protein complexes have been captured. In addition, the annotation of these proteins may not accurately reflect their function. The identification of a given protein in my studies was assigned based on an algorithm used in the database search tool. Abundant proteins with homologous peptides could confound the detection of less abundant proteins and bias the annotation of that protein. However, despite these caveats, the altered protein patterns, functional elucidation and their roles in the pathogenesis of FAODs reported here should serve as a useful starting point for more extensive experimental characterization of core biological findings.

In conclusion, diverse changes in energy metabolism in SCAD and VLCAD deficient mice help explain heterogeneous symptoms in these two disorders. Differential compensatory or secondary deleterious effects may play a dominant role in determining the pathophysiology of these deficiencies. I anticipate that functional studies and direct investigations suggested from these studies on patients will help to elucidate the complex mechanisms underlying phenotypic variability, provide more accurate diagnosis, and improve clinical outcome in patients with these life-threatening disorders.

APPENDIX A

DEFINITION OF ANNOTATED FUNCTIONS

Functional analysis in Ingenuity Pathway Analysis associates biological functions and diseases to the experimental results by leveraging the complex biological interactions that are stored in the Ingenuity Knowledge Base. IPA Functional Analysis has three primary categories of functions: Molecular and Cellular Functions; Physiological System Development and Function; and Diseases and Disorders. There are 85 high-level functional categories that are classified under these categories. Lower level functions are classified within the high-level categories. Specific functions are the lowest level functions found in IPA. Each lowest level function has a population of associated molecules. Specific functions come from the Findings that are stored within the Ingenuity Knowledge Base. Lower level functions and specific functions may be classified within multiple high-level categories.

Amino Acid Metabolism Describes functions associated with the metabolism of amino acids, for example the generation of serine and the degradation of tryptophan.

Carbohydrate Metabolism Describes functions associated with the metabolism of carbohydrates, for example the activation of glycogen and consumption of carbohydrate.

DNA replication, recombination and repair Describes functions associated with the replication, recombination and repair of DNA. Examples of these functions include formation of replication fork, homologous recombination of DNA, and damage of DNA.

Lipid Metabolism Describes functions associated with the metabolism of lipids, for example absorption of cholesterol and adiposis.

Molecular Transport Describes functions associated with the intra- and extracellular movement of molecules, including small molecules, ions, DNA, RNA, protein, lipids and carbohydrates. Examples include efflux of glutamate and depletion of DNA.

Small Molecule Biochemistry Describes functions associated with small molecules, for example the generation of nitric oxide and metabolism of indole. Functions associated with DNA, RNA, protein, lipids and carbohydrates are described by more specific categories and therefore are not included in this category.

Neurological Disease Describes diseases and abnormalities of the neurological system. Some examples include atrophy of axons, convulsion, dyskinesia and swelling of brain.

Skeletal and Muscular Disorders Describes diseases and abnormalities of the skeletal and muscular system. Some examples include destruction of bone, hyperplasia of muscle and osteosclerosis.

Metabolic Disease Describes metabolic diseases. Some examples include acidosis of cells, diabetes and hypolipidemia.

Significance in Functional Analysis for a Dataset. The significance value associated with Functional Analysis for a dataset is a measure of the likelihood that the association between a set of Functional Analysis molecules in your experiment and a given process or pathway is due to random chance. The smaller the *p*-value the less likely that the association is random and the

more significant the association. In general, p-values less than 0.05 indicate a statistically significant, non-random association. The *p*-value is calculated using the right-tailed Fisher Exact Test.

In this method, the p-value for a given function is calculated by considering

1) the number of functional analysis molecules that participate in that function and

2) the total number of molecules that are known to be associated with that function in the Ingenuity Knowledge Base

APPENDIX B

LEGEND OF INGENUITY PATHWAY ANALYSIS

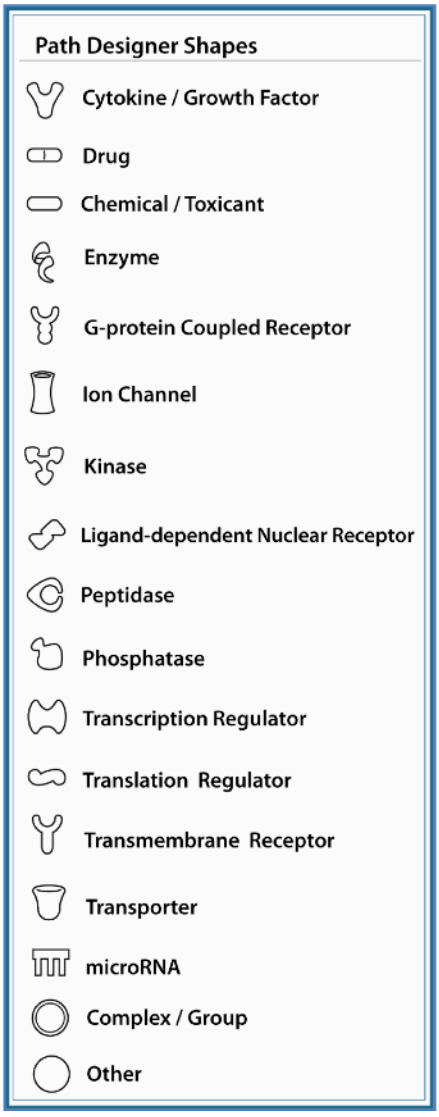

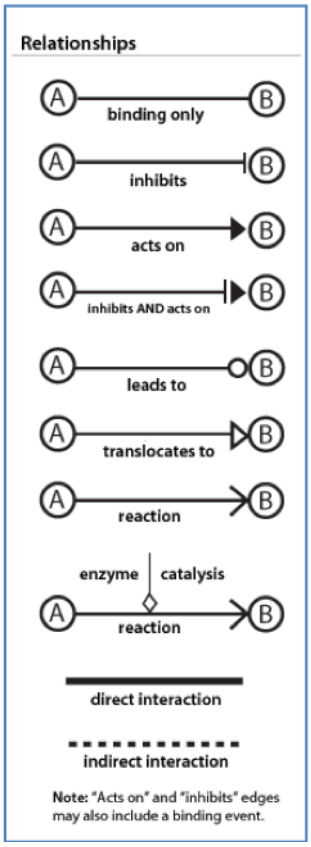

This legend is provided by IPA with a key of the main features in the networks and canonical pathways including molecule shapes and colors as well as relationship labels and types.

APPENDIX C

DATA TRANFORMATION AND NORMALIZATION

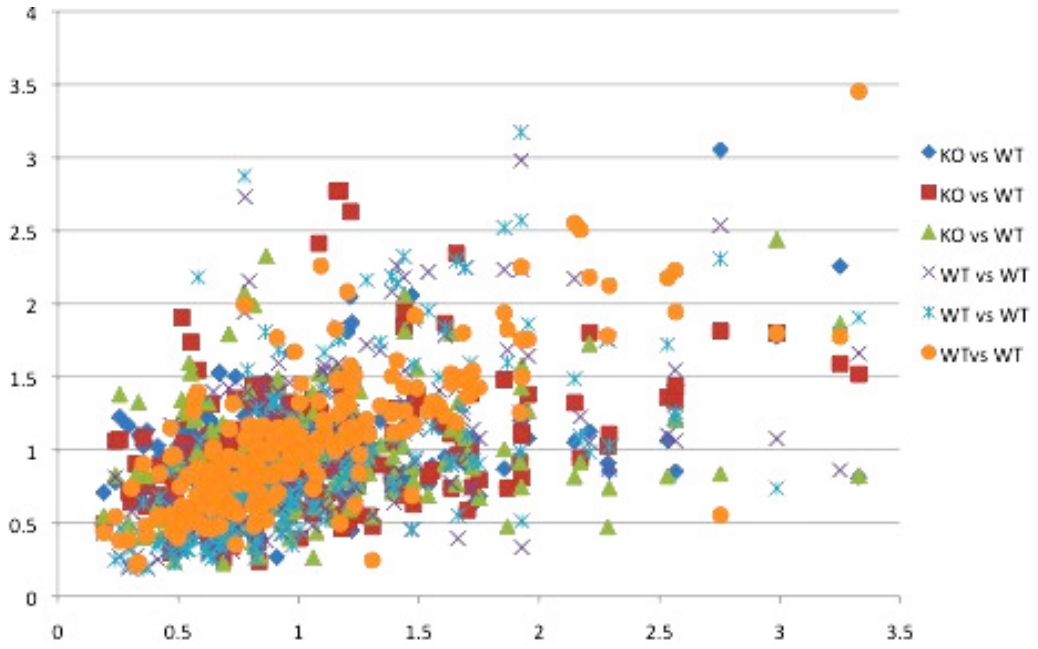

Figure 28. Example of data distribution before normalization and transformation

Data distribution of iTRAQ labeled values in fasted VLCAD deficient mice and wild type mice. X-axis-iTRAQ value of a protein in wild type mice. Y-axis-iTRAQ values of the same protein in VLCAD deficient mice or wild type mice. Each color represents the corresponding label value for the same protein either in VLCAD deficient mice or other wild type mice as replicates. KO denotes data from deficient mice. WT denotes data from wild type mice.

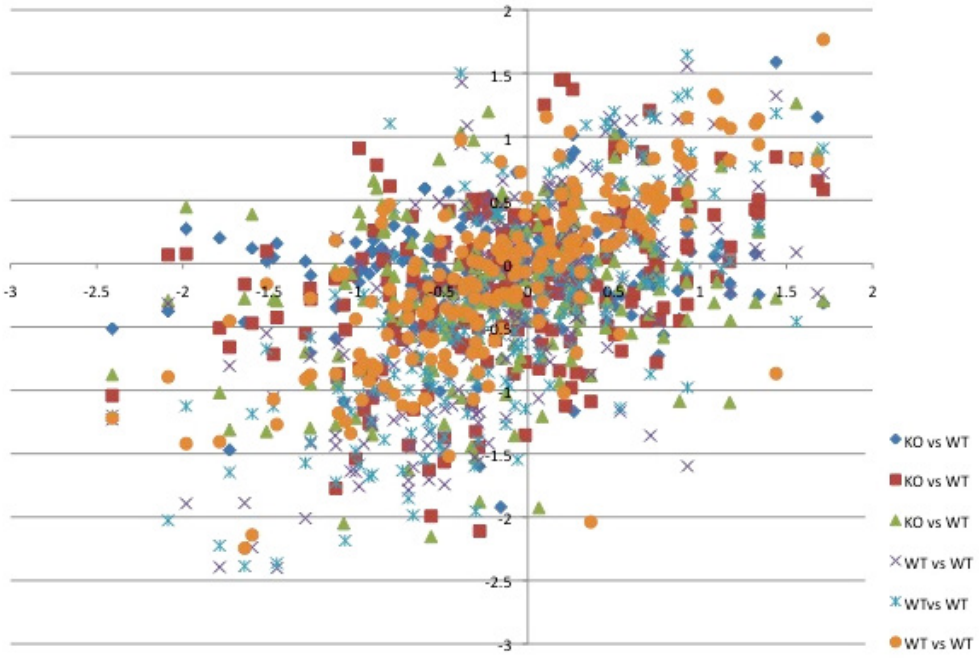

Figure 29. Example of data distribution after normalization and transformation

Data distribution of iTRAQ labeled values in fasted VLCAD deficient mice and wild type mice after normalization and log2 transformation as described in Chapter 3 (Page 76). X-axis- iTRAQ value of a protein in wild type mice. Y-axis-iTRAQ values of the same protein in VLCAD deficient mice or wild type mice. Each color represents the corresponding label value for the same protein either in VLCAD deficient mice or other wild type mice as replicates. KO denotes data from deficient mice. WT denotes data from wild type mice.

APPENDIX D

AN EXAMPLE OF INFERRED INFORMATION FROM IPA ANALYSIS

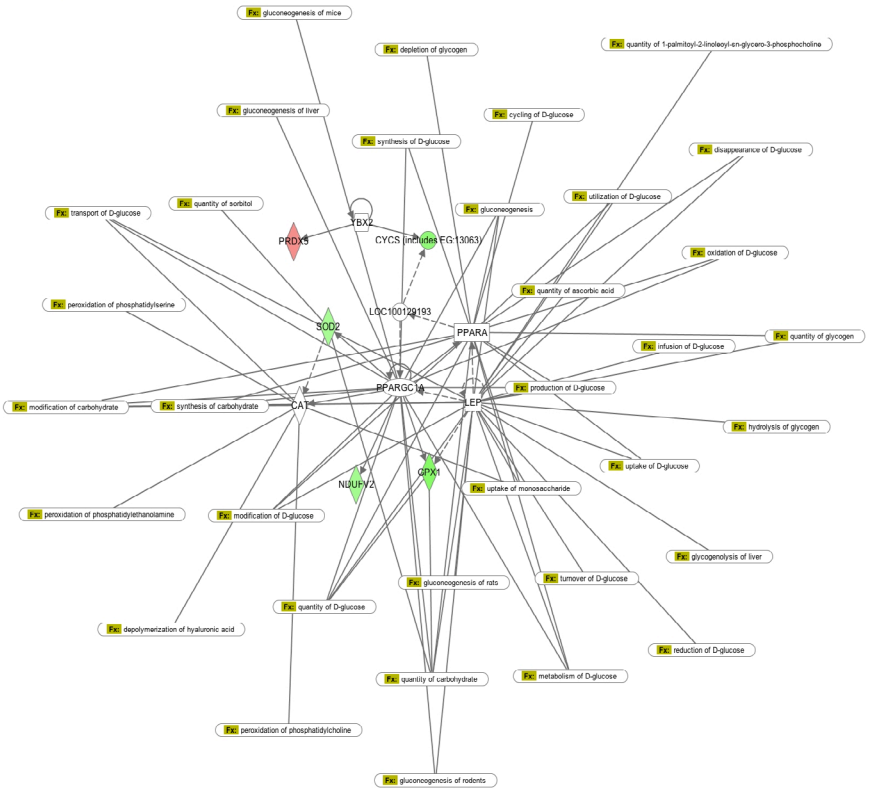

Figure 30. Network of Carbohydrate Metabolism and Inferred Information from IPA

This picture is generated by IPA based on Figure 18 overlay with function of carbohydrate metabolism. Red nodes indicate that the protein is up-regulated in the fasted VLCAD deficient mice as compared to fed deficient mice. Green indicates that the protein is down-regulated in the fasted VLCAD deficient mice. Proteins in white are those inferred from the Ingenuity Pathways Knowledge Base. The shapes denote the molecular class of the protein. An oval frame indicates a relation to carbohydrate metabolism.

BIBLIOGRAPHY

Amendt B, Green C, Sweetman L, Cloherty H, Shih V, Moon A, Teel L, Rhead W (1987) Short chain acyl-CoA dehydrogenase deficiency: clinical and biochemical studies in two patients. J Clin Invest 79: 1303-1309

Andersen JS, Lyon CE, Fox AH, Leung AK, Lam YW, Steen H, Mann M, Lamond AI (2002) Directed proteomic analysis of the human nucleolus. Curr Biol 12: 1-11

Andresen BS, Olpin S, Poorthuis BJ, Scholte HR, Vianey-Saban C, Wanders R, Ijlst L, Morris A, Pourfarzam M, Bartlett K, Baumgartner ER, deKlerk JB, Schroeder LD, Corydon TJ, Lund H, Winter V, Bross P, Bolund L, Gregersen N (1999) Clear correlation of genotype with disease phenotype in very-long-chain acyl-CoA dehydrogenase deficiency. Am J Hum Genet 64: 479-494

Aoyama T, Souri M, Ushikubo S, Kamijo T, Yamaguchi S, Kelley RI, Rhead WJ, Uetake K, Tanaka K, Hashimoto T (1995) Purification of human very-long-chain acyl-coenzyme A dehydrogenase and characterization of its deficiency in seven patients. J Clin Invest 95: 2465-2473

Arendt CW, Ostergaard HL (1997) Identification of the CD45-associated 116-kDa and 80-kDa proteins as the alpha- and beta-subunits of alpha-glucosidase II. *J Biol Chem* **272:** 13117-13125

Arendt CW, Ostergaard HL (2000) Two distinct domains of the beta-subunit of glucosidase II interact with the catalytic alpha-subunit. *Glycobiology* 10**:** 487-492

Armstrong DL, Masiowski ML, Wood PA (1993) Pathologic characterization of short-chain acyl-CoA dehydrogenase deficiency in BALB/cByJ mice. Am J Med Genet 47: 884-892

Beckner ME, Chen X, An J, Day BW, Pollack IF (2005) Proteomic characterization of harvested pseudopodia with differential gel electrophoresis and specific antibodies. Lab Invest 85: 316-327

Begriche K, Igoudjil A, Pessayre D, Fromenty B (2006) Mitochondrial dysfunction in NASH: causes, consequences and possible means to prevent it. Mitochondrion 6: 1-28

Bennett MJ, Rinaldo P, Strauss AW (2000) Inborn errors of mitochondrial fatty acid oxidation. Crit Rev Clin Lab Sci 37: 1-44

Bhala A, Willi SM, Rinaldo P, Bennett MJ, Schmidt-Sommerfeld E, Hale DE (1995) Clinical and biochemical characterization of short-chain acyl-coenzyme A dehydrogenase deficiency. J Pediatr 126: 910-915

Binzak B, Willard J, Vockley J (1998) Identification of the catalytic residue of human short/branched chain acyl-CoA dehydrogenase by in vitro mutagenesis. Biochim Biophys Acta 1382: 137-142

Boneh A, Andresen BS, Gregersen N, Ibrahim M, Tzanakos N, Peters H, Yaplito-Lee J, Pitt JJ (2006) VLCAD deficiency: pitfalls in newborn screening and confirmation of diagnosis by mutation analysis. Mol Genet Metab 88: 166-170

Bortolami S, Comelato E, Zoccarato F, Alexandre A, Cavallini L (2008) Long chain fatty acyl-CoA modulation of H(2)O (2) release at mitochondrial complex I. J Bioenerg Biomembr 40: 9-18

Bross P, Li Z, Hansen J, Hansen JJ, Nielsen MN, Corydon TJ, Georgopoulos C, Ang D, Lundemose JB, Niezen-Koning K, Eiberg H, Yang H, Kolvraa S, Bolund L, Gregersen N (2007) Single-nucleotide variations in the genes encoding the mitochondrial Hsp60/Hsp10 chaperone system and their disease-causing potential. J Hum Genet 52: 56-65

Brown-Harrison MC, Nada MA, Sprecher H, Vianey-Saban C, Farquhar J, Jr., Gilladoga AC, Roe CR (1996) Very long chain acyl-CoA dehydrogenase deficiency: successful treatment of acute cardiomyopathy. Biochem Mol Med 58: 59-65

Burns DL, Kessel M, Arciniega JL, Karpas A, Gould-Kostka J (1992) Immunochemical localization of a region of chaperonin-60 important for productive interaction with chaperonin-10. J Biol Chem 267: 25632-25635

Coates PM, Hale DE, Finocchiaro G, Tanaka K, Winter S (1988) Genetic deficiency of short chain acyl-CoA dehdrogenase in cultured fibroblasts from a patient with muscle carnitine deficiency and severe skeletal muscle weakness. J Clin Invest 81: 171-175

Corydon MJ, Andresen BS, Bross P, Kjeldsen M, Andreasen PH, Eiberg H, Kolvraa S, Gregersen N (1997) Structural organization of the human short-chain acyl-CoA dehydrogenase gene. Mamm Genome 8: 922-926

Corydon MJ, Gregersen N, Lehnert W, Ribes A, Rinaldo P, Kmoch S, Christensen E, Kristensen TJ, Andresen BS, Bross P, Winter V, Martinez G, Neve S, Jensen TG, Bolund L, Kolvraa S (1996) Ethylmalonic aciduria is associated with an amino acid variant of short chain acyl-coenzyme A dehydrogenase. Pediatric Research 39: 1059-1066

Corydon MJ, Vockley J, Rinaldo P, Rhead WJ, Kjeldsen M, Winter V, Riggs C, Babovic-Vuksanovic D, Smeitink J, De Jong J, Levy H, Sewell AC, Roe C, Matern D, Dasouki M, Gregersen N (2001) Role of common gene variations in the molecular pathogenesis of short-chain acyl-CoA dehydrogenase deficiency. Pediatr Res 49: 18-23

Coughlin CR, 2nd, Ficicioglu C (2010) Genotype-phenotype correlations: sudden death in an infant with very-long-chain acyl-CoA dehydrogenase deficiency. J Inherit Metab Dis

Cox GF, Souri M, Aoyama T, Rockenmacher S, Varvogli L, Rohr F, Hashimoto T, Korson MS (1998a) Reversal of severe hypertrophic cardiomyopathy and excellent neuropsychologic outcome in very-long-chain acyl-coenzyme A dehydrogenase deficiency. J Pediatr 133: 247-253

Cox KB, Hamm DA, Millington DS, Matern D, Vockley J, Rinaldo P, Pinkert CA, Rhead WJ, Lindsey JR, Wood PA (2001a) Gestational, pathologic and biochemical differences between very long-chain acyl-CoA dehydrogenase deficiency and long-chain acyl-CoA dehydrogenase deficiency in the mouse. Hum Mol Genet 10: 2069-2077

Cox KB, Hamm DA, Millington DS, Matern D, Vockley J, Rinaldo P, Pinkert CA, Rhead WJ, Lindsey JR, Wood PA (2001b) Gestational, pathologic and biochemical differences between very long-chain acyl-CoA dehydrogenase deficiency and long-chain acyl-CoA dehydrogenase deficiency in the mouse. Hum Mol Genet 10: 2069-2077

Cox KB, Johnson KR, Wood PA (1998b) Chromosomal locations of the mouse fatty acid oxidation genes Cpt1a, Cpt1b, Cpt2, Acadvl, and metabolically related Crat gene. Mamm Genome 9: 608-610

de Lonlay P, Valnot I, Barrientos A, Gorbatyuk M, Tzagoloff A, Taanman JW, Benayoun E, Chretien D, Kadhom N, Lombes A, de Baulny HO, Niaudet P, Munnich A, Rustin P, Rotig A (2001) A mutant mitochondrial respiratory chain assembly protein causes complex III deficiency in patients with tubulopathy, encephalopathy and liver failure. Nat Genet 29: 57-60

Deshmukh DR, Remington PL (1984) Ornithine carbamyl transferase in Reye's syndrome. Biochemical medicine 32: 337-340

Deshmukh DR, Thomas PE, McArthur B, Sarnaik AP (1985) Serum glutamate dehydrogenase and ornithine carbamyl transferase in Reye's syndrome. Enzyme 33: 171-174

Douette P, Navet R, Gerkens P, de Pauw E, Leprince P, Sluse-Goffart C, Sluse FE (2005) Steatosis-induced proteomic changes in liver mitochondria evidenced by two-dimensional differential in-gel electrophoresis. *J Proteome Res* **4:** 2024-2031

Eaton S, Bartlett K, Pourfarzam M (1996) Mammalian mitochondrial beta-oxidation. Biochem J 320 (Pt 2): 345-357

Exil VJ, Sims H, Kovacs A, Qin W, Boero J, Khuchua Z, Strauss AW (1998). Physiologic stressors inducing sudden death in the very-long-chain acyl-CoA dehydrogenase deficient mice. Circulation 98:I-5.

Exil VJ, Roberts RL, Sims H, McLaughlin JE, Malkin RA, Gardner CD, Ni G, Rottman JN, Strauss AW (2003) Very-long-chain acyl-coenzyme a dehydrogenase deficiency in mice. Circ Res 93: 448-455

Ferdinandusse S, Zomer AW, Komen JC, van den Brink CE, Thanos M, Hamers FP, Wanders RJ, van der Saag PT, Poll-The BT, Brites P (2008) Ataxia with loss of Purkinje cells in a mouse model for Refsum disease. Proc Natl Acad Sci U S A 105: 17712-17717

Ficicioglu C, Coughlin CR, 2nd, Bennett MJ, Yudkoff M (2010) Very long-chain acyl-CoA dehydrogenase deficiency in a patient with normal newborn screening by tandem mass spectrometry. J Pediatr 156: 492-494

Ghaemmaghami S, Huh WK, Bower K, Howson RW, Belle A, Dephoure N, O'Shea EK, Weissman JS (2003) Global analysis of protein expression in yeast. *Nature* **425:** 737-741

Ghisla S, Thorpe C, Massey V (1984) Mechanistic Studies with General Acyl-CoA Dehydrogenase and Butyryl-CoA Dehydrogenase: Evidence for the Transfer of the b-Hydrogen to the Flavin N(5)-Position as a Hydride. Biochemistry 23: 3154-3161

Gianazza E, Vergani L, Wait R, Brizio C, Brambilla D, Begum S, Giancaspero TA, Conserva F, Eberini I, Bufano D, Angelini C, Pegoraro E, Tramontano A, Barile M (2006) Coordinated and reversible reduction of enzymes involved in terminal oxidative metabolism in skeletal muscle mitochondria from a riboflavin-responsive, multiple acyl-CoA dehydrogenase deficiency patient. Electrophoresis 27: 1182-1198

Gibson KM, Sweetman L, Nyhan WL, Jansen I (1985) Demonstration of 4-aminobutyric acid aminotransferase deficiency in lymphocytes and lymphoblasts. J Inherit Metab Dis 8: 204-208

Goetzman ES, Tian L, Wood PA (2005) Differential induction of genes in liver and brown adipose tissue regulated by peroxisome proliferator-activated receptor-alpha during fasting and cold exposure in acyl-CoA dehydrogenase-deficient mice. Mol Genet Metab 84: 39-47

Gregersen N, Andresen BS, Corydon MJ, Corydon TJ, Olsen RK, Bolund L, Bross P (2001) Mutation analysis in mitochondrial fatty acid oxidation defects: Exemplified by acyl-CoA dehydrogenase deficiencies, with special focus on genotype-phenotype relationship. Hum Mutat 18: 169-189

Gregersen N, Olsen RK (2010) Disease mechanisms and protein structures in fatty acid oxidation defects. J Inherit Metab Dis 33: 547-553

Gygi SP, Corthals GL, Zhang Y, Rochon Y, Aebersold R (2000) Evaluation of two-dimensional gel electrophoresis-based proteome analysis technology. Proc Natl Acad Sci U S A 97: 9390-9395

Haack TB, Danhauser K, Haberberger B, Hoser J, Strecker V, Boehm D, Uziel G, Lamantea E, Invernizzi F, Poulton J, Rolinski B, Iuso A, Biskup S, Schmidt T, Mewes HW, Wittig I, Meitinger T, Zeviani M, Prokisch H (2010) Exome sequencing identifies ACAD9 mutations as a cause of complex I deficiency. Nat Genet 42: 1131-1134

He M, Rutledge SL, Kelly DR, Palmer CA, Murdoch G, Majumder N, Nicholls RD, Pei Z, Watkins PA, Vockley J (2007) A new genetic disorder in mitochondrial fatty acid beta-oxidation: ACAD9 deficiency. Am J Hum Genet 81: 87-103

Hinsdale ME, Kelly CL, Wood PA (1993) Null allele at Bcd-1 locus in BALB/cByJ mice is due to a deletion in the short-chain acyl-CoA dehydrogenase gene and results in missplicing of mRNA. Genomics 16: 605-611

Holt JT, Arvan DA, Mayer T, Smith TJ, Bell JE (1983) Glutamate dehydrogenase in Reye's syndrome. Evidence for the presence of an altered enzyme in serum with increased susceptibility to inhibition by GTP. Biochimica et biophysica acta 749: 42-46

Ikeda Y, Keese S, Fenton WA, Tanaka K (1987) Biosynthesis of four rat liver mitochondrial acyl-CoA dehydrogenases. Import into mitochondria and processing of their precursors in a cell-free system and in cultured cells. *Arch Biochem Biophys* **252:** 662-674

Jiang XS, Dai J, Sheng QH, Zhang L, Xia QC, Wu JR, Zeng R (2005) A comparative proteomic strategy for subcellular proteome research: ICAT approach coupled with bioinformatics prediction to ascertain rat liver mitochondrial proteins and indication of mitochondrial localization for catalase. Mol Cell Proteomics 4: 12-34

Kelly CL, Wood PA (1996) Cloning and characterization of the mouse short-chain acyl-CoA dehydrogenase gene. Mamm Genome 7: 262-264

Kersey PJ, Duarte J, Williams A, Karavidopoulou Y, Birney E, Apweiler R (2004) The International Protein Index: an integrated database for proteomics experiments. Proteomics 4: 1985-1988

Kislinger T, Cox B, Kannan A, Chung C, Hu P, Ignatchenko A, Scott MS, Gramolini AO, Morris Q, Hallett MT, Rossant J, Hughes TR, Frey B, Emili A (2006) Global survey of organ and organelle protein expression in mouse: combined proteomic and transcriptomic profiling. Cell 125: 173-186

Kurian MA, Hartley L, Zolkipli Z, Little MA, Costigan D, Naughten ER, Olpin S, Muntoni F, King MD (2004) Short-chain acyl-CoA dehydrogenase deficiency associated with early onset severe axonal neuropathy. Neuropediatrics 35: 312-316

Lai JC, Liang BB, Zhai S, Jarvi EJ, Lu DR (1994) Brain mitochondrial citrate synthase and glutamate dehydrogenase: differential inhibition by fatty acyl coenzyme A derivatives. Metabolic brain disease 9: 143-152

Iacobellis A, Marcellini M, Andriulli A, Perri F, Leandro G, Devito R, Nobili V (2006) Non invasive evaluation of liver fibrosis in paediatric patients with nonalcoholic steatohepatitis. World J Gastroenterol 12: 7821-7825

Lanpher B, Brunetti-Pierri N, Lee B (2006) Inborn errors of metabolism: the flux from Mendelian to complex diseases. Nat Rev Genet 7: 449-460

Lebon S, Rodriguez D, Bridoux D, Zerrad A, Rotig A, Munnich A, Legrand A, Slama A (2007) A novel mutation in the human complex I NDUFS7 subunit associated with Leigh syndrome. Mol Genet Metab 90: 379-382

Lebovitz RM, Zhang H, Vogel H, Cartwright J, Jr., Dionne L, Lu N, Huang S, Matzuk MM (1996) Neurodegeneration, myocardial injury, and perinatal death in mitochondrial superoxide dismutase-deficient mice. Proc Natl Acad Sci U S A 93: 9782-9787

Lehr S, Kotzka J, Avci H, Knebel B, Muller S, Hanisch FG, Jacob S, Haak C, Susanto F, Muller-Wieland D (2005) Effect of sterol regulatory element binding protein-1a on the mitochondrial protein pattern in human liver cells detected by 2D-DIGE. *Biochemistry* 44**:** 5117-5128

Lindner M, Hoffmann GF, Matern D (2010) Newborn screening for disorders of fatty-acid oxidation: experience and recommendations from an expert meeting. J Inherit Metab Dis 33: 521-526

Martin J (1997) Molecular chaperones and mitochondrial protein folding. J Bioenerg Biomembr 29: 35-43

Mathur A, Sims HF, Gopalakrishnan D, Gibson B, Rinaldo P, Vockley J, Hug G, Strauss AW (1999) Molecular heterogeneity in very-long-chain acyl-CoA dehydrogenase deficiency causing pediatric cardiomyopathy and sudden death. Circulation 99: 1337-1343

Matsubara Y, Indo Y, Naito E, Ozasa H, Glassberg R, Vockley J, Ikeda Y, Kraus J, Tanaka K (1989) Molecular cloning and nucleotide sequence of cDNAs encoding the precursors of rat long chain acyl-coenzyme A, short chain acyl-coenzyme A, and isovaleryl-coenzyme A dehydrogenases. Sequence homology of four enzymes of the acyl-CoA dehydrogenase family. J Biol Chem 264: 16321-16331

Medina-Kauwe LK, Tobin AJ, De Meirleir L, Jaeken J, Jakobs C, Nyhan WL, Gibson KM (1999) 4-Aminobutyrate aminotransferase (GABA-transaminase) deficiency. J Inherit Metab Dis 22: 414-427

Mitchell RA, McArthur B, Sarnaik AP (1985) Absence of diffusible inhibitor of glutamate dehydrogenase in the hepatocytes of Reye syndrome patients. Pediatric Research 19: 110-112

Mitchell RA, Ram ML, Arcinue EL, Chang CH (1980) Comparison of cytosolic and mitochondrial hepatic enzyme alterations in Reye's syndrome. Pediatric Research 14: 1216-1221

Mootha VK, Bunkenborg J, Olsen JV, Hjerrild M, Wisniewski JR, Stahl E, Bolouri MS, Ray HN, Sihag S, Kamal M, Patterson N, Lander ES, Mann M (2003) Integrated analysis of protein composition, tissue diversity, and gene regulation in mouse mitochondria. Cell 115: 629-640

Murayama K, Fujimura T, Morita M, Shindo N (2001) One-step subcellular fractionation of rat liver tissue using a Nycodenz density gradient prepared by freezing-thawing and two-dimensional sodium dodecyl sulfate electrophoresis profiles of the main fraction of organelles. Electrophoresis 22: 2872-2880

Nishikawa T, Edelstein D, Du XL, Yamagishi S, Matsumura T, Kaneda Y, Yorek MA, Beebe D, Oates PJ, Hammes HP, Giardino I, Brownlee M (2000) Normalizing mitochondrial superoxide production blocks three pathways of hyperglycaemic damage. *Nature* **404:** 787-790

Olsen JV, de Godoy LM, Li G, Macek B, Mortensen P, Pesch R, Makarov A, Lange O, Horning S, Mann M (2005) Parts per million mass accuracy on an Orbitrap mass spectrometer via lock mass injection into a C-trap. Mol Cell Proteomics 4: 2010-2021

Ong SE, Foster LJ, Mann M (2003) Mass spectrometric-based approaches in quantitative proteomics. Methods 29: 124-130

Pedersen CB, Kolvraa S, Kolvraa A, Stenbroen V, Kjeldsen M, Ensenauer R, Tein I, Matern D, Rinaldo P, Vianey-Saban C, Ribes A, Lehnert W, Christensen E, Corydon TJ, Andresen BS, Vang S, Bolund L, Vockley J, Bross P, Gregersen N (2008) The ACADS gene variation spectrum in 114 patients with short-chain acyl-CoA dehydrogenase (SCAD) deficiency is dominated by missense variations leading to protein misfolding at the cellular level. Hum Genet 124: 43-56

Pedersen CB, Zolkipli Z, Vang S, Palmfeldt J, Kjeldsen M, Stenbroen V, Schmidt SP, Wanders RJ, Ruiter JP, Wibrand F, Tein I, Gregersen N (2010) Antioxidant dysfunction: potential risk for neurotoxicity in ethylmalonic aciduria. J Inherit Metab Dis 33: 211-222

Phizicky E, Bastiaens PI, Zhu H, Snyder M, Fields S (2003) Protein analysis on a proteomic scale. *Nature* 422**:** 208-215

Prochazka, M, Leiter, EH (1986). A null activity variant found at the butyryl CoA dehydrogenase (Bcd-1) locus in BALB/cByJ subline. Mouse News Lett. 75, 31.

Ribes A, Riudor E, Garavaglia B, Martinez G, Arranz A, Invernizzi F, Briones P, Lamantea E, Sentis M, Barcelo A, Roig M (1998) Mild or absent clinical signs in twin sisters with short-chain acyl-CoA dehydrogenase deficiency. Eur J Pediatr 157: 317-320

Ross PL, Huang YN, Marchese JN, Williamson B, Parker K, Hattan S, Khainovski N, Pillai S, Dey S, Daniels S, Purkayastha S, Juhasz P, Martin S, Bartlet-Jones M, He F, Jacobson A, Pappin DJ (2004) Multiplexed protein quantitation in Saccharomyces cerevisiae using amine-reactive isobaric tagging reagents. Mol Cell Proteomics 3: 1154-1169

Saheki T, Iijima M, Li MX, Kobayashi K, Horiuchi M, Ushikai M, Okumura F, Meng XJ, Inoue I, Tajima A, Moriyama M, Eto K, Kadowaki T, Sinasac DS, Tsui LC, Tsuji M, Okano A, Kobayashi T (2007) Citrin/mitochondrial glycerol-3-phosphate dehydrogenase double knock-out mice recapitulate features of human citrin deficiency. J Biol Chem 282: 25041-25052

Saudubray JM, Martin D, de Lonlay P, Touati G, Poggi-Travert F, Bonnet D, Jouvet P, Boutron M, Slama A, Vianey-Saban C, Bonnefont JP, Rabier D, Kamoun P, Brivet M (1999) Recognition and management of fatty acid oxidation defects: a series of 107 patients. J Inherit Metab Dis 22: 488-502

Sauer SW, Okun JG, Hoffmann GF, Koelker S, Morath MA (2008) Impact of short- and medium-chain organic acids, acylcarnitines, and acyl-CoAs on mitochondrial energy metabolism. Biochim Biophys Acta 1777: 1276-1282

Schiffer, SP, Prochaska, M, Jezyk, PF, Roderick, TH, Yudhoff, M, Patterson, DF (1989). Organic aciduria and butryl CoA dehydrogenase deficiency in BALB/cByJ mice. Biochem. Genet. 27, 47-58.

Schmidt SP, Corydon TJ, Pedersen CB, Bross P, Gregersen N (2010) Misfolding of short-chain acyl-CoA dehydrogenase leads to mitochondrial fission and oxidative stress. Mol Genet Metab 100: 155-162

Schuck PF, Ferreira Gda C, Tonin AM, Viegas CM, Busanello EN, Moura AP, Zanatta A, Klamt F, Wajner M (2009) Evidence that the major metabolites accumulating in medium-chain acyl-CoA dehydrogenase deficiency disturb mitochondrial energy homeostasis in rat brain. Brain Res 1296: 117-126

Schuler AM, Gower BA, Matern D, Rinaldo P, Vockley J, Wood PA (2005) Synergistic heterozygosity in mice with inherited enzyme deficiencies of mitochondrial fatty acid beta-oxidation. Mol Genet Metab 85: 7-11

Schuler AM, Wood PA (2002) Mouse models for disorders of mitochondrial fatty acid beta-oxidation. ILAR J 43: 57-65

Spiekerkoetter U, Lindner M, Santer R, Grotzke M, Baumgartner MR, Boehles H, Das A, Haase C, Hennermann JB, Karall D, de Klerk H, Knerr I, Koch HG, Plecko B, Roschinger W,

Schwab KO, Scheible D, Wijburg FA, Zschocke J, Mayatepek E et al (2009a) Management and outcome in 75 individuals with long-chain fatty acid oxidation defects: results from a workshop. J Inherit Metab Dis 32: 488-497

Spiekerkoetter U, Lindner M, Santer R, Grotzke M, Baumgartner MR, Boehles H, Das A, Haase C, Hennermann JB, Karall D, de Klerk H, Knerr I, Koch HG, Plecko B, Roschinger W, Schwab KO, Scheible D, Wijburg FA, Zschocke J, Mayatepek E et al (2009b) Treatment recommendations in long-chain fatty acid oxidation defects: consensus from a workshop. J Inherit Metab Dis 32: 498-505

Spiekerkoetter U, Tokunaga C, Wendel U, Mayatepek E, Exil V, Duran M, Wijburg FA, Wanders RJ, Strauss AW (2004) Changes in blood carnitine and acylcarnitine profiles of very long-chain acyl-CoA dehydrogenase-deficient mice subjected to stress. Eur J Clin Invest 34: 191-196

Spiekerkoetter U, Wood PA (2010) Mitochondrial fatty acid oxidation disorders: pathophysiological studies in mouse models. J Inherit Metab Dis 33: 539-546

Strauss AW, Powell CK, Hale DE, Anderson MM, Ahuja A, Brackett JC, Sims HF (1995) Molecular basis of human mitochondrial very-long-chain acyl-CoA dehydrogenase deficiency causing cardiomyopathy and sudden death in childhood. Proc Natl Acad Sci U S A 92: 10496-10500

Su AI, Cooke MP, Ching KA, Hakak Y, Walker JR, Wiltshire T, Orth AP, Vega RG, Sapinoso LM, Moqrich A, Patapoutian A, Hampton GM, Schultz PG, Hogenesch JB (2002) Large-scale analysis of the human and mouse transcriptomes. Proc Natl Acad Sci U S A 99: 4465-4470

Swigonova Z, Mohsen AW, Vockley J (2009) Acyl-CoA dehydrogenases: Dynamic history of protein family evolution. J Mol Evol 69: 176-193

Tanaka K, Indo Y (1992) Evolution of the acyl-CoA dehydrogenase/oxidase superfamily. Prog Clin Biol Res 375: 95-110

Tein I, Elpeleg O, Ben-Zeev B, Korman SH, Lossos A, Lev D, Lerman-Sagie T, Leshinsky-Silver E, Vockley J, Berry GT, Lamhonwah AM, Matern D, Roe CR, Gregersen N (2008) Short-chain acyl-CoA dehydrogenase gene mutation (c.319C>T) presents with clinical heterogeneity and is candidate founder mutation in individuals of Ashkenazi Jewish origin. Mol Genet Metab 93: 179-189

Thorpe C, Kim JJP (1995) Structure and mechanism of action of the Acyl-CoA dehydrogenases. FASEB 9: 718-725

Tiranti V, Jaksch M, Hofmann S, Galimberti C, Hoertnagel K, Lulli L, Freisinger P, Bindoff L, Gerbitz KD, Comi GP, Uziel G, Zeviani M, Meitinger T (1999) Loss-of-function

mutations of SURF-1 are specifically associated with Leigh syndrome with cytochrome c oxidase deficiency. Ann Neurol 46: 161-166

Tonge R, Shaw J, Middleton B, Rowlinson R, Rayner S, Young J, Pognan F, Hawkins E, Currie I, Davison M (2001) Validation and development of fluorescence two-dimensional differential gel electrophoresis proteomics technology. Proteomics 1: 377-396

Triepels RH, van den Heuvel LP, Loeffen JL, Buskens CA, Smeets RJ, Rubio Gozalbo ME, Budde SM, Mariman EC, Wijburg FA, Barth PG, Trijbels JM, Smeitink JA (1999) Leigh syndrome associated with a mutation in the NDUFS7 (PSST) nuclear encoded subunit of complex I. Ann Neurol 45: 787-790

Tucci S, Primassin S, Ter Veld F, Spiekerkoetter U (2010) Medium-chain triglycerides impair lipid metabolism and induce hepatic steatosis in very long-chain acyl-CoA dehydrogenase (VLCAD)-deficient mice. Mol Genet Metab 101: 40-47

Unlu M, Morgan ME, Minden JS (1997) Difference gel electrophoresis: a single gel method for detecting changes in protein extracts. Electrophoresis 18: 2071-2077

van Maldegem BT, Duran M, Wanders RJA, Niezen-Koning KE, Hogeveen M, Ijlst L, Waterham HR, Wijburg FA (2006) Clinical, biochemical, and genetic heterogeneity in short-chain acyl-coenzyme A dehydrogenase deficiency. Jama 296: 943-952

van Maldegem BT, Wanders RJA, Wijburg FA (2010) Clinical aspects of short-chain acyl-CoA dehydrogenase deficiency. J Inherit Metab Dis 33: 507-511

Viswanathan S, Unlu M, Minden JS (2006) Two-dimensional difference gel electrophoresis. Nat Protoc 1: 1351-1358

Vockley J, Rinaldo P, Bennett MJ, Matern D, Vladutiu GD (2000) Synergistic heterozygosity: disease resulting from multiple partial defects in one or more metabolic pathways. Mol Genet Metab 71: 10-18

Vockley J, Whiteman DA (2002) Defects of mitochondrial beta-oxidation: a growing group of disorders. Neuromuscul Disord 12: 235-246

Waisbren SE, Levy HL, Noble M, Matern D, Gregersen N, Pasley K, Marsden D (2008) Short-chain acyl-CoA dehydrogenase (SCAD) deficiency: an examination of the medical and neurodevelopmental characteristics of 14 cases identified through newborn screening or clinical symptoms. Mol Genet Metab 95: 39-45

Wang Y, Mohsen A-W, Mihalik SJ, Goetzman ES, Vockley J (2010) Evidence for physical association of mitochondrial fatty acid oxidation and oxidative phosphorylation complexes. The Journal of biological chemistry 285: 29834-29841

Wheeler MD, Nakagami M, Bradford BU, Uesugi T, Mason RP, Connor HD, Dikalova A, Kadiiska M, Thurman RG (2001) Overexpression of manganese superoxide dismutase prevents alcohol-induced liver injury in the rat. J Biol Chem 276: 36664-36672

Wiese S, Reidegeld KA, Meyer HE, Warscheid B (2007) Protein labeling by iTRAQ: a new tool for quantitative mass spectrometry in proteome research. Proteomics 7: 340-350

Wilcken B (2010) Fatty acid oxidation disorders: outcome and long-term prognosis. J Inherit Metab Dis 33: 501-506

Wilcken B, Wiley V, Hammond J, Carpenter K (2003) Screening newborns for inborn errors of metabolism by tandem mass spectrometry. N Engl J Med 348: 2304-2312

Wood PA, Amendt BA, Rhead WJ, Millington DS, Inoue F, Armstrong D (1989) Short-chain acyl-coenzyme A dehydrogenase deficiency in mice. Pediatr Res 25: 38-43

Wu WW, Wang G, Baek SJ, Shen RF (2006) Comparative study of three proteomic quantitative methods, DIGE, cICAT, and iTRAQ, using 2D gel- or LC-MALDI TOF/TOF. J Proteome Res 5: 651-658

Zhang D, Liu ZX, Choi CS, Tian L, Kibbey R, Dong J, Cline GW, Wood PA, Shulman GI (2007) Mitochondrial dysfunction due to long-chain Acyl-CoA dehydrogenase deficiency causes hepatic steatosis and hepatic insulin resistance. Proc Natl Acad Sci U S A 104: 17075-17080

Zhao Q, Wang J, Levichkin IV, Stasinopoulos S, Ryan MT, Hoogenraad NJ (2002) A mitochondrial specific stress response in mammalian cells. EMBO J 21: 4411-4419

Zolkipli Z, Pedersen CB, Lamhonwah AM, Gregersen N, Tein I (2011) Vulnerability to oxidative stress in vitro in pathophysiology of mitochondrial short-chain acyl-CoA dehydrogenase deficiency: response to antioxidants. PLoS One 6: e17534

Zuber C, Fan JY, Guhl B, Parodi A, Fessler JH, Parker C, Roth J (2001) Immunolocalization of UDP-glucose:glycoprotein glucosyltransferase indicates involvement of pre-Golgi intermediates in protein quality control. *Proc Natl Acad Sci U S A* **98:** 10710-10715